MODEL ANALYSIS OF THE ROLE OF MARINE GATEWAYS IN THE PALAEOCEANOGRAPHY OF THE MIOCENE MEDITERRANEAN AND PARATETHYS

Members of the dissertation committee:

Prof. dr. ir. H.A. Dijkstra
Institute for Marine and Atmospheric Research (IMAU), Utrecht University
Utrecht, The Netherlands

Dr. R. Flecker
School of Geographical Sciences, University of Bristol
Bristol, United Kingdom

Prof. dr. J. García Lafuente
Department of Applied Physics II, University of Malaga
Malaga, Spain

Prof. dr. W. Krijgsman
Department of Earth Sciences, Utrecht University
Utrecht, The Netherlands

Prof. dr. G.J. de Lange
Department of Earth Sciences, Utrecht University
Utrecht, The Netherlands

Cover picture of the Strait of Gibraltar by Alba de la Vara, Tarifa, 2015.
Picture of the sea by Alba de la Vara, Cadiz, 2015.

Model analysis of the role of marine gateways in the palaeoceanography of the Miocene Mediterranean and Paratethys

Modelanalyse van de rol van zeestraten in de paleo-oceanografie van de Middellandse Zee en de Paratethys tijdens het Mioceen

(met een samenvatting in het Nederlands)

Análisis numérico de la influencia de los estrechos marinos en la paleoceanografía del Mediterráneo y el Paratetis durante el Mioceno

(con resumen en Español)

Proefschrift
ter verkrijging van de graad van doctor aan de Universiteit Utrecht op gezag van de rector magnificus, prof. dr. G.J. van der Zwaan, ingevolge het besluit van het college voor promoties in het openbaar te verdedigen op vrijdag 4 december 2015 des middags te 12.45 uur

door
Alba de la Vara Fernández
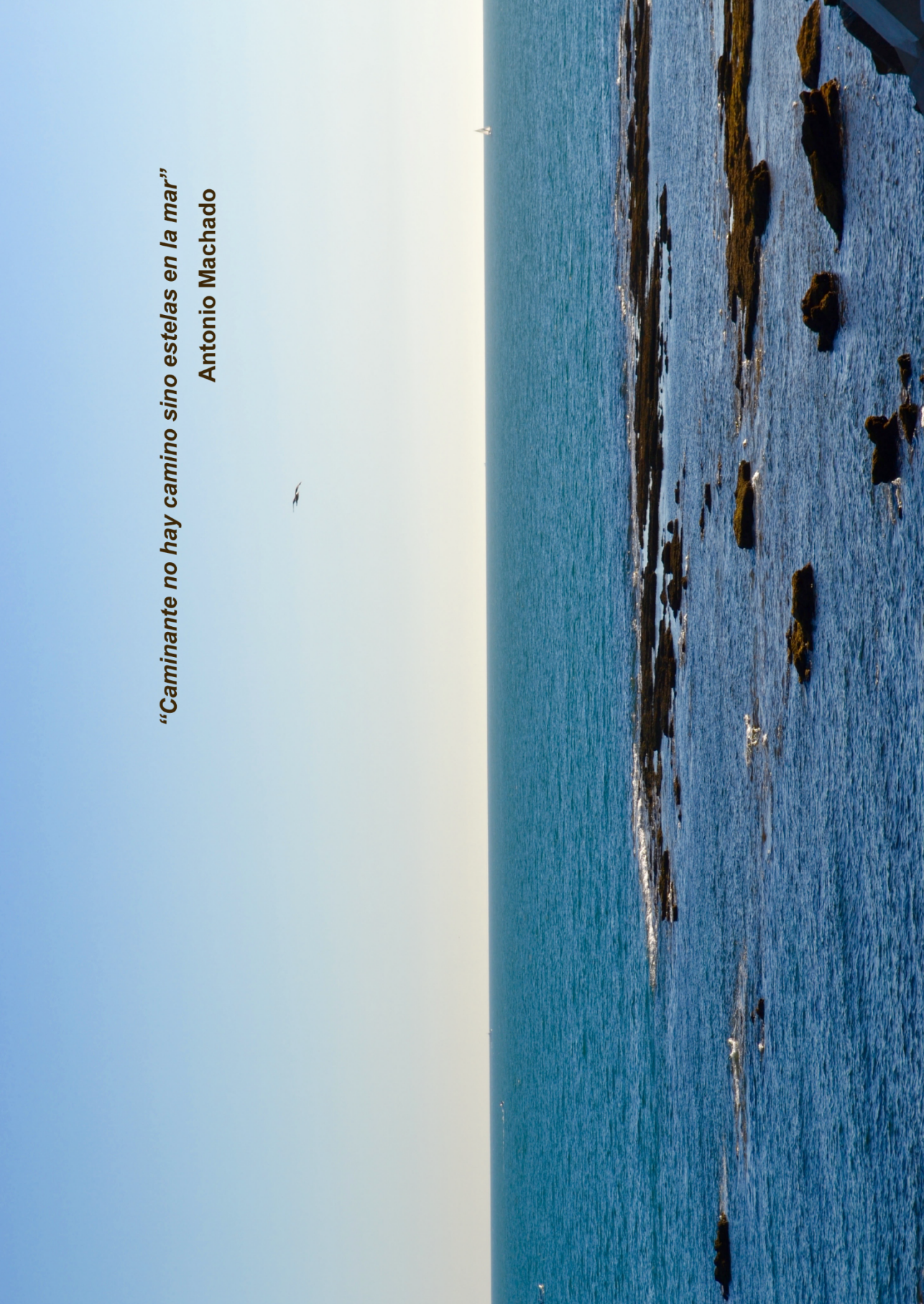geboren op 28 november 1985
te Valencia, Spanje

For my grandfather and friend, Pepe

"*Caminante no hay camino sino estelas en la mar*"

Antonio Machado

Index

Chapter 1: Introduction

The circulation of the oceans is driven by fluxes of water, heat and momentum across the interface between the ocean and the atmosphere. In turn, the ocean affects the state of the atmosphere and plays an important role in determining Earth's climate. Ocean currents are constrained by the shape of the basins, i.e. by the distribution of land and sea and by the bathymetry. Although often thought of as stationary, basin shape is as mobile as the ocean and the atmosphere, albeit on the much longer time scale of plate tectonics (millions of years). Viewed over geological time then, the oceans, the atmosphere (climate), and the solid Earth form a closely linked system. It is in the form of sediments, and in particular those sediments accumulating on the seafloor, that this system records changes in ocean circulation (e.g., Woodruff and Savin, 1989; Maier-Reimer et al., 1990; Heinze and Crowley, 1997; Ramsay et al., 1998). These changes are especially well expressed in land-locked basins, which are more sensitive to changes in climate due to their limited connection to the ocean.

A very direct way in which plate tectonics affects the evolution of ocean circulation is by means of the opening and closure of marine gateways. Marine gateways are oceanic passages between neighbouring basins which allow interbasinal exchange of water, heat, and salt, nutrients and biota (e.g., deConto, 2009). The key role of marine gateways is well exemplified by the Strait of Gibraltar, which at present forms the only connection between the Mediterranean Sea and the Atlantic Ocean. The Strait of Gibraltar has a length of 60 km, a minimum depth of 290 m near Camarinal Sill and a minimum width of 15 km close to Tarifa Narrows (e.g., Sannino et al., 2002). Because of these small dimensions the strait limits the exchange between the Mediterranean basin and the Atlantic Ocean. This, together with the high evaporative loss over the basin, increases Mediterranean salinity (and therefore density) relative to that in the Atlantic Ocean at the same depth. The resulting horizontal pressure gradient drives a dense outflow from the Mediterranean at depth through the strait, towards the Atlantic Ocean (e.g., Bryden and Kinder, 1991; Figure 1.1). This outflow causes the Mediterranean surface to tend towards a lower level and the implied surface gradient triggers Atlantic inflow at shallow levels (Figure 1.1). In
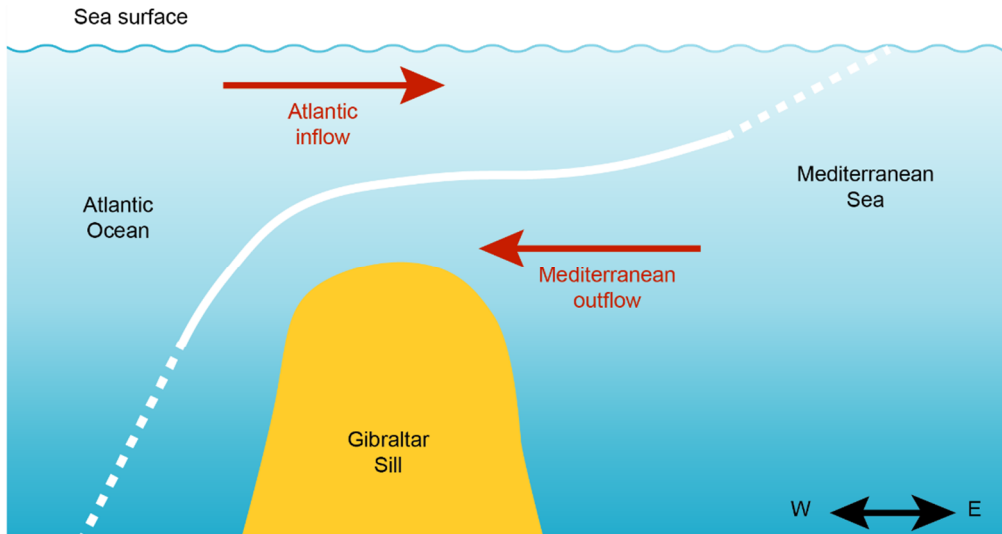
Figure 1.1. Schematic east-west cross-section of the Strait of Gibraltar illustrating the Mediterranean-Atlantic water exchange at the sill based on Bryden and Kinder (1991). The white line corresponds to the interface between the upper Atlantic inflow and the lower Mediterranean outflow.

terms of volume transport, inflow slightly exceeds outflow which compensates for the net evaporative loss over the Mediterranean Sea and allows the basin volume to be constant with time. With an annual mean of 0.78±0.05 Sv (Soto-Navarro et al., 2010; 1 Sv = 10^6 m^3/s) the volume of Mediterranean outflow waters is relatively small but it has been proposed to be sufficient to enhance the Atlantic Meridional Overturning Circulation (e.g., Hernández-Molina et al., 2014 and references therein) and thus to play a role in the global climate system. Particularly interestingly, in the recent geological past, marine gateways existed between the Mediterranean Sea and the adjacent Indian and Atlantic oceans.

In general terms, this thesis is about applying theory and models for ocean circulation, to questions stemming from the sedimentary evidence, regarding the influence of tectonics. More specifically, I aim to achieve physics-based insight into the role of the marine gateways of the Mediterranean region at a time when these were subject to important changes, the Miocene period (see Figure 1.2). The focus is on the

Series/Epoch		Age/Stage	Age (Ma)
			2.58
Pliocene		Piacenzian	3.600
		Zanclean	5.333
Miocene	Late	Messinian	7.246
		Tortonian	11.63
	Middle	Serravallian	13.82
		Langhian	15.97
	Early	Burdigalian	20.44
		Aquitanian	23.03
Oligocene		Chattian	28.1
		Rupelian	33.9

Figure 1.2. Oligocene to Pliocene geologic time scale based on the International Chronostratigraphic Chart of 2015/01 (Cohen et al., 2013; updated).

control that gateways exert on first-order aspects such as basin temperature and salinity, the basin-scale (overturning) circulation, and patterns of exchange in the gateways. For this I use regional-scale ocean general circulation models. In addition, I perform a quantitative analysis of what may be thought of as an extreme consequence of gateway closure, the lowering of sea level in the satellite basins of the Mediterranean, the predecessors of the Black Sea and the Caspian Sea. By comparing model results to available data I am able to discard previously proposed scenarios and formulate new ones. My research focuses on three outstanding issues, which played a role at different times: (i) the Early to Middle Miocene closure of the Tethys Seaway which used to connect the proto-Mediterranean Sea to the Indo-Pacific Ocean (the "Indian Gateway"); (ii) the interplay of the two marine corridors that connected the Mediterranean and the Atlantic during the Late Miocene, before the Strait of Gibraltar was formed; and (iii) the sea level variations of the Black Sea and the Caspian Sea in response to the fall of the level of the Mediterranean Sea during the deposition of the Messinian evaporites.

1.1. From the Neo-Tethys to the Mediterranean Sea and its satellite basins

From the Eocene-Oligocene onwards, the motion of the African-Arabian plate relative to the Eurasian plate turned the once open western Neo-Tethys Ocean into the proto-Mediterranean Sea (e.g., Rögl, 1999; Figure 1.3a). The convergence of the two plates was accommodated by subduction of the African plate below the Eurasian plate and, subsequently, resulted in collision of the approaching continents (e.g., Jolivet et al., 2006). The ensuing lithospheric deformation uplifted the Alpine chains in a long-term process of tectonic interaction (e.g., Schmid et al., 1996; Bellahsen et al., 2014). Due to the development of the Alpine chains a new marine realm north of the proto-Mediterranean Sea came into existence: the Paratethys (Seneš, 1973; Báldi, 1980; Rögl, 1999). This vast sea extended over the southern flank of Europe and had connections with the North Sea and the proto-Mediterranean Sea (Rögl, 1999; Harzhauser and Piller, 2007; Figure 1.3a). With the plate boundary pinned at certain points by collision, subduction of the remaining African lithosphere resulted in slab retreat and extension of the overriding southern edge of Eurasia (Jolivet and Faccenna, 2000; Wortel and Spakman, 2000). As a result, the main basins of the western Mediterranean developed as back-arc basins floored by oceanic crust since the Oligocene (e.g., Jolivet and Faccenna, 2000; Jolivet et al., 2006).

On the eastern side of the proto-Mediterranean Sea, rifting and spreading of the Red Sea occurred, leading to the separation of Arabia from Africa (McKenzie et al., 1970; Coleman, 1974; Figure 1.3b). At some point, Arabia collided with Eurasia which resulted in closure of the marine gateway that used to connect the proto-Mediterranean Sea to the Indo-Pacific Ocean: the Indian Gateway. The consensual view is that closure of the Indian Gateway occurred during the Middle Miocene after several short-lived disconnections during the Early Miocene (e.g., Rögl, 1999; Harzhauser et al., 2007), but the precise age is still debated (e.g., Wang et al., 2002; Allen and Armstrong, 2008; Hüsing et al., 2009). By the end of the Middle Miocene the formation of the Carpathians divided the Paratethys into an eastern domain (Euxinic-Caspian basins) and a central domain (Pannonian basin; Figure 1.3c; e.g., Steininger et al., 1988; Rögl, 1996).

Figure 1.3. Schematic palaeogeographic maps of the circum-Mediterranean region modified from Harzhauser and Piller (2007) at different points in time. "C. P." and "E. P." refer to Central and Eastern Paratethys, respectively. "BeC" corresponds to the Betic corridor and "RiC" to the Rifian corridor.

In the Late Miocene, the communication between the Mediterranean Sea and the Atlantic Ocean was established by means of two marine passages, the Betic corridor of southern Spain and the Rifian corridor through the north of Morocco (Santisteban and Taberner, 1983; Benson et al., 1991; Figure 1.3d). Closure of these gateways would terminate the connection between the Mediterranean Sea and the Atlantic Ocean (e.g., Krijgsman et al., 1999a; Martín et al., 2001, 2009) and result in

the deposition of evaporites over the Mediterranean basin during the so-called Messinian Salinity Crisis (Roveri et al., 2014). As to the Paratethys, further differentiation between the Eastern and Central Paratethys took place and episodic connections with the Mediterranean Sea have also been documented (e.g., Clauzon et al., 2005; Krijgsman et al., 2010; Vasiliev et al., 2011).

The Pliocene starts when the Zanclean flooding terminates the Messinian Salinity Crisis (e.g., Cita and Gartner, 1973). Vertical motions in the Mediterranean, the Black Sea and the Caspian Sea shaped their modern geometry and bathymetry, as well as the present-day river systems (e.g., Meulenkamp and Sissingh, 2003; Popov et al., 2006).

1.2. Marine gateways, ocean circulation and climate

The key role that marine gateways played in the Cenozoic evolution of ocean circulation and climate is well exemplified by the Drake Passage. Although estimates of the opening of this marine passage between South America and Antarctica range from the Middle Eocene (Livermore et al., 2007) to the Early Miocene (Barker, 2001), the opening has been related to abrupt changes in ocean circulation and climate (e.g., Kennett, 1977; Nong et al., 2000; Toggweiler and Bjornsson, 2000). Formation of the passage allowed the gradual establishment of the Antarctic Circumpolar Current (ACC; Latimer and Filipelli, 2002), which resulted in thermal isolation of Antarctica (e.g., Kennett, 1977). Model studies have shown that the opening of Drake Passage weakened the Southern Ocean Meridional Overturning Circulation (Mikolajewicz et al., 1993; Sijp and England, 2004; Pfister et al., 2014).

Estimates of the time of closure of the Panama Seaway, which used to separate North and South America, range between the Middle Miocene (Montes et al., 2015) and the Pliocene (Coates et al., 2004). The formation of the Isthmus of Panama is thought to have had an important effect on ocean circulation, climate and the exchange of faunas (e.g., Maier-Reimer et al., 1990; Prange and Schulz, 2004; von der Heydt and Dijkstra, 2005; Schneider and Schmittner, 2006; Leigh et al., 2014). Closure of the Panama Seaway has been argued to have increased the North Atlantic Deep Water (NADW) production (Burton et al, 1997; Haug and Tiedemann., 1998; Schneider and Schmittner, 2006) and enhanced the Atlantic Meridional Overturning

Circulation (e.g., Bartoli et al., 2005; Sepulchre et al., 2014). Although this aspect remains controversial, formation of the isthmus has also been proposed as a factor contributing to northern hemisphere glaciation (Bartoli et al., 2005; Lunt et al., 2008).

Regarding the Mediterranean region, arguably the most prominent example of changing gateways is the closure of the Indian Gateway. Early to Middle Miocene closure of the Indian Gateway has been suggested to have terminated the so-called Tethys Circumequatorial Current (von der Heydt and Dijkstra, 2005): a westward current that was possible due to the existing continental geometry before the Indian Gateway closed (Berggren and Hollister, 1977; Bush, 1997). Although currently under debate (e.g., Butzin et al., 2011; Hamon et al., 2013), for decades closure of this gateway has been related to the development of the East Antartic Ice Sheet (e.g., Woodruff and Savin, 1989; Flower and Kennett, 1994). On the regional scale, closure of the Indian Gateway increased the sensitivity of the Paratethys and Mediterranean Sea water properties to climate and favoured the transition towards the present-day Mediterranean circulation (Karami et al., 2009, 2011).

The Late Miocene tectonic restriction of the marine connections between the Mediterranean and the Atlantic, together with glacioeustatic sea level fluctuation, caused the deposition of a thick and complex sequence of evaporites throughout the Mediterranean during the Messinian Salinity Crisis (see Roveri et al., 2014 for a recent review). During the climax of the crisis (5.61–5.55 Ma; Krijgsman et al., 1999a; Manzi et al., 2013), the Mediterranean sea level presumably dropped by 1200 - 1500 m. This triggered halite deposition as well as the formation of the so-called Messinian Erosional Surface (MES) and river incisions over the Mediterranean shelves (Ryan, 1978; Ryan and Cita, 1978). The sea level drop also affected the communication between the Mediterranean and the Paratethys. Mediterranean inflow into this realm disappeared and the sea level in the Paratethys sub-basins was more prone to fluctuate (e.g., Gillet et al., 2007). Although some authors speculate that in the Black Sea and the Caspian Sea a lowering of the order of 1000 m may have occurred in response to the Messinian Salinity Crisis (e.g., Hsü and Giovanoli, 1979; Abdullayev et al., 2012), the amplitude and timing of these lowstands are still controversial (Krijgsman et al., 2010; Grothe et al., 2014; Tari et al., 2015; van Baak et al., in press, 2015).

1.3. The model approach

Over the last decades significant improvements in computational power have allowed the development of sophisticated models capable of simulating physical processes in the ocean with high accuracy. One of the strengths of numerical modelling is that it allows us to test hypotheses and understand the behaviour of the system under study. In reconstructing palaeoenvironments, when a present-day analog of the system does not exist, modelling represents an essential tool to gain insight into the functioning of the system. In this case, the comparison of the model results to geological evidence allows us to determine the processes and conditions responsible for the observations.

In Chapters 2 and 3 I use ocean general circulation models (OGCMs). These models are based on the primitive equations, which describe the large-scale ocean circulation. General circulation models provide a detailed, three-dimensional output. Diagnostic variables are temperature, salinity, water surface elevation and the components of velocity. Output is conveniently processed to study the target variable (e.g., overturning streamfunction, basin averaged temperature, basin averaged salinity). From a computational perspective, these models are expensive to run and therefore cannot be integrated over long time scales. OGCMs are applied when the research question to tackle involves spatial variation of the basin dynamics. Results obtained correspond to the equilibrium state of the system. This snapshot approach is justified given that palaeogeographic changes are much slower than changes in ocean circulation. The input required to run the OGCMs includes: (i) a bathymetry; (ii) atmospheric forcing; (iii) lateral boundary conditions to simulate the exchange with the adjacent ocean(s); and (iv) initial conditions for the basin (i.e., temperature and salinity). More specifically I use sbPOM (Jordi and Wang, 2012), which is the parallel version of the Princeton Ocean Model (POM; Blumberg and Mellor, 1987). POM is a three-dimensional, sigma-coordinate, free-surface, hydrostatic ocean model. POM was applied to the dynamics of the Mediterranean Sea for the first time by Zavatarelli and Mellor (1995) and has been extensively used for this basin since then (e.g., Drakopoulos and Laskaratos, 1999; Alhammoud et al., 2010). SbPOM was applied to the Mediterranean Sea for the first time by Topper and Meijer (2015).

In Chapter 4 I perform budget calculations to investigate sea level variations in response to changes in hydrologic fluxes (i.e., evaporation, precipitation and river

discharge). The essential element of this analysis is a reconstructed hypsometry of the basin under investigation.

1.4. Thesis outline

The chapters of this thesis are arranged in chronological order of the period under investigation. **Chapter 2** focuses on the effect of the Early to Middle Miocene shoaling and closure of the Indian Gateway on the exchange patterns with the adjacent oceans, as well as on Mediterranean circulation and water properties. For this I use sbPOM and a series of bathymetries constructed from an early Burdigalian (20.5-19 Ma) palaeogeography from which I solely modify the depth of the Indian Gateway. To simulate a progressive closure, the Indian Gateway is set to 1000, 450, 200 and 0 m. In view of the lack of a unique Early Miocene climate data set, I start with idealised atmospheric conditions based on the present and then examine the sensitivity of the system to different climates. The effect of a westward net flow through the gateways on the patterns of exchange is investigated for the first time with a regional-scale model. Results show the complex reorganisation of flows that the gradual closure of the Indian Gateway entails, especially when this gateway is shallow. Comparing our results to observational evidence I propose patterns of exchange consistent with data for different stages of closure, as well as the conditions required for those patterns to occur.

In **Chapter 3** I examine the functioning of the double gateway formed by the Betic and Rifian corridors that existed at the time just preceding the Messinian Salinity Crisis. Understanding the exchange patterns through these gateways is essential to be able to interpret geological evidence and reconstruct the events leading up to the salinity crisis. To this end I use sbPOM and a reference bathymetry based on a late Tortonian (8-7 Ma) palaeogeography. From this bathymetry, multiple gateway geometries are created by changing the depths of the gateways only. Because the Late Miocene climate is uncertain, various idealised atmospheric forcings are considered. In all cases, regardless of the atmospheric conditions assumed, results show that only two exchange patterns are possible in the gateways and that these patterns are a function of the depth of one corridor with respect to that of the other. The insight derived from our model is essential to understand whether geological evidence from

a corridor indicates one- or two-layer flow, reconstruct the relative depths of the gateways, and determine the age of gateway closure.

During the Late Miocene, at the same time as the Messinian Salinity Crisis in the Mediterranean Sea, the Paratethys sea level may have been subject to a lowering. However, estimates of the sea level fall range from a few meters to more than 1500 m. In **Chapter 4,** I therefore assess the sensitivity of the level of the Late Miocene Black Sea and Caspian Sea to hydrologic fluxes when no connection to the Mediterranean exists. Using budget calculations I quantify the amplitude of the sea level drop, the resulting salinity, and the time to reach equilibrium for a wide range of negative hydrologic budgets (i.e., evaporation exceeds precipitation and river discharge). Comparing the model results to hydrologic budgets derived from a recent global climate simulation and to salinity estimates based on geological evidence I find that a sea level drop as large as 1000 m is unlikely to have occurred in the Caspian Sea. For the Black Sea, the possibility of a drop in sea level of the order of 1000 m would appear unlikely but cannot be fully discarded.

Chapter 2: Response of Mediterranean circulation to Miocene shoaling and closure of the Indian Gateway; A model study

ABSTRACT

In this regional ocean model study we explore the effect of the Early to Middle Miocene shoaling and closure of the Indian Gateway on Mediterranean circulation and its exchange with the adjacent oceans. For this we use the regional ocean circulation model "sbPOM" and a collection of bathymetries created from an early Burdigalian palaeogeographical base map in which the depth of the Indian Gateway is set to 1000, 450, 200, or 0 m. A significant improvement of this work relative to previous regional modelling studies is that we also consider the possibility that the Indian and Atlantic gateways accommodated net westward flow—as reported in many global climate model studies. To this end we superimpose net westward flows of different magnitudes to the gateways. Because the Early-Middle Miocene climate is uncertain, we start with atmospheric conditions based on the present and subsequently explore alternative atmospheric forcings. Similarly, we first assume a relatively shallow Atlantic Gateway of 500 m depth and then study the effect of a connection of 900 m. The extensive set of experiments performed allows us to gain detailed physics-based insight into the role of the different factors mentioned above and provides a solid background to interpret observational evidence. By comparing our modelled exchange patterns to data we are able to propose the flow configurations consistent with observations—some of them not considered until now—during the different stages of closure and infer the conditions (climate, presence/absence of net flow, Atlantic Gateway depth) under which these patterns arise.

2.1. Introduction

The configuration of the proto-Mediterranean Sea during the Early Miocene was very different from that at present. To the north, the Mediterranean was connected to the Paratethys: a large intracontinental sea that started to isolate from the Tethys Ocean during the Eocene-Oligocene due to the formation of the Alpine chain (see Figure 2.1; Báldi et al., 1980). In addition to being connected to the Atlantic Ocean, the Mediterranean Sea was also open to the Indian Ocean through what we will refer to as the Indian Gateway. The exchange through this gateway terminated when the Arabian plate collided with the Eurasian plate. The age of closure of the Indian Gateway has been estimated using various criteria: examination of the deformation of the Arabian and Eurasian margins (Allen and Armstrong, 2008), analysis of stable isotopes (e.g., Woodruff and Savin, 1989; Ramsay et al., 1998), study of the Mediterranean-Indian Ocean faunal affinities (e.g., Harzhauser et al., 2009) and investigation of the sedimentary record (e.g., Wang et al., 2002; Hüsing et al., 2009) among others. Although the age estimates differ depending on the approach used, the most commonly accepted scenario is that final closure of this gateway occurred around the Middle Miocene after several short-lived disconnections during the Early Miocene (Rögl, 1999; Harzhauser et al., 2007).

In general, marine gateways control interbasinal exchange, as well as the water properties of the two connected basins. There are many examples that illustrate the key role of the evolving gateways on the regional and global-scale oceanic and, indirectly, atmospheric circulation in the geological past (e.g., Cane and Molnar, 2001; Zhang et al., 2014). For instance, the deepening of the Tasman Seaway during the Late Eocene has been related to a global deep ocean cooling (Sijp et al., 2011). The shoaling and closure of the Panama Seaway is suggested to have enhanced the Atlantic Meridional Overturning Circulation (AMOC; e.g., Sepulchre et al., 2014 and references therein). It has also been proposed to have contributed to ice-sheet expansion—although this aspect is now disputed (e.g., Haug and Tiedemann, 1998; Bartoli et al., 2005; Lunt et al., 2008). Extant gateways are exemplified by the modern Strait of Gibraltar which accommodates a dense Mediterranean outflow into the Atlantic, which is considered an important factor in the Atlantic Meridional Overturning Circulation (Hernández-Molina et al., 2014).

Also the closure of the Indian Gateway triggered important changes. Many modelling studies report that, with a deep and wide connection to the Indian Ocean this gateway, as well as the Atlantic Gateway, accommodated a net westward flow (Butzin et al., 2011; Krapp and Jungclaus, 2011; Herold et al., 2012). This westward flow is often considered the result of a west-directed circum-equatorial current, the so-called Tethys Circumglobal Current, which has been found not only in modelling studies (Bush, 1997; Omta and Dijkstra, 2003; von der Heydt and Dijkstra, 2006), but also inferred from biogeographic evidence (Hallam, 1969; Stanley, 1995). Some authors argue that the closure of the Indian Gateway, together with widening of Drake Passage, led to a reversal of this global current (Omta and Dijkstra, 2003; von der Heydt and Dijkstra, 2005). Furthermore, the closing of the Indian Gateway is thought to have triggered warming of the northern Indian Ocean at shallow levels and cooling at depth (Butzin et al., 2011). Although controversial (Butzin et al., 2011; Hamon et al., 2013), closure has been suggested to have caused a decrease in the heat transport to high southern latitudes that cooled the Antarctic surface waters and induced the formation of the East Antarctic Ice Sheet during the Middle Miocene (Woodruff and Savin, 1989). On the regional scale, faunal and stable isotope studies indicate changes in water properties in both the Mediterranean and Paratethys throughout the time interval accepted for closure (e.g., Bicchi et al., 2003; Bosellini and Perrin, 2008; Kocsis et al., 2008, 2012). However, proxy data are limited in spatial and temporal coverage and do not provide an unambiguous story of the evolution of the Mediterranean exchange with the Atlantic and Indian oceans and its effects. This is exacerbated by the fact that other factors such as climate change and the conditions of the Atlantic Gateway have played an as yet unknown role.

The purpose of this paper is to try and achieve a more complete understanding of the response to closure through the use of a regional-scale ocean circulation model. The model permits us to formulate hypotheses, rooted in physics, as to which changes will result from shoaling and closure and provides a solid framework that we use to interpret existing data. Comparison between data and model results allows us (i) to determine which of the modelled exchange patterns is consistent with observations and (ii) to specify the conditions required for these patterns to develop. In our analysis we will focus on the circulation of the Mediterranean basin and the exchange at the Atlantic and Indian gateways but also address the changes in basin temperature and salinity. Specific attention will be paid to the role of a net westward flow. We use the

Figure 2.1. Reference bathymetry based on the early Burdigalian palaeogeographic map of the Peri-Tethys Atlas (Dercourt et al., 2000).

model "sbPOM" (Jordi and Wang, 2012) in combination with a set of idealised bathymetries constructed from the Peri-Tethys Atlas (Dercourt et al., 2000). The uncertainty as to atmospheric forcing is handled by considering different atmospheric conditions and we also examine the role of the Atlantic Gateway depth.

The first-order response of the Mediterranean Sea and Paratethys to closure of the Indian Gateway has been extensively studied with box models (Karami et al., 2009, 2011). Furthermore, in Karami (2011), a regional ocean circulation model was used for the first time in this context. The most relevant improvements of this study compared to Karami (2011) are the use of a more realistic bathymetry, a greater vertical resolution, and the simulation of net westward flow through the gateways.

2.2. Model description

2.2.1. Ocean circulation model

SbPOM, which is the parallel version of the Princeton Ocean Model (POM; Blumberg and Mellor, 1987), only differs from the 2008 version of POM in the parallelisation. SbPOM is a three-dimensional ocean model based on the primitive equations that uses sigma-grid coordinates. The latter guarantees the same amount of vertical levels (in our case 40) regardless of the water depth. This increases the vertical resolution in shallow areas and allows us to study in detail the flows during the last stages of the process of closure. The horizontal grid is rectangular and has a uniform resolution of ¼ by ¼ degree. POM has been extensively applied to investigate the circulation of the Mediterranean Sea (e.g., Zavatarelli and Mellor, 1995; Drakopoulos and Laskaratos, 1999; Alhammoud et al., 2010). Lately sbPOM was used for the first time to investigate the sensitivity of the Mediterranean basin to changes in the depth of the Strait of Gibraltar (Topper and Meijer, 2015). For a given basin/gateway configuration the model is run into equilibrium, which is generally achieved after 800-1000 model years. Results shown here represent the average over the last 100 years of each experiment (during all of which steady state prevails). This approach is justified because palaeogeographic changes are slower than the establishment of the new circulation pattern.

2.2.2. Set of bathymetries

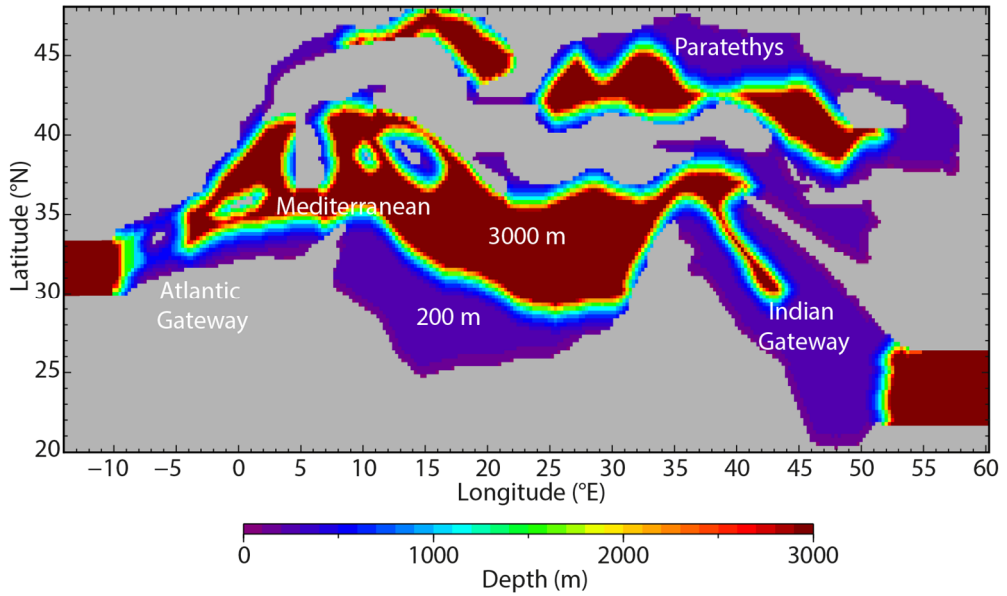Our reference bathymetry is based on the early Burdigalian palaeogeographic map of the Peri-Tethys Atlas (Dercourt et al., 2000). The past position of the basin in an absolute sense was brought up-to-date using rotation poles for Africa and Eurasia from Müller et al. (2008). The atlas distinguishes between deep and shallow domains which we set to 200 and 3000 m, respectively (see Figure 2.1). To avoid computational instabilities and artefacts related to large topographic variability, we introduce a continental slope between the deep and shallow domains. To simulate the process of closure a set of alternative geometries is created by changing solely the depth of the Indian Gateway. This allows us to isolate the effect of the Indian Gateway in our results. The southern portion of the Indian Gateway is set to 1000, 450, and 200
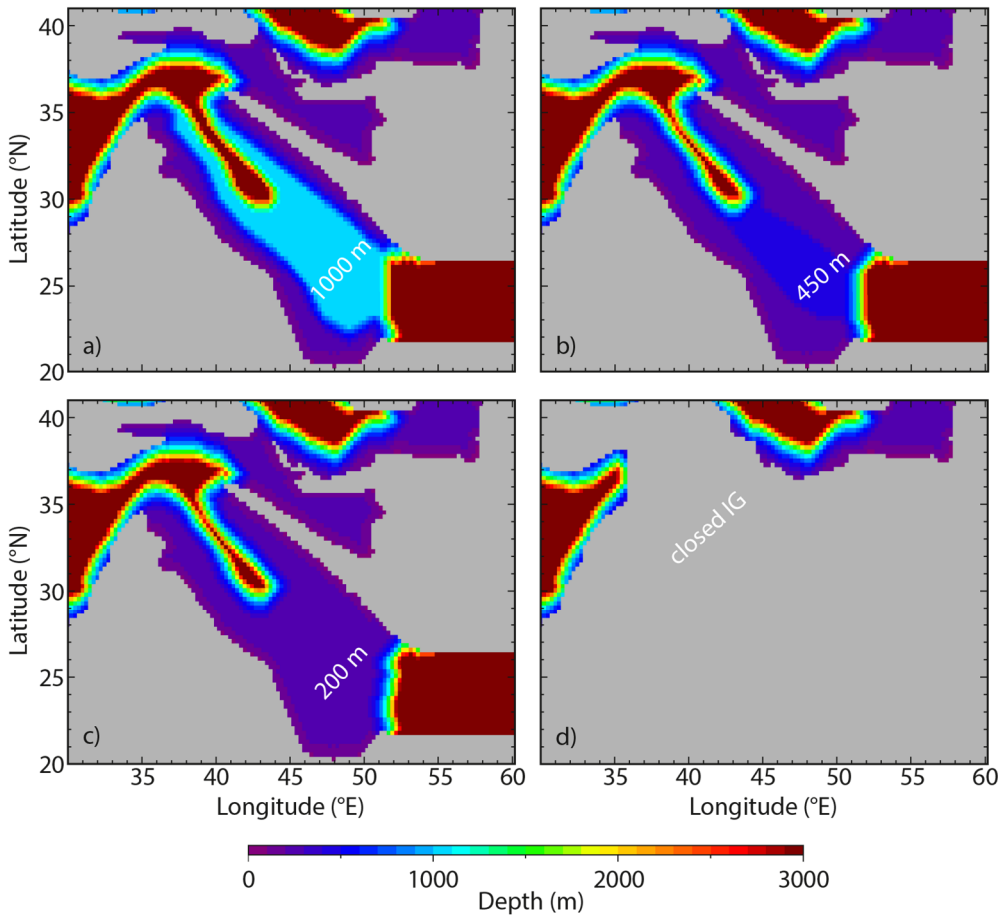
Figure 2.2. Alternative geometries of the Indian Gateway which allow us to examine the process of closure. The Indian Gateway depth is set to 1000, 450, 200 m in panels (a-c), respectively. The gateway is closed in panel (d).

m depth or is considered closed (Figure 2.2). Both Mediterranean-Paratethys connections are defined as shallow areas in the atlas and are hence assigned a maximum depth of 200 m (see Figure 2.1). Although the Paratethys is thus included in our model to capture, to first approximation, the effect it has on the Mediterranean, in our analysis below we will focus on the Mediterranean circulation and exchange at the ocean gateways. The Atlantic Gateway depth is set at 500 m—a value deeper than

the present-day Strait of Gibraltar (300 m) but not as deep as the deepest basin. Due to the complex tectonic history, the past water depth in the Atlantic-Mediterranean transition zone is essentially unknown. In a set of additional experiments we will increase the Atlantic Gateway depth to 900 m to explore its role. The Atlantic and Indian gateways have a width of 417 and 1056 km, respectively.

2.2.3. Atmospheric forcing

Because there is no consensus as to the climate of the Early to Middle Miocene and global climate model simulations do not converge towards a single climatic data set, we start from boundary conditions based on the present day. Subsequently, we test the sensitivity of the results to alternative atmospheric forcings. This approach allows us to understand the role of climate and to incrementally build knowledge about the functioning of the system. We use idealised atmospheric forcing constant in time, which has been shown to conveniently reproduce the main features of the Mediterranean circulation (Meijer and Dijkstra, 2009; Topper and Meijer, 2015). In the reference setup (i.e., based on the present day) the heat exchange between the atmosphere and the basin is achieved by relaxation of the upper water layer to the present-day zonally averaged annual mean sea-surface temperature. For the latter we use the reconstruction based on satellite data proposed by Steppuhn et al. (2006) shown in Figure 2.3a. As in Topper and Meijer (2015) the relaxation time scale is set to one day. The freshwater flux (evaporation minus precipitation and river runoff) is set to a uniform and constant value of 0.5 m/yr all over the entire model domain. This value, which is within the range of present-day values for the Mediterranean Sea (Mariotti et al., 2002), has also been found to be adequate for the Late Miocene (e.g., Gladstone et al., 2007).

The alternative atmospheric forcings only differ from the reference setup in that we either modify the atmospheric temperature prescribed or the freshwater flux. Specifically, we consider a Middle Miocene sea-surface temperature profile constructed on the basis of proxy data by You et al. (2009; see Figure 2.3c). Although at lower latitudes temperatures are similar to those at present, values are significantly higher at northern latitudes. This thus permits us to investigate the effect of a reduced north-south sea-surface temperature gradient. Because the Paratethys was probably less evaporative than the Mediterranean due to the large river discharge over this area
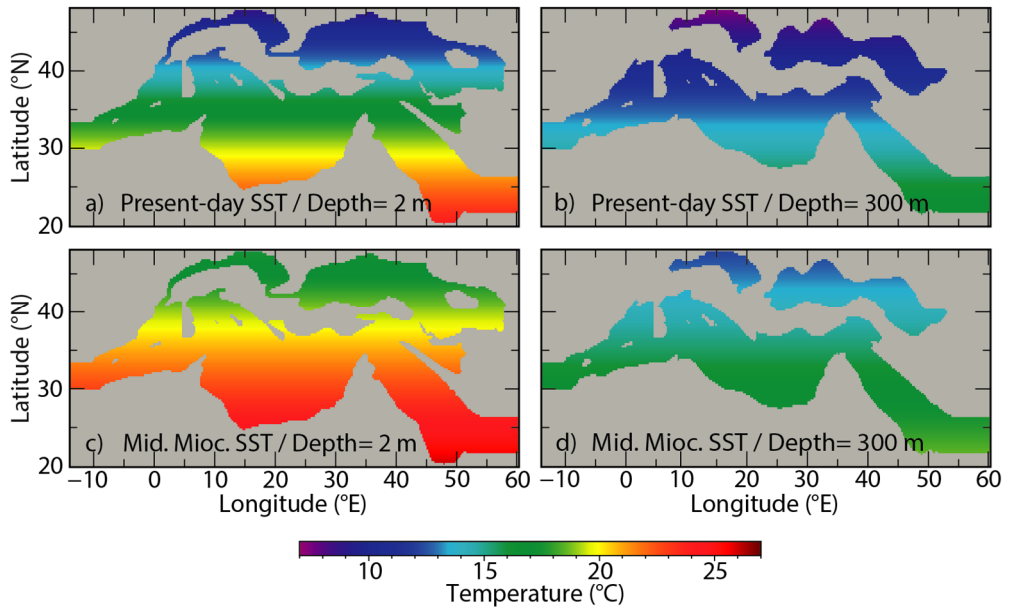
Figure 2.3. Initial temperature at the surface (2 m; panels (a) and (c)) and at depth (300 m; panels (b) and (d)). In panels (a) and (b) the initial fields derive from the present-day zonally averaged annual mean sea-surface temperature reconstructed by Steppuhn et al (2006) from satellite data. In panels (c) and (d) the initial temperature derives from one of the Middle Miocene zonally averaged annual mean sea-surface temperature profiles proposed by You et al. (2009) based on proxy data.

(e.g., Pippèrr and Reichenbacher, 2010), in another set of experiments, we set the freshwater flux over this realm to 0 m/yr. Both atmospheric forcings entail a greater change in the water properties over the Paratethys compared to the Mediterranean. These experiments will thus shed light on the effect of the Paratethys on Mediterranean circulation.

We do not prescribe winds because (i) the Early Miocene wind pattern is uncertain and (ii) earlier sensitivity model studies demonstrate that winds mainly intensify the circulation at shallow depths and are not essential to reproduce the first-order features of the basin-scale circulation (e.g., Meijer and Dijkstra, 2009). In a general sense, the horizontal oceanic circulation is determined, to some extent, by the

geometry of the existing gateways and winds (Krapp and Jungclaus, 2011). By imposing a westward flow our model can be considered to partly account for winds.

2.2.4. Open-ocean boundaries and initial conditions

On the western and eastern limits of the model domain we implement open ocean boundaries representing the communication with the Atlantic and Indian oceans. We impose a Sommerfield radiation condition to the baroclinic (depth-dependent) mode of the boundary-normal velocity and set the velocity component parallel to the boundaries to zero. To ensure water volume conservation, the barotropic (depth-averaged) component of the velocity normal to the boundaries compensates for the net evaporative loss over the basin. To be precise, each of the boundaries compensates for exactly half of the total water volume lost by evaporation in the basin. This flux is distributed homogeneously over the open boundary. When a net westward flow is prescribed, the boundary condition on the barotropic mode of the open boundary is adjusted according to the water flux specified (1, 3, or 5 Sv). In each experiment net flows of the same magnitudes are prescribed on the Atlantic and Indian open-ocean boundaries.

In line with our general approach, we wish to keep the required prescribed values for temperature and salinity at the open boundaries and in the adjacent "ocean boxes" as simple as possible. Following Karami et al. (2009) we take the Atlantic Ocean to be saltier than the Indian Ocean. Salinities are set to constant and uniform values of 35 and 36 psu in the Indian and Atlantic oceans, respectively (while we are aware that psu is not a formal unit we use it to be consistent with the formulation in sbPOM). Because a match to the imposed surface forcing needs to be ensured and sharp temperature contrasts between the open boundaries and the Mediterranean waters next to them are not desirable, temperature cannot be defined as a uniform value. Instead, temperature is made to decrease exponentially with depth from the latitude-dependent sea-surface temperature. The exponential function is a best fit of present-day potential temperature from the Levitus Atlas (Locarnini et al., 2013). This approach automatically adjusts the vertical temperature profile near the open boundaries when the prescribed atmospheric temperature changes (see Figures 2.3b, 2.3d). Our setup results in an Atlantic Ocean that is denser than the Indian Ocean, the implications of which have been extensively discussed in Karami et al. (2009).

Within the basin, initial salinity varies smoothly between the values of the oceans at both ends of the model domain. Initial temperature decreases exponentially with depth from the sea-surface temperature (Figures 2.3b, 2.3d). As in Topper and Meijer (2015), to ensure a smooth transition towards the open boundaries, water properties are gradually restored to the initial values over the part of the model grid just inward of the boundaries (extending over 18 grid cells in the east-west direction).

2.3. Results and analysis

In our analysis we will focus on the Mediterranean zonal overturning streamfunction (calculated excluding the velocity field of the Paratethys), which conveniently captures the main features of the basin-scale circulation. The zonal overturning streamfunction corresponds to all water transport projected on a vertical, east-west section through the basin. In Figures 2.4, 2.5, and 2.6 the sense of overturning is defined as viewed from the south. Negative cells (shown in blue) indicate anticlockwise circulation and a positive sign (yellow to red) points to clockwise motion.

2.3.1. Reference experiments

Experiments performed with the reference atmospheric forcing are presented in Figure 2.4. First, we assume that there is no net flow in the gateways and then we superimpose net flows of different magnitudes.

Effect of shoaling and closure of the Indian Gateway without a net flow

As observed in Figure 2.4a, with a deep Indian Gateway (1000 m), the Mediterranean is dominated by a strong, anticlockwise cell that occupies the whole basin. The streamlines indicate that the Indian Gateway accommodates inflow from the surface until an intermediate depth and that outflow occurs below the inflow (i.e., exchange is antiestuarine). In the westernmost Mediterranean, part of the Indian waters coming from the east flow out of the basin while below about the mid-depth of the Atlantic Gateway water flows in from the ocean (i.e., exchange is estuarine). The streamlines also show that exchange is largest on the Indian side.

When the Indian Gateway has an intermediate depth of 450 m (Figure 2.4e) an anticlockwise cell still occupies the basin but it does not extend into the Atlantic Gateway. There, a small clockwise cell associated with the Atlantic Ocean has now developed. Even though the exchange with the Atlantic is still very limited, a transition towards antiestuarine exchange has started. The weaker magnitude of the anticlockwise (Indian-related) cell indicates that the Mediterranean-Indian exchange is not as large as with a deep Indian Gateway. Note that even though the two gateways have similar depths, the greater width of the Indian Gateway causes water transport through this gateway to be largest.

With a shallow Indian Gateway of 200 m (Figure 2.4i) the circulation pattern is substantially different in that large clockwise and anticlockwise motion cells appear. The clockwise cell, which shows well-developed antiestuarine exchange with the Atlantic, extends from the surface until 800-1000 m depth all over the basin. The anticlockwise cell, which is much weaker than with an intermediate-depth Indian Gateway, extends over the Indian Gateway and sits below the upper cell. This deep cell is mainly fed by deep water formation and is enhanced by Indian inflow. Studying in detail several cross-sections of temperature and salinity over the basin we determined that deep water forms in the northernmost Mediterranean Sea. At locations where deep water is formed, temperatures are low due to the interaction with the atmosphere at high latitudes and salinities are high.

Finally, when the Indian Gateway is closed (Figure 2.4m), the Mediterranean general circulation resembles that with a shallow Indian Gateway but it becomes even more similar to the present-day Mediterranean. The deep cell is only related to deep water formation because the complete closure of the Indian Gateway blocks the exchange with the Indian Ocean.

To summarise, when atmospheric values based on the present are used and no net flow is prescribed in the gateways, the shoaling and closure of the Indian Gateway imply a progressive transition from a circulation pattern dominated by the Indian Ocean towards a pattern that resembles the present-day Mediterranean circulation. This shift involves an increase of the importance of the Atlantic Ocean relative to the Indian Ocean on the Mediterranean circulation and a change of the exchange type between the Mediterranean and the Atlantic (i.e., from estuarine to antiestuarine). In this respect, antiestuarine exchange occurs when, at levels above the
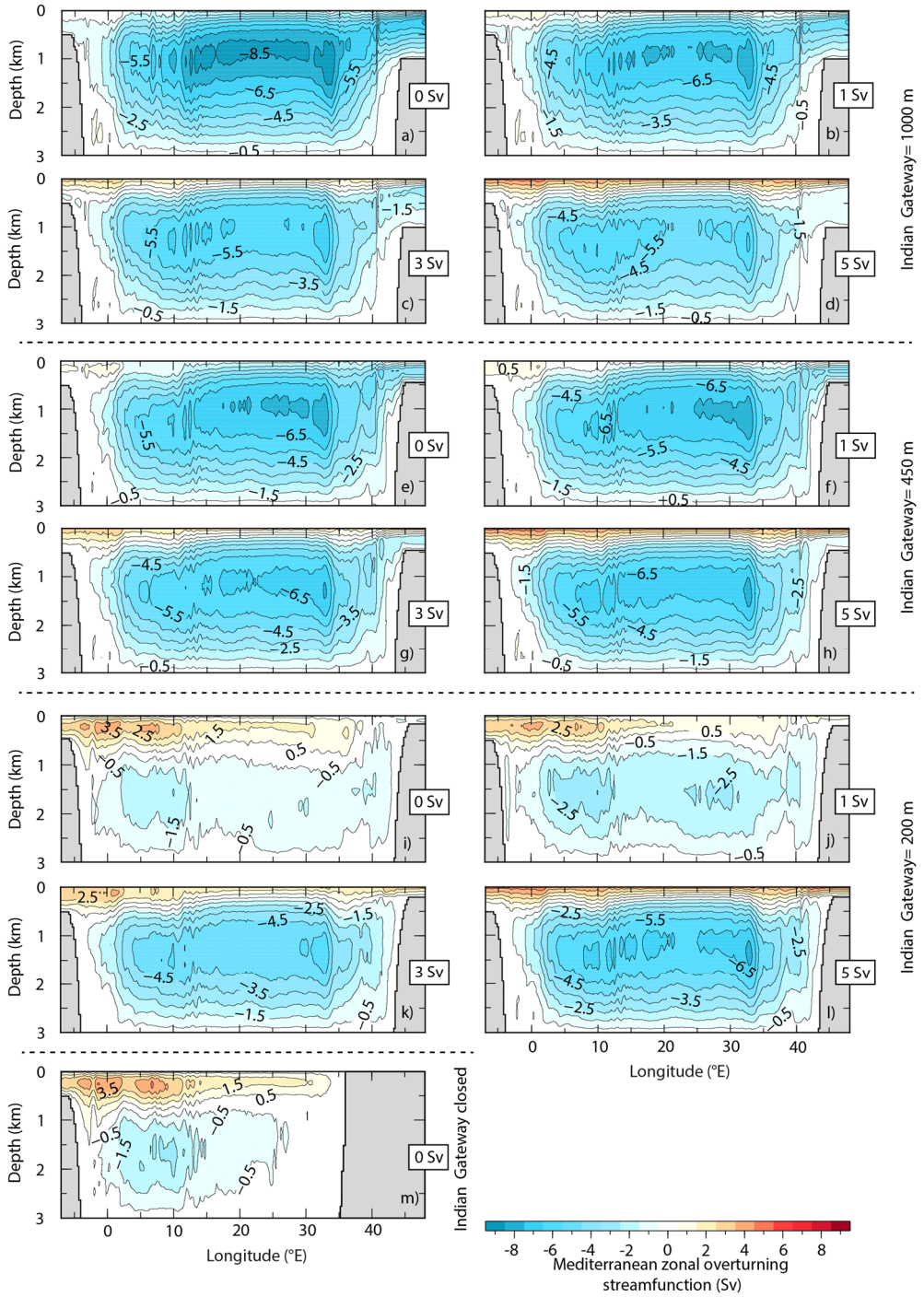
Figure 2.4. (Previous page) Mediterranean zonal overturning streamfunction for several Indian Gateway depths and different amounts of net westward flow. The Indian Gateway is set to 1000 m (a-d), 450 m (e-h), 200 m (i-l), and it is closed in (m). As indicated in the figure, in the first panel of each block of four no net flow is imposed and, in the following ones, 1, 3 and 5 Sv are prescribed, respectively. In this set of experiments reference atmospheric forcing based on the present day is used. The contour interval is 1 Sv.

sill, the Mediterranean density is larger than the density of the adjacent ocean. We observe that estuarine exchange arises when oceanic density exceeds the Mediterranean density, at least, in the lower portion of the water column above the sill (more details about the development of estuarine exchange will be given in Section 2.3.2). The reversal of the exchange type with the Atlantic thus results from the increase of the Mediterranean density as the basin becomes more enclosed. Although in Karami (2011) a much more idealised bathymetry is used and different atmospheric conditions are assumed, these authors also find that, without a net flow, a shoaling of the connections to the Atlantic and Indian oceans results in a reversal of the exchange type with the Atlantic.

Effect of the addition of a net flow

The net flow, which is imposed uniformly at both open ocean boundaries, is found to be accommodated mainly at the surface. This is expressed by the disappearance of closed overturning contours at shallow levels (Figures 2.4b-2.4d, 2.4f-2.4h, 2.4j-2.4l). Whereas with a small net flow the Mediterranean general circulation does not change substantially, when a large net flow is prescribed (i.e., 5 Sv), the Indian inflow is able to reach the Atlantic Ocean at shallow depths, even with a shallow Indian Gateway. This can be seen in Figures 2.4d, 2.4h and 2.4l, where streamlines extend at the surface from east to west all over the basin.

When the Indian Gateway is deep, or has an intermediate depth, the exchange with the Indian Ocean remains antiestuarine regardless of the magnitude of the net flow prescribed (Figures 2.4b-2.4d and 2.4f-2.4h). This is explained by the fact that Mediterranean densities are greater than those of the Indian Ocean (the latter being relatively warm and less salty than the Mediterranean). However, if the Indian

Gateway is shallow, the addition of a net flow substantially reduces the outflow and the Indian Gateway features mainly inflow due to the lack of space to accommodate the flows (Figures 2.4j, 2.4k, 2.4l). With a deep Indian Gateway, the exchange with the Atlantic Ocean remains estuarine even if large net flows are prescribed (Figures 2.4b to 2.4d). However, with an intermediate-depth or shallow Indian Gateway, when net flows larger than 1 Sv are added, the Atlantic Gateway accommodates mainly Mediterranean outflow over its entire depth range (Figures 2.4g, 2.4h, 2.4k, 2.4l).

   In our simulations we always find a large anticlockwise cell that extends until the bottom of the basin (Figure 2.4). Without net flow the magnitude of this cell is not the same with a deep or a shallow Indian Gateway and the cell responds differently to the progressive addition of a net flow. Whereas larger net flows weaken this cell when the Indian Gateway is deep, the cell strengthens if the gateway is shallow (Figures 2.4a to 2.4d and 2.4i to 2.4l). It appears that several mechanisms are at play. On the one hand, westward inflow imposed on the eastern boundary reduces the Mediterranean outflow through the Indian Gateway, which decreases the magnitude of the deep cell. On the other hand, part of the Indian inflow coming from the eastern Mediterranean is not able to reach the Atlantic Ocean due to the shallow nature of the Atlantic Gateway and recirculates over the basin strengthening the deep cell. While with a deep Indian Gateway the first mechanism prevails, when this gateway is shallow the second becomes more important.

   To sum up, the prescription of a net flow has a greater impact on the exchange with the adjacent oceans when the Indian Gateway is relatively shallow. In this case, although without a net flow the exchange with the Atlantic Ocean tends to be antiestuarine, the addition of throughflow results in mostly outflow all over the Atlantic Gateway. On the Indian side, when this gateway is shallow, the addition of a net flow terminates the antiestuarine exchange, which is replaced by mostly Indian inflow over the Indian Gateway. The deep anticlockwise cell responds differently to the prescription of an increasing net flow depending on the Indian Gateway depth. The implication is that the magnitude of the deep cell with a shallow and a deep Indian Gateway is comparable when a large net flow is prescribed (i.e., 5 Sv; Figures 2.4d and 2.4l).

2.3.2. Additional experiments

In the following sections the sensitivity of the basin to changes in the atmospheric forcing and Atlantic Gateway depth is examined.

Sensitivity to atmospheric forcing

In Figures 2.5a and 2.5b we assume no net evaporation over the Paratethys and, in Figures 2.5c and 2.5d, we use the Middle Miocene sea-surface temperature profile (see Figure 2.3). Whereas in 2.5a and 2.5c we do not prescribe net flows, in 2.5b and 2.5d intermediate-magnitude net flows of 3 Sv are added. In the reference experiments we find that the pattern of exchange with the adjacent oceans is more sensitive to the boundary conditions applied when the Indian Gateway is shallow (i.e., 200 m). For this reason the shallow Indian Gateway geometry is considered in this section.

Figures 2.5a and 2.5c show that, when no net flow is prescribed, the use of neither of the two alternative atmospheric forcings changes the overall circulation pattern compared to the equivalent experiment with reference atmospheric forcing (Figure 2.4i). However, the new atmospheric conditions substantially reduce the strength of the Mediterranean zonal overturning. Both the use of a flatter north-south temperature profile and the decrease of the net evaporation over the Paratethys lead to a reduced meridional density gradient. Assuming thermal-wind balance, a weaker meridional gradient in density corresponds to a decrease of the vertical gradient of zonal (east-west) velocity, which is consistent with a less strong zonal overturning (see Karami, 2011).When throughflow is added (Figures 2.5b and 2.5d) the basin accommodates the flows as in the corresponding experiment with reference atmospheric forcing (Figure 2.4k): at shallow levels the Indian inflow extends from east to west all over the basin, the Indian Gateway does not accommodate two-layer flow anymore and the deep cell becomes stronger compared to the cases without a net flow. Again, the flatter meridional density gradient corresponds to a weaker Mediterranean zonal overturning. Different from the reference case, the Indian-derived water now enters the Atlantic Gateway over a reduced depth range. When the Middle Miocene sea-surface temperature is used this shoaling is more pronounced and Atlantic inflow develops at depth in the gateway (i.e., estuarine exchange; Figure
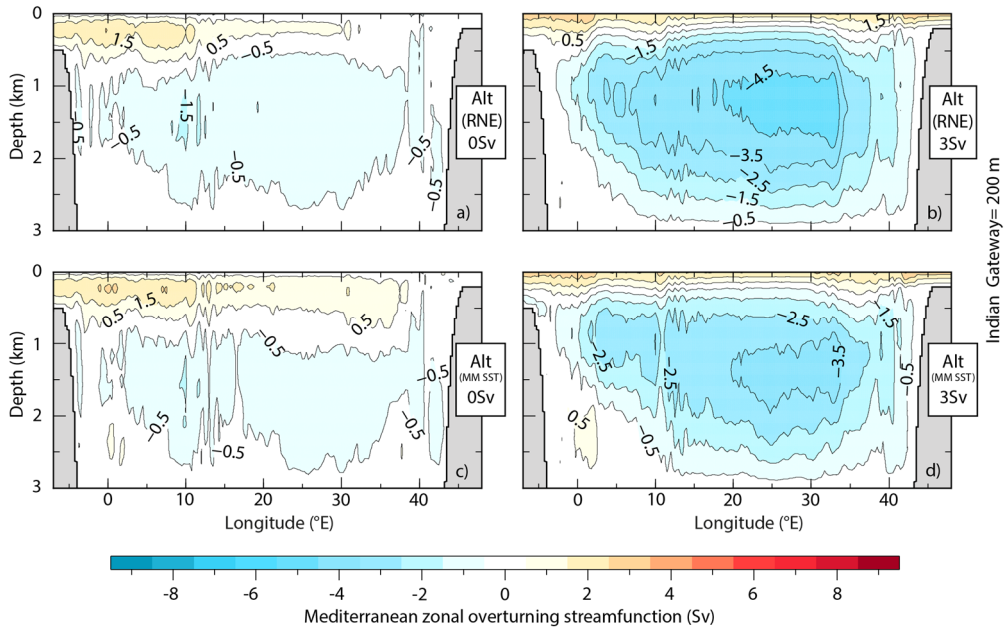
Figure 2.5. Mediterranean zonal overturning streamfunction for a shallow Indian Gateway when alternative atmospheric forcings (Alt.) are considered. In panels (a) and (b) the net evaporation is reduced over the Paratethys (RNE) and in panels (c) and (d) the Middle Miocene sea-surface temperature is prescribed (MM SST). In panels (a) and (c) the gateways do not accommodate net flow and, in (b) and (d), 3 Sv are imposed. The contour interval is 1 Sv.

2.5d). Our analysis strongly suggests that the occurrence of Atlantic inflow at depth in the gateway depends on the Mediterranean-Atlantic pressure gradient. Although this is mainly determined by the density gradient, an effect of sea-surface elevation is expected also. In our experiments Mediterranean water is denser than Atlantic water from the surface until a certain level below which the pattern reverses because Atlantic temperature decreases more strongly with depth. In this case, when net flow is prescribed in combination with the use of alternative atmospheric forcing, the Mediterranean densities are lower causing the deep inflow to start at shallower levels. As to the exchange type with the Indian Ocean, this remains the same as in the equivalent experiments with a shallow Indian Gateway (Figures 2.4i and 2.4k).

Sensitivity to Atlantic Gateway depth

Here we increase the depth of the Atlantic Gateway to 900 m in order to study its influence on the Mediterranean circulation. In panels 2.6a and 2.6b the Indian Gateway is deep (i.e., 1000 m) and, in 2.6c and 2.6d, it is shallow (i.e., 200 m). While in 2.6a and 2.6c we assume no net flow, in 2.6b and 2.6d intermediate-magnitude net flows of 3 Sv are again prescribed in the Atlantic and Indian gateways. In these four experiments reference atmospheric forcing is used. In the final panels (2.6e and 2.6f) the Indian Gateway is closed. In 2.6e reference atmospheric conditions are used and in 2.6f the Middle Miocene sea-surface temperature profile is prescribed.

Starting with the deep Indian Gateway configuration we observe that, with and without a net flow (Figures 2.6a and 2.6b), the exchange with the Atlantic Ocean remains estuarine. The deep nature of the Atlantic Gateway ensures that the level below which the Atlantic is denser than the Mediterranean is situated above the sill. Although the Indian Gateway is also deep, deep oceanic inflow in this gateway never develops due to the relative low density of the Indian Ocean (this being warmer and less salty than the Atlantic).

When the Indian Gateway is shallow and there is no net flow (Figure 2.6c), the overall circulation pattern does not show important differences in comparison with the equivalent run with a shallow Atlantic Gateway (Figure 2.4i). Although the Atlantic Gateway is deep, the shallow nature of the Indian Gateway promotes less exchange with the Indian Ocean. This increases the Mediterranean density and antiestuarine exchange with the Atlantic Ocean develops. When net flow is prescribed, estuarine exchange with the Atlantic similar to that in Figure 2.5d occurs (Figure 2.6d). The mechanism by which estuarine exchange develops is the same as explained in the previous subsection. In this case, the greater depth of the Atlantic connection, together with the lowering of the Mediterranean density associated with prescribing a net flow, guarantee that the change in sign of the Mediterranean-Atlantic density gradient occurs above the sill depth.

After closure, if a deep Atlantic Gateway is considered, the exchange with the Atlantic can be substantially different from that at present depending on the atmospheric conditions prescribed (Figure 2.6e and 2.6f). If reference atmospheric forcing is used, the upper antiestuarine cell extends until the bottom of the sill (Figure 2.6e). In contrast, if the Middle Miocene sea-surface temperature is prescribed, the
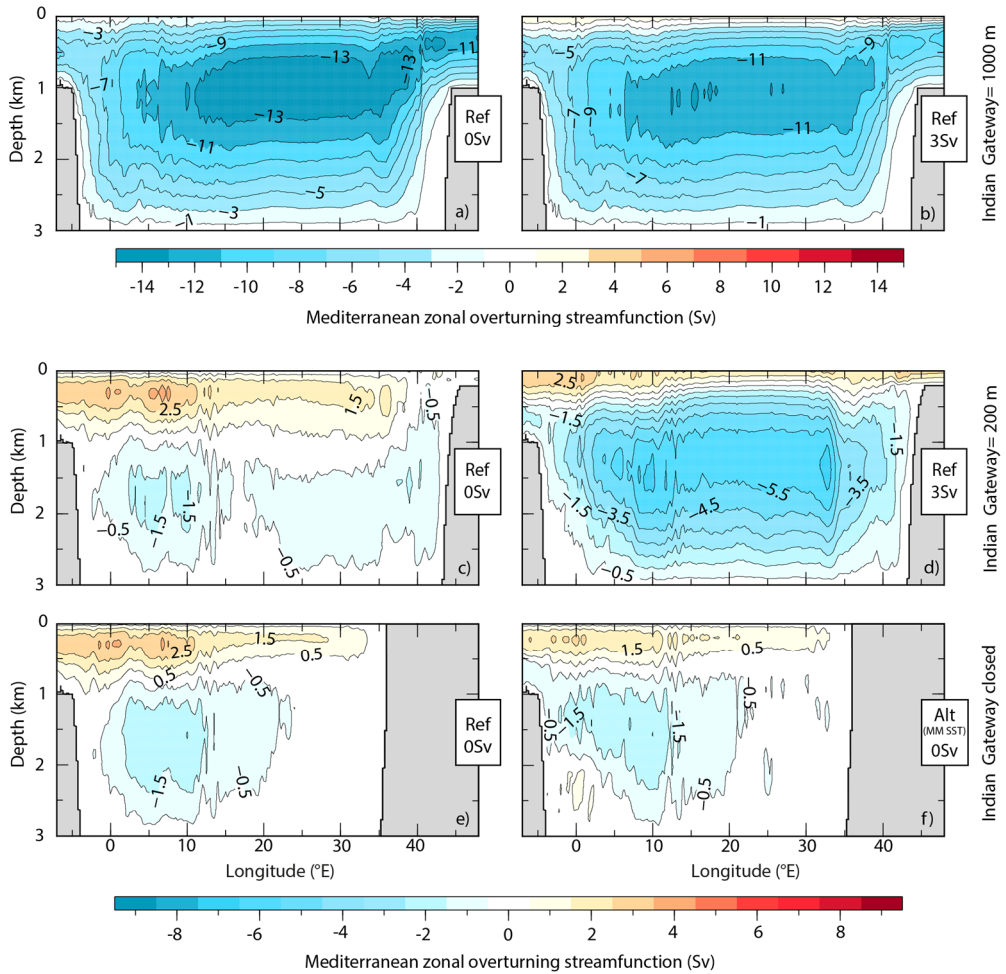
Figure 2.6. Mediterranean zonal overturning streamfunction for a deep Atlantic Gateway and a deep (a-b), shallow (c-d) and closed (e-f) Indian Gateway. In panels (a) to (d) reference atmospheric forcing is used (i.e., Ref) and, in (b) and (d), a net flow of 3 Sv is superimposed. In panel (e) reference atmospheric conditions are used again and, in (f), alternative atmospheric forcing (i.e., Alt) consisting of the Middle Miocene sea-surface temperature is prescribed (MM SST). The contour interval is 2 Sv in panels (a) and (b) and 1 Sv in panels (c) to (f).

upper antiestuarine cell extends only until an intermediate depth and deep Atlantic inflow occurs below it, resulting in three-layer flow (Figure 2.6f). The causes for its development are again those explained in the preceding subsection. In the six experiments the exchange pattern with the Indian Ocean is unchanged compared to the equivalent experiments with a shallow Atlantic Gateway.

To sum up, in terms of mechanisms, the additional experiments offer two relevant insights: (i) forcing that decreases the meridional density gradient leads to a weaker zonal overturning streamfunction, and (ii) when the Mediterranean densities are relatively low Atlantic inflow may occur over the sill.

2.4. Discussion

2.4.1. Exchange through the Indian Gateway

Carbon and oxygen isotope studies indicate that the Mediterranean was a source of warm and salty deep outflow into the Indian Ocean until about 14-14.5 Ma (e.g., Woodruff and Savin, 1989; Wright et al., 1992; Flower and Kennett, 1994; Ramsay et al., 1998). These observations are in agreement with the model experiments for an Indian Gateway depth greater than 200 m, which show that the exchange with the Indian Ocean consists of Indian inflow at the surface and Mediterranean outflow from an intermediate depth. This antiestuarine exchange with the Indian Ocean has also been reported in other regional studies (Karami et al., 2009; Karami, 2011) and global climate models (e.g., Butzin et al., 2011) with an open Indian Gateway. In our results, only when the Indian Gateway is as shallow as 200 m do deviations from this pattern occur. In this case, Mediterranean outflow still enters the Indian Ocean if the Indian Gateway does not accommodate net flow. However, if a net westward flow is imposed, the gateway shows mainly inflow into the Mediterranean (Figures 2.4, 2.5, 2.6). The latter is consistent with the global climate model experiments of Hamon et al. (2013), who find Mediterranean outflow into the Indian to end when this gateway has a depth of 250 m. However, these authors did not consider intermediate depths of the Indian Gateway between 1000 m and 250 m. We find that an Indian Gateway of 450 m is still deep enough to permit in- and outflow regardless of the atmospheric conditions and net flow prescribed.

Although the effects of the disappearance of the Mediterranean outflow into the Indian Ocean on global circulation and climate are beyond the scope of this regional work, our results show that, with a deep connection to the Indian Ocean there is a net heat transport from the Indian Ocean into the Indian Gateway in the order of 10^{-1} - 10^{-2} PW. Furthermore, both the Indian inflow and the Mediterranean outflow carry a heat content in the order of 1 PW—being greater the heat transported by the inflow. Based on this we speculate that, although closure may have increased the heat content of the Indian Ocean, warming at shallow levels and cooling at deeper depths could have occurred in the Indian Ocean in response to closure, the latter reported in the model study by Butzin et al. (2011).

Even when the Indian Gateway accommodates anti-estuarine exchange, like the present-day Strait of Gibraltar, there is a fundamental difference in the way these gateways connect to the basin circulation. Atmospheric forcing of water temperature causes density to be greater in the northern parts of the basin than in the south—at least—at shallow levels. Assuming thermal-wind balance, this density gradient would correspond to an increase in the magnitude of the east-directed flow going upwards in the water column. This is, indeed, the nature of the upper circulation cell in the present-day Mediterranean, which is composed as it is of westward flow at intermediate depth and eastward surface flow. Anti-estuarine exchange with the Atlantic Ocean matches this pattern of circulation in the basin. However, anti-estuarine exchange with the Indian Ocean does not: the gateway flows go against the "geostrophic sense" of overturning of upper waters set by the atmospheric forcing. Inspection of map views of salinity, temperature and currents demonstrates that this is achieved by the Indian inflow occupying mostly the southern part of the basin where, locally, the meridional density gradient is reversed.

2.4.2. Atlantic exchange with an open Indian Gateway

Consistent with previous modelling studies (e.g., Karami et al., 2009; Karami, 2011; Krapp and Jungclaus, 2011), our experiments show that with a deep Indian Gateway the Mediterranean-Atlantic exchange is estuarine. In contrast, when the Indian Gateway is shallow, multiple exchange patterns with the Atlantic Ocean are found possible depending on the boundary conditions (i.e., net flow prescribed, climate, and depth of the Atlantic Gateway). Exactly which exchange develops is a

function of the density (pressure) gradient between the basin and the ocean. In our results we observe that a deep connection to the Atlantic Ocean and a lowering of the Mediterranean density promote Atlantic inflow at depth in the Atlantic Gateway (e.g., Figure 2.5d). Similarly, the vertical density profile on the Atlantic Ocean (i.e., Atlantic open boundary) determines the Mediterranean-Atlantic density gradient and hence also sets the depth at which the inflow at depth starts.

Observational evidence concerning the Atlantic exchange during the Early and Middle Miocene comes from faunal and isotopic studies performed at several sites of the western and central Mediterranean. These studies postulate the presence of cold Atlantic waters (4 – 10°C) at depth in the Mediterranean basin during the Langhian (e.g., Benson, 1978; Vergnaud-Grazzini, 1983; Gebhardt, 1999; Dall´Antonia et al., 2001; Dall'Antonia, 2003). Given that most estimates of the time of closure of the Indian Gateway lie in the range from the Early to the Middle Miocene, we assume that deep Atlantic inflow was coeval, at least during some time, with a still open—but probably shallow—Indian Gateway. In our model results there are two flow configurations consistent with Atlantic inflow at depth in the Atlantic Gateway: estuarine exchange and three-layer flow (the latter not shown, but similar to that presented in Figure 2.6f). Both flow configurations prove favoured by: (i) a relatively deep Atlantic Gateway and (ii) climatic conditions leading to lower Mediterranean densities than in the case with reference atmospheric forcing, which is consistent with the early Langhian climate being more humid (Böhme et al., 2011) and warmer (coeval with the late Middle Miocene Climatic Optimum; Zachos et al., 2001) than presently. For estuarine exchange to develop a large net flow is required. In panels (a), (b), and (c) of Figure 2.7 the flow configurations consistent with the entrance of Atlantic waters at depth in the Atlantic Gateway for a shallow Indian Gateway, as well as the conditions under which these flow patterns arise, are summarised. Note that although estuarine exchange can also develop when the connection to the Atlantic is shallow, only with a relatively deep Atlantic Gateway (i.e., 900 m) does the temperature of the Atlantic inflow lie within the inferred from faunas (see Dall'Antonia, 2003). The possibility that the estuarine exchange was related to a positive Mediterranean water budget (i.e., precipitation and river runoff being greater than evaporation)—as indicated in Karami et al. (2009)—cannot be excluded.

Shallow Indian Gateway   **Closed Indian Gateway**

a)
200 m
~1000 m
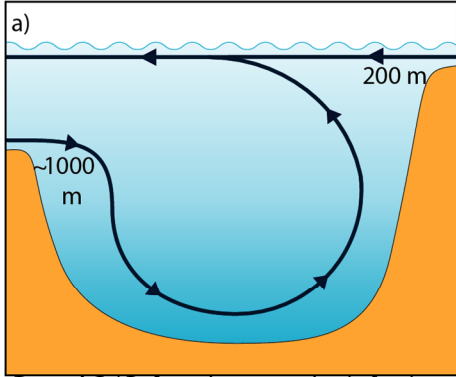
Deep AG / Ref. or alt. atmospheric forcing
/ Net flow

d)
~1000 m

Deep AG / Ref. atmospheric forcing

b)
200 m
~1000 m
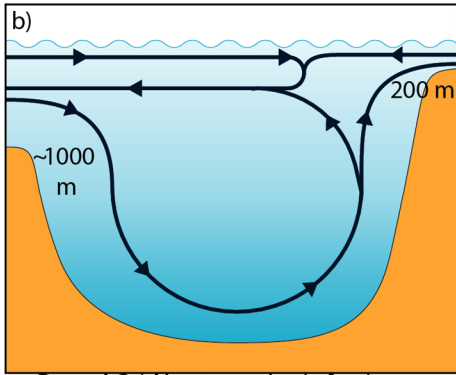
Deep AG / Alt. atmospheric forcing
/ No net flow

e)
~1000 m

Deep AG / Alt. atmospheric forcing

c)
200 m
500 m
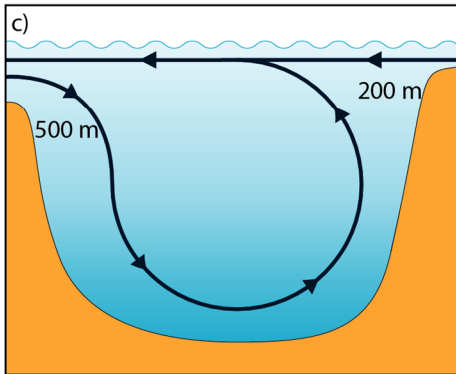
Shallow AG / Alt. atmospheric forcing
/ Net flow

f)
500 m
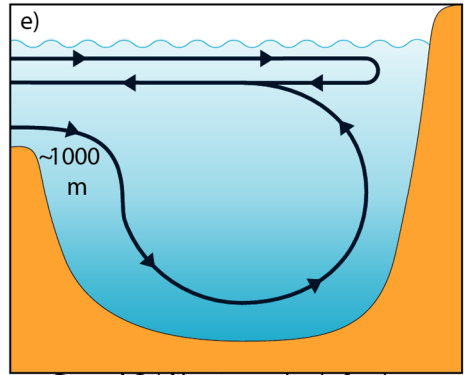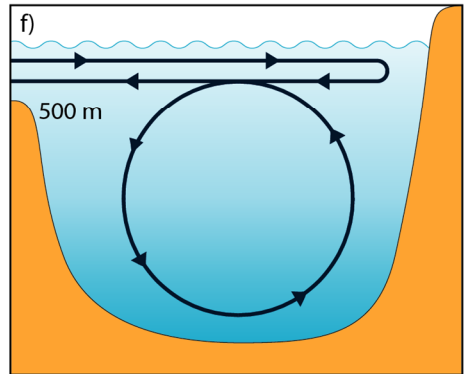
Shallow AG / Ref. or alt. atmospheric forcing

W ◄──► E   W ◄──► E

Figure 2.7. (Previous page). Panels (a), (b), and (c): modelled Mediterranean-Atlantic exchange patterns consistent with data from the Langhian for a shallow Indian Gateway. Panels (d), (e), and (f): all possible exchange patterns found after closure. The conditions under which the flows develop are also indicated. "AG" refers to the Atlantic Gateway; "Ref" and "Alt" to reference and alternative atmospheric conditions, respectively (see text for details). Note that not all the exchange patterns here presented have been shown in the preceding figures.

Thus, although the presence of deep Atlantic inflow during the Langhian has generally been related to estuarine exchange (e.g., Gebhardt, 1999), by comparing our model results to data we learn that there are other patterns of exchange that also feature Atlantic inflow at deep levels. The depth of the Atlantic Gateway, the magnitude of the net flow, and the atmospheric conditions prescribed play an essential role in the configuration of the flows when the connection to the Indian Ocean is restricted.

2.4.3. Atlantic exchange after closure of the Indian Gateway

As explained in the previous section, deep Atlantic inflow in the Mediterranean during the Langhian is evidenced by observations. Because the exact date of closure of the Indian Gateway is still under debate (e.g., Hüsing et al., 2009), we also need to consider the possibility that deep Atlantic inflow persisted after closure. In our set of results three-layer flow is the only flow configuration consistent with deep Atlantic inflow after closure (Figure 2.6f). Although three-layer flow has been found to occur in other regions at present (e.g., Red Sea-Gulf of Aden; Smeed, 2000), this is the first time that this is suggested as a possible exchange pattern between the Atlantic and the Mediterranean in the past. If this happened, the transition towards present-day antiestuarine exchange would have required a change in climate leading to greater densities of the Mediterranean (i.e., lower atmospheric temperatures or greater net evaporation) and/or a shoaling of the Atlantic connection. Panels (d), (e), and (f) of Figure 2.7 show all the exchange patterns found after closure and the conditions under which each of them appear. If, after closure, deep Atlantic inflow occurred in a setting of simple two-layer estuarine exchange, the Mediterranean must have had a positive water budget. In this case, the evolution towards antiestuarine

exchange would necessarily have required a change in the sign of the water budget. Because most authors maintain that after the Langhian there is no evidence for cold inflowing Atlantic waters in the Mediterranean, if the age of closure is younger than this, the exchange with the Atlantic after closure may have been antiestuarine directly (see Figure 2.7).

Our results also show that if (i) a shallow Indian Gateway does not feature significant net flow (e.g., smaller than 1 Sv) and (ii) climatic conditions and Atlantic Gateway depth persist while the Indian Gateway changes from shallow to closed, then the Mediterranean circulation before and after closure is very similar. Although the transition from a shallow to a closed Indian Gateway may have changed temperature and salinity, the configuration of flows in the Mediterranean may have been essentially the same (i.e., Mediterranean circulation dominated by the Atlantic Ocean and limited exchange with the Indian). This, which was also found in the global model study by Hamon et al. (2013), implies that a shallow Indian Gateway can be taken to be effectively closed from a palaeoceanographic perspective. In other words, the overall circulation pattern prior and after closure would not have been subjected to important changes.

We may conclude that available data and model results do not converge on a single, most likely response to closure of the Indian Gateway. However, whatever the details, the transition from estuarine (i.e., deep Indian Gateway) towards present-day antiestuarine exchange through the Atlantic Gateway may well have had important consequences for the circulation of the Atlantic Ocean. During this process, the outflow shifted its position from the surface to deeper parts of the gateway. Also, the outflow became saltier (denser) due to the more landlocked configuration of the Mediterranean basin. According to several modelling studies (see Hamon et al., 2013; Ivanovic et al., 2014), the latter configuration may have enhanced the Atlantic Meridional Overturning Circulation.

In this context, more information about the Mediterranean hydrological budget during the Early-Middle Miocene would represent a major step forward towards the understanding of the communication between the Mediterranean-Atlantic during the last stages of closure. This would allow the discard of certain flow configurations and hence to gain insight into the conditions that may have existed for the possible exchange/s to develop (i.e., climate, Atlantic Gateway depth, net flow).

If, for instance, during the Langhian the Mediterranean water budget was negative, then the influx of deep Atlantic waters into the Mediterranean needs to be related to (i) estuarine exchange associated with a large net westward flow or (ii) three-layer flow. The former entails that the Indian Gateway was still open and was able to accommodate large water volumes; the latter necessarily requires a relatively deep Atlantic connection (i.e., 900 m).

2.4.4. Effect of closure of the Indian Gateway on basin temperature and salinity

Our analysis shows that there are many exchange patterns possible between the Mediterranean and the adjacent oceans—especially with the Atlantic—for the different stages of the process of closure. Consequently, how basin salinity and temperature change in response to closure is dependent on the specific combination of boundary conditions. An aspect that all cases do have in common is that closure entails a complex reorganisation of the flows and this leads to non-uniform temperature and salinity changes all over the basin (not shown). This behaviour, also found in the sensitivity study of Karami (2011) and observed in data (e.g., Bicchi et al., 2003), implies that variations observed in a certain region or depth interval are not automatically applicable to the rest of the basin.

As reported in previous modelling studies (e.g., Karami, 2011; Hamon et al., 2013), we observe a general salinity increase when the connection with the Indian becomes shallower. This is direct consequence of the reduced exchange with the adjacent oceans. Comparing the corresponding deep and closed Indian Gateway geometries included in our sets of experiments we find that this rise is generally more pronounced in the Paratethys (Paratethys: from about 1 to 6 psu; Mediterranean: from 1 to 2 psu). This relates to the greater sensitivity of the Paratethys to atmospheric forcing due to its small water volume and limited connection with the Mediterranean.

Temperature changes are more complex. Using a simplified bathymetry constructed from the same palaeogeography we use, Karami (2011) found that warming or cooling could happen after closure depending on the boundary conditions assumed. In our analysis we find that, on the local scale, cooling or warming can occur. On the basin scale, however, we observe an increase of the average temperature

of the Paratethys and Mediterranean (Paratethys: from 0.1 to 0.3ºC; Mediterranean: from 0.1 to 2ºC). The fact that only small temperature changes occur in the Paratethys is a direct consequence, again, of its high sensitivity to atmospheric forcing. For this reason, the average temperature over this realm tends to stay close to the prescribed atmospheric values. After closure, changes in the heat transport through the gateways occur as a result of the new circulation pattern. On the one hand, the transition from estuarine (deep Indian Gateway) to antiestuarine or three-layer flow (closed Indian Gateway) entails a change in the sign of the heat transported through the Atlantic Gateway. Whereas with a deep Indian Gateway the basin loses heat to the Atlantic Ocean, the basin gains heat from the Atlantic when the gateway is closed. This may contribute to the higher temperature after closure. On the other hand, whereas with a deep Indian Gateway the Paratethys acts as a source of heat for the Mediterranean, the Paratethys becomes a sink of heat after closure. More specifically, when the Indian Gateway is deep, part of the Indian inflow enters the Paratethys from the eastern Mediterranean-Paratethys connection and flows into the Mediterranean through the western connection transporting heat into the basin. After closure, the eastern connection disappears and the Paratethys becomes a sink of heat for the Mediterranean. However, it is not straightforward to establish a link between changes in the heat budget and variations in temperature because of the dynamic role of the atmosphere.

2.4.5. Role of depth of the Paratethys connections

Because the alternative atmospheric conditions that we explore affect to a relatively large extent the Paratethys, the corresponding experiments provide insight into the role of the Paratethys on the Mediterranean circulation. However, we do not explore how changing the depth of the Mediterranean-Paratethys connections—set to 200 m in all the experiments—would affect the two marine domains. With an open Indian Gateway shallower connections may have reduced the volume of Mediterranean-Indian waters entering the Paratethys through the eastern connection and decreased the total water exchange between the Mediterranean and the Paratethys. As found by Karami et al. (2011) the latter would reduce the influence of each marine domain onto the other and is expected to increase the sensitivity of the Paratethys to climate. Although the same effects are expected after the closure of the Indian

Gateway, given that in this scenario only the western Mediterranean-Paratethys connection may have persisted (see Figure 2.2d), the previously mentioned effects would be even more enhanced. On the contrary, the opposite effects are expected if before and after closure deeper connections existed. Given that in the palaeogeography we use as a reference the Mediterranean-Paratethys connections are very narrow, we do not expect relatively small changes in the depth of these connections to introduce significant deviations from the results found in this analysis.

2.5. Conclusions

Using a regional ocean model we investigated the changes in Mediterranean circulation due to shoaling and closure of the Indian Gateway. To understand the functioning of the system and test the robustness of the results we imposed several atmospheric conditions, modified the Atlantic Gateway depth, and prescribed net westward flows of different magnitudes for each of the stages of closure. Our main conclusions are:

- Shoaling of the Indian Gateway progressively increases the importance of the Atlantic Ocean with respect to the Indian Ocean when the gateways do not accommodate net flow. However, when a net westward flow is prescribed, important changes in the Mediterranean large-scale circulation occur—especially if the gateways are shallow.

- We find antiestuarine exchange with the Indian Ocean unless the Indian Gateway is 200 m and the gateways accommodate net flow.

- The exchange with the Atlantic Ocean is estuarine if the Indian Gateway is deep. However, if this is shallow or closed, there are several possible Mediterranean-Atlantic exchange patterns depending on the atmospheric conditions, the Atlantic Gateway depth and net flow prescribed.

- For the case of a shallow Indian Gateway, a comparison between the modelled exchange patterns and proxy data from the Langhian suggests that estuarine exchange or three-layer flow are the most likely configurations to have occurred between the Mediterranean and the Atlantic. These patterns are favoured by a deep Atlantic Gateway and/or climatic conditions that reduce the Mediterranean density. Estuarine exchange additionally requires a relatively large net flow to develop.

- After closure, with a negative Mediterranean water budget, model results show antiestuarine exchange with the Atlantic unless the Atlantic Gateway is deep and alternative atmospheric conditions are applied. Then, three-layer flow develops.

- Temperature and salinity changes due to closure are not spatially homogeneous in either the horizontal or vertical direction in the Mediterranean and Paratethys.

Acknowledgements

Chapter 3: Water exchange through the Betic and Rifian corridors prior to the Messinian Salinity Crisis: A model study

ABSTRACT

Although the present-day Mediterranean-Atlantic water exchange has been extensively studied, little is known about the dynamics of the Betic and Rifian corridors that existed before the Messinian Salinity Crisis. Due to the difficulties in studying the palaeogeographic evolution of these corridors, physics-based knowledge of their behaviour is essential to interpret observational evidence and to relate flow structures to gateway geometries. Here we present the first systematic model study of the water exchange through these gateways. We use the parallel version of the Princeton Ocean Model (sbPOM) and a set of idealised bathymetries based on a late Tortonian palaeogeography. This analysis represents a major step forward in the understanding of the behaviour of the double-gateway system constituted by the Late Miocene Betic and Rifian corridors. We demonstrate that the "siphon" scenario, involving inflow of cold upwelled Atlantic water through the Rifian corridor and outflow of Mediterranean water only via the Betic corridor, is unlikely from a physics perspective. It is shown that two exchange patterns are possible depending solely on the relative depths of the corridors. The implication of this is that geological evidence for the behaviour of one corridor provides information about the dimensions of the other. We show that disappearance of outflow in one corridor does not necessarily imply its closure and we establish a guideline to determine how geological evidence can be interpreted as indicating one- or two-layer flow. Based on the model results, we propose new physics-based scenarios for the time interval defined for the siphon.

3.1. Introduction

During the Late Miocene, the Mediterranean and the Atlantic were connected by at least two marine gateways: the Betic and Rifian corridors through southern Spain and northern Morocco, respectively (e.g., Santisteban and Taberner, 1983; Benson et al., 1991; see Figure 3.1). Tectonic restriction, in combination with glacioeustatic sea level fluctuations, led to the Messinian Salinity Crisis during which evaporites were deposited throughout the Mediterranean basin (e.g., Roveri et al., 2014). Knowledge about the palaeogeographic evolution of these two gateways is essential to reconstruct the sequence of events resulting in the salinity crisis. However, it is difficult to identify the gateways because of the local nature of the strait deposits and the erosion inherent to regression and uplift (e.g., Martín et al., 2009). For this reason, most of the information about gateway dimensions and evolution derives from the study of the past exchange. For this, indirect methods such as faunal (e.g., Pérez-Asensio et al., 2012) or isotope (e.g., Ivanovic et al., 2013) studies are used. However, the lack of insight regarding the functioning of a double gateway limits the interpretation of results. It is generally assumed that each gateway either behaves in the same way as a single gateway or that the two corridors acted together as in the "siphon" scenario proposed by Benson et al. (1991). The siphon theory entails that in a double-gateway scenario prior to the Messinian Salinity Crisis, the Rifian corridor (RiC) accommodated only upwelled inflow from the Atlantic while the Betic corridor (BeC) was the sole conduit for Mediterranean outflow.

The purpose of our study is to gain physics-based insight into the interplay of the two gateways prior to the salinity crisis in order to (i) establish a solid framework that provides information relevant to data acquisition and (or) interpretation and (ii) test the validity of the "siphon theory". For this we use a regional-scale ocean general circulation model. The experiments include multiple gateway geometries created from a reference bathymetry based on a late Tortonian palaeogeography from which only the depths of the gateways are modified. Our model study allows us to assess the significance of observational evidence for patterns of exchange and provides a basis for relating observed flow configurations to the associated gateway geometries. To the extent that our work provides insight regarding the behaviour of the Mediterranean

Figure 3.1. Earliest Messinian palaeogeography modified from Martín et al. (2001) showing the location of the Taza-Guercif basin, Bou Regreg valley and the Guadalhorce corridor. The black line corresponds to the present-day coastline. Note that this map is a snapshot in the evolving palaeogeography and our model geometry (Figure 3.2) is more generic.

outflow in a double gateway it is relevant also for ongoing efforts to reconstruct the pathway of outflow water from contourites (e.g., ODP Leg-339; see Hernández-Molina et al., 2014).

3.2. Model setup

We use the parallel version of the Princeton Ocean Model (Blumberg and Mellor, 1987) sbPOM (Jordi and Wang, 2012). This is a three-dimensional, sigma-grid coordinate, free-surface, hydrostatic, primitive equation numerical model. The use of sigma coordinates gives the same amount of vertical levels regardless of the water depth, which is optimal for the study of shallow (strait) areas. The horizontal grid is curvilinear and has a resolution between 12 and 63 km in the i direction and between 11 and 70 km in the j direction of the grid (Figure 3.2). For brevity, we will refer to the i direction as "east-west" and j direction as "north-south". Starting with
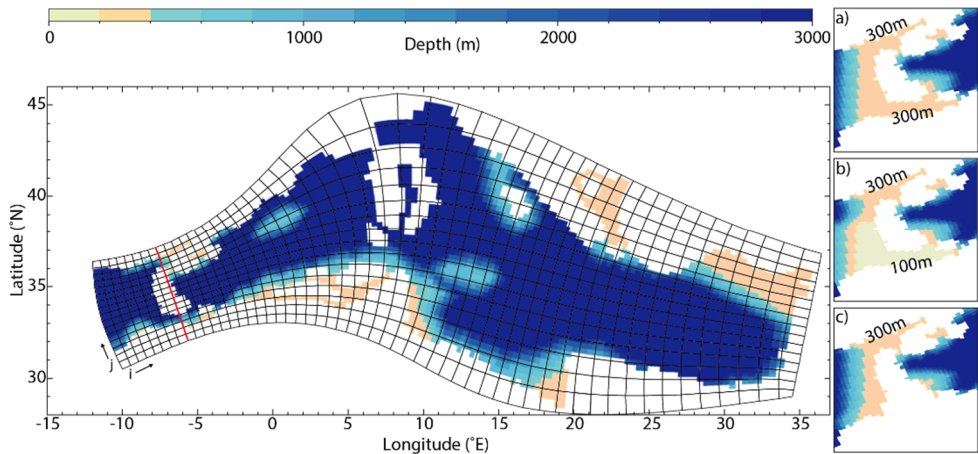
Figure 3.2. Reference bathymetry based on the late Tortonian palaeogeographic map from the Peri-Tethys Atlas and the orthogonal curvilinear grid (only one out of three gridlines is drawn). Right-hand side panels illustrate in detail the gateway area to exemplify the alternative bathymetries. The BeC is set to 300 m, and the RiC is (a) 300, (b) 100 and (c) 0 m. The red line shows the transect where horizontal velocities are illustrated (Figures 3.4-3.6).

Zavatarelli and Mellor (1995), POM has been widely applied to investigate the oceanography of the Mediterranean Sea. Recently, sbPOM has been successfully used to study the Mediterranean circulation (Topper and Meijer, 2015). A series of idealised bathymetries based on the late Tortonian map of the Peri-Tethys Atlas (Dercourt et al., 2000) is considered. The Paratethys is not included because we focus on the functioning of the Betic and Rifian corridors and the presence of the Paratethys is not necessary to reproduce the basin-scale circulation of the Mediterranean. To construct the reference bathymetry, the deep and shallow levels distinguished on the atlas are set to 3000 and 220 m, respectively. Between these two levels, a continental slope is introduced to create a smooth transition (Figure 3.2). In the alternative geometries, we only change the depth of the gateway areas, which are set before the continental slope is implemented (Figures 3.2a-3.2c). The coastline is not modified so as to enable the isolation of the effect of the straits. Although the Atlantic region is always 3000 m deep, the smoothing introduces a continental slope that extends toward the west over different distances depending on strait depth. The

maximum gateway depth we consider is that of the present Strait of Gibraltar (300 m) arguing that in a double-gateway scenario just prior to the Messinian crisis—during which the corridors were severely restricted (e.g., Roveri et al., 2014)—these gateways were most likely shallower than that. We do not include geometries where both corridors are shallower than 25 m because these configurations lead to very high salinities, which are not expected before the crisis. The Betic and Rifian corridors have, at the red transect shown in Figure 3.2, a width of 89 and 70 km, respectively.

We use idealised atmospheric forcing which has been shown to be able to capture the first-order features of the thermohaline circulation (e.g., Meijer and Dijkstra, 2009) and allows us to isolate the basin's response to bathymetric changes in the gateways. Because the Late Miocene climate is uncertain (e.g., Roveri et al., 2014), atmospheric values based on the present day are used. The freshwater flux (evaporation minus precipitation and river discharge) is set to a uniform and constant value of 0.5 m/yr. This is close to the value for the present day and also appropriate for the Mediterranean region during the Late Miocene (Gladstone et al., 2007; see discussion in Topper et al., 2011). To simulate heat exchange with the atmosphere, the upper layer of the model is relaxed to the modern latitudinal profile of zonal and annual mean sea-surface temperature of Steppuhn et al. (2006). To test the sensitivity of the model results to changes in climate we ran several experiments with alternative atmospheric conditions (this aspect will be addressed in the discussion). Because former sensitivity studies conclude that the main effect of the addition of winds is the enhancement of the circulation in the uppermost water column (e.g., Meijer and Dijkstra, 2009), winds are neglected. In the Atlantic, west of the gateways, our model features an open boundary that represents the communication with the Atlantic Ocean and through which an amount of water flows that exactly compensates for the evaporative loss in the Mediterranean. Atlantic water flowing into the Mediterranean is given a salinity of 35 psu independent of latitude and depth. The temperature of the top layer of the model is set equal to that used for the atmospheric forcing. The vertical distribution of temperature is an exponential curve approximating the vertical distribution of potential temperature in the Atlantic Ocean (10°W, 35°N) from the Levitus' World Ocean Atlas (Locarnini et al., 2013). The Mediterranean basin and the Atlantic are initialised with a salinity of 35 psu, and temperature decreases with depth from the sea-surface value. To ensure a progressive transition from the open boundary

to the Mediterranean, water properties are gradually relaxed toward conditions equal to the initial values over the first 18 grid columns as in Topper and Meijer (2015). Each experiment is run until steady state, and all results shown are averages over 100 years of equilibrium. This snapshot approach is warranted because palaeogeographic changes are slower than the establishment of the new circulation pattern. The implications of the model parameters here used have been tested in Topper and Meijer (2015).

3.3. Analysis and results

3.3.1. Exchange pattern

In Figure 3.3 the zonal (i.e., east-west) overturning streamfunction illustrates the basin circulation for a double-gateway scenario where both corridors have a depth of 300 m. The overturning streamfunction may be thought of as all water transport projected on a vertical east-west section through the basin. Although variations in the depth of the gateways affect the strength of the overturning cells, the basin-scale circulation remains unchanged in the experiments. The model simulates well the overall behaviour of the present-day Mediterranean, where the thermohaline circulation is characterised by shallow and deep cells. The shallow cell extends to an intermediate depth and shows antiestuarine exchange with the Atlantic: oceanic inflow occurs at the surface, extends to the eastern Mediterranean where it sinks due to net evaporation, and returns back to the Atlantic. The underlying deep circulation cell is fed by deep water formation. Detailed analysis shows that deep water forms in the northern parts of the basin where temperature is low and salinity is high (see also Topper and Meijer, 2015).

To gain insight into the Mediterranean-Atlantic exchange, we study profiles of east-west velocities averaged over the j direction of the grid at the transect shown in red in Figure 3.2 for a range of gateway-depth configurations. This location is chosen because it coincides with the shallowest region of the gateways and, consequently, determines the particular type of exchange within the corridors.

The modelled exchange patterns are summarised in Figure 3.4 in the form of coloured dots. The blue dots indicate that we find two-way flow consisting of Atlantic inflow at the surface and Mediterranean outflow at depth through both corridors, and
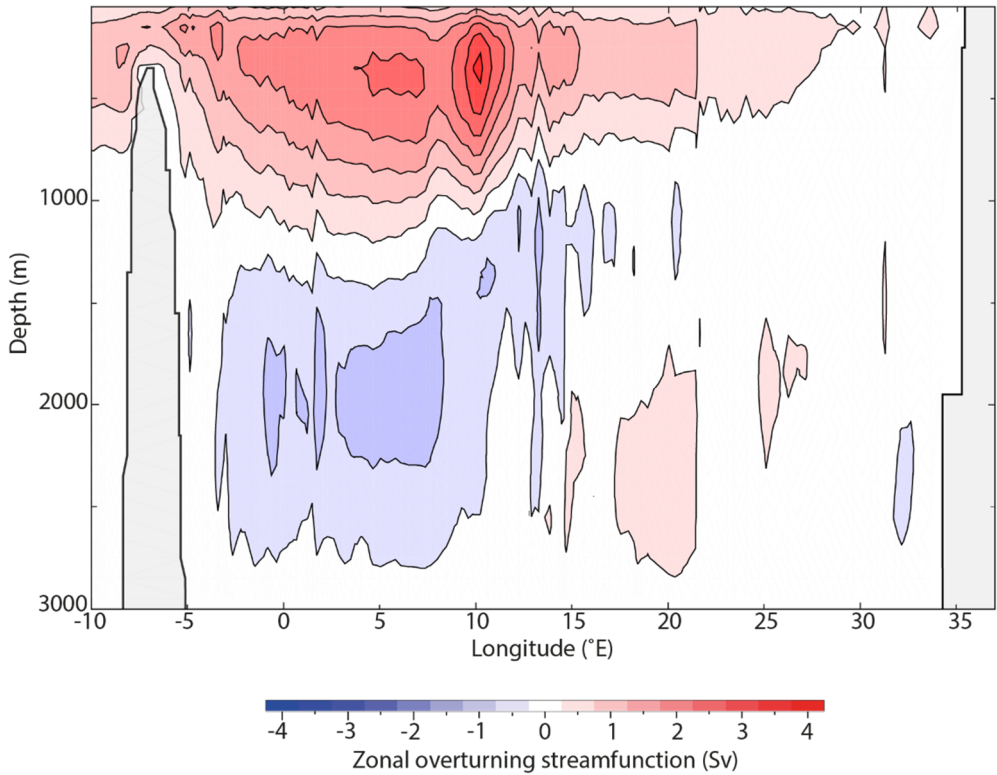
Figure 3.3. Zonal overturning streamfunction for a double-gateway scenario where both corridors have 300 m. Red colours indicate a clockwise sense of flow in this projection and blue colours counterclockwise. The seafloor is depicted at the maximum depth that occurs at each longitude and the contour interval is 0.5 Sv.

the red dots correspond to two-way flow in the deep corridor and only Atlantic inflow in the shallower one. The overall behaviour that emerges from the large set of runs we carried out is that the pattern of exchange depends on the relative depth of the two corridors. Specifically, two-way flow in both corridors occurs when the shallow corridor is deeper than about half the depth of the deep corridor; one-way flow develops when the shallow corridor is shallower than this.

Small deviations from a completely regular pattern occur near the lines that limit the segment with two-way flow in both corridors, especially when the corridors are deep. On the one hand, the Mediterranean basin is less sensitive to bathymetric
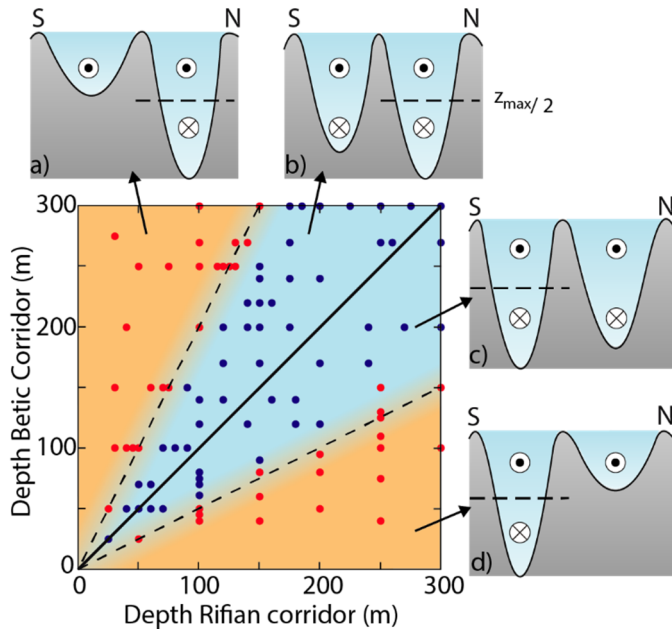
Figure 3.4. Exchange patterns through the corridors. The blue dots indicate that we find two-way flow in both gateways. The red dots represent two-layer flow in the deep corridor and only Atlantic inflow in the shallower one. The continuous line designates that both gateways have the same depth, and the dashed lines that one corridor is twice the depth of the other. Panels (a-d) show various gateway configurations as seen from the Mediterranean. The discontinuous line indicates the mid-depth of the deep corridor.

changes in the gateways when these are deep. This causes the shift from one circulation pattern to the other to occur slightly further away from the halfway position. On the other hand, the transition from one- to two-layer flow is gradual and we only classify a gateway as presenting outflow when the latitudinally-averaged velocity at depth is oceanward.

3.3.2. Velocity profiles

Figure 3.4 demonstrates that the exchange in a gateway depends on the depth of one corridor relative to the other. Profiles of east-west velocity averaged by latitude (j direction) are shown in Figure 3.5 for the following gateway configurations: the
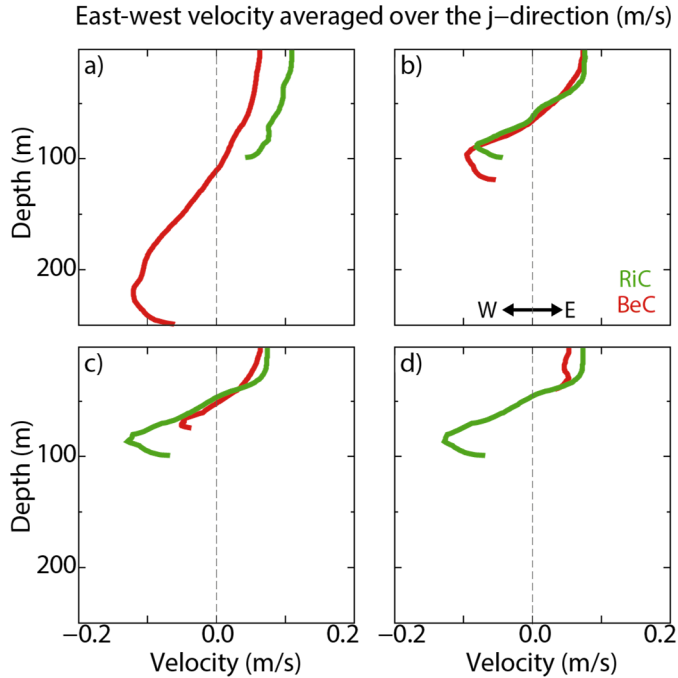
Figure 3.5. Profiles of east-west velocities averaged over the north-south direction, measured at i=25 (red line in Figure 3.2) for the Betic and Rifian corridors. The RiC (green) is set to 100 m, and the BeC (red) is (a) 250, (b) 120, (c) 75 and (d) 40 m. Positive velocities indicate eastward flow.

RiC has a constant depth of 100 m, and the BeC is set to 250, 120, 75 and 40 m in Figures 3.5a-3.5d. In Figures 3.5b and 3.5c, the shallow corridor is deeper than half the depth of the other corridor and both gateways have two-way flow. In contrast, in Figures 3.5a and 3.5d, where the shallow corridor is shallower than this halfway position, it only accommodates Atlantic inflow.

Next, we illustrate in detail the flow structure when the shallow corridor approaches the mid-depth of the deeper one. Figure 3.6 shows velocity profiles for several depth combinations where the BeC has a constant depth of 300 m and the RiC is 300, 200, 150, 100 and 0 m in panels (a) to (e), respectively. In Figure 3.6a both gateways have the same depth and present eastward velocities at the surface and westward flow at depth. When the RiC is set to a depth slightly shallower than the

BeC, the outflow occurs only at the bottom of the corridor and its velocity decreases (Figure 3.6b). If the shallow gateway is half the depth of the deep corridor or shallower outflow disappears in the RiC (Figures 3.6c and 3.6d). In Figures 3.6b-3.6d the BeC is always deeper than the RiC and it accommodates two-way flow. In the last configuration, where the RiC is closed, the positive velocities in the BeC increase compared with a double-gateway scenario (Figure 3.6e).

3.3.3. Interface between inflow and outflow

Figures 3.6a-3.6e also serve to examine the average depth of the interface, i.e., the level at which velocities are zero. When both gateways have the same depth, the interfaces are close to the middle of the water column but not exactly at the same position probably due to the complex gateway geometry (Figure 3.6a). In Figure 3.6b, the interface is shallower in the BeC than in the RiC. Moreover, with two gateways, the interface in the deep corridor is always located at its mid-depth or shallower levels (Figures 3.6b-3.6d). Finally, with a closed RiC, the interface in the BeC deepens (Figure 3.6e).

To investigate the interface configuration in more detail, we study east-west velocities through the same transect again (Figures 3.6f-3.6j). The gateway geometries are the same as before and presented in the same order. When the two corridors are 300 m deep, both interfaces are tilted down to the south (Figure 3.6f). This indicates that at the location of the profiles the flows are affected by Coriolis force, which causes water accumulation to the right of the flow direction. Note that at locations where the gateways are narrower, Coriolis force does not play a role and the interface is flat. When the RiC is shallower than the BeC, but still deeper than half the depth of the latter, the interface configuration in the RiC is substantially different (Figure 3.6g). In this corridor the outflow is restricted to a small triangle at the bottom in the northernmost part of the gateway. In Figure 3.6h, where the RiC is half the depth of the BeC, the interfaces look similar to Figure 3.6g but the outflow in the RiC is closer to the bottom due to the smaller water depth. When the RiC is shallower than half the depth of the BeC (Figure 3.6i) we find that while the RiC presents Atlantic inflow only, the BeC still accommodates two-way flow and has a similar interface to Figures 3.6g and 3.6h. With a closed RiC the interface in the BeC resembles the previous configuration but positive (eastward) velocities increase (Figure 3.6j). In the
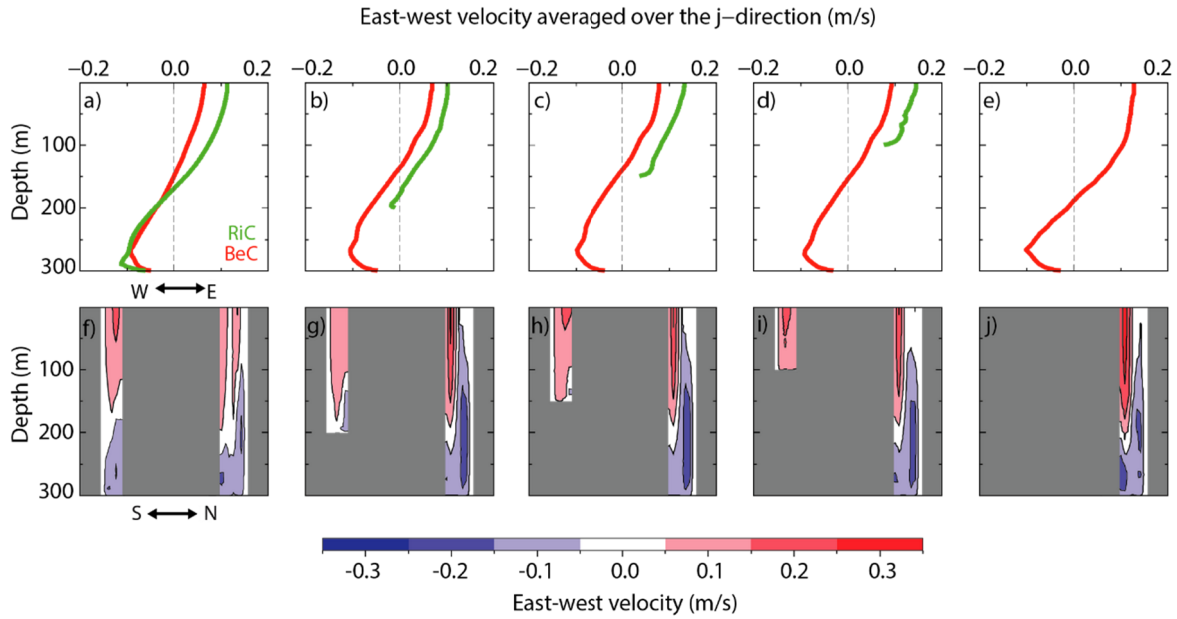
Figure 3.6. Profiles of latitudinally-averaged east-west velocity (a-e) and east-west velocity (f-j) both calculated at the same transect (i=25). The BeC has a constant depth of 300 m and the RiC is set to 300, 200, 150, 100 and 0 m from (a) to (e) and from (f) to (j). The contour interval is 0.1 m/s.

shallow corridor of a double gateway, rotational effects cause the interface, located relatively close to its bottom, to reach the floor of the corridor (Figures 3.6g and 3.6h). However, in the deeper corridor or in a single-gateway setting, where the interface is at about the mid-depth of the corridor, the interface is tilted but it does not reach the seafloor (Figures 3.6f to 3.6j). An interface located at an intermediate depth in a corridor would only reach the bottom when the effect of rotation increases (i.e., in a wider gateway, see Timmermans and Pratt (2005)).

Figure 3.7 shows the salinity and trajectory of the flow at the bottom in the gateway area. The BeC is set to 300 m and the RiC to 150 m (same geometry as in Figures 3.6c and 3.6h). The purpose of this figure, in which salinity is used as a tracer to distinguish between the low salinity Atlantic waters and the saltier Mediterranean outflow, is to illustrate how the exchange pattern would be recorded in the sediments of the corridor. Although in this specific case both corridors accommodate two-layer flow, only in the shallower RiC, rotational effects allow the upper inflowing layer to reach the bottom on the southern side of the gateway.
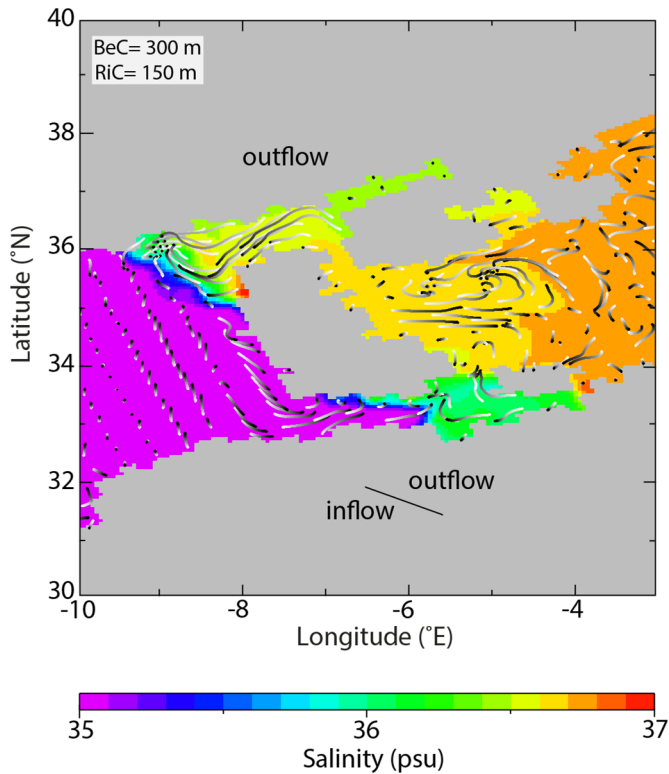
Figure 3.7. (Previous page). Salinity (psu) and flow trajectories just above the seafloor in the gateway area (shown is the deepest sigma layer). Trajectories show the paths water would travel in 30 days, on the basis of the velocity field at steady state. Tails are white and heads are black. The BeC is set to 300 m and the RiC to 150 m.

3.4. Discussion

3.4.1. Causal mechanism

The finding that the behaviour of the shallower corridor depends on its depth relative to the mid-depth level of the deep corridor indicates that the deeper corridor controls the behaviour of the double gateway. The antiestuarine exchange in the deep corridor is the same as in the present-day Strait of Gibraltar and for the same reason: evaporation leads to a salinity and, thus, density, increase in the Mediterranean basin. The resulting pressure gradient between basin water and lower density Atlantic waters drives outflow over the sill. This outflow causes the Mediterranean Sea surface to drop, which drives a compensating inflow at the surface. The deep corridor apparently always has the interface positioned near its mid-depth (it is never exactly halfway and the reasons for this are discussed shortly) and imposes this position of the interface on the shallower corridor. If the bottom of the shallow corridor is above the interface level, this corridor does not accommodate outflow. Because the gateways are geographically close to each other, the sea-surface gradient is similar in both, and both therefore accommodate surface inflow.

In the deeper corridor the interface is near mid-depth most likely because for a given density (pressure) gradient along the strait, an intermediate position of the interface is associated with the greatest inflow and outflow (e.g., Bryden and Stommel, 1984; see also Meijer, 2012). In their turn, these flows are driven toward a maximum by the intrinsic tendency of the Mediterranean to be well mixed, subject as it is to net evaporation and buoyancy loss of its surface water (e.g., Bryden and Stommel, 1984). A well-mixed basin implies a small difference between density of inflow and outflow and this—from budget considerations—is associated with relatively large exchange flows. Note that we neither wish nor need to argue that our

modelled gateways and basin are in the rather precisely defined states of maximal exchange and overmixing, respectively.

Viewed in more detail, we find that in the deep corridor of a two-gateway system, the interface is shallower than it would be in a single gateway of the same depth (Figures 3.6b-3.6e). The shallow gateway acts as an extra source of Atlantic inflow into the basin; hence, less inflow needs to be accommodated in the deep corridor, causing the interface to shoal there (Figures 3.6b-3.6d). Finally, when both corridors accommodate two-way flow, the interface is always deeper in the shallow corridor than in the deeper corridor (Figure 3.6b). As the shallow corridor shoals, the space available for the outflow gets smaller. Friction from the overlying layer and the bottom increases in importance and this reduces the outflow—deepens the interface—even more.

3.4.2. Sensitivity of the Mediterranean circulation to climate

To investigate how sensitive the Mediterranean large-scale circulation and Mediterranean-Atlantic exchange patterns are to changes in climate, we ran a large set of experiments with alternative atmospheric conditions. In particular, we considered a warmer than present-day temperature profile based on the Middle Miocene latitudinal profile of zonal and annual mean sea-surface temperature proposed by You et al. (2009). This profile was used instead of a Late Miocene one because this is warmer and thus represents a more extreme case to test. In addition to this, in another collection of experiments, we set the freshwater flux to 1 m/yr (instead of 0.5 m/yr). Overall, these experiments show that the main features of the Mediterranean large-scale circulation remain unchanged. Similar to when present-day atmospheric conditions are prescribed, the zonal overturning streamfunction presents deep and shallow cells (see Figure 3.3) and only variations of the magnitude of these cells occur depending on the specific atmospheric forcing applied. This implies that although changes in the properties and amount of outflow produced in response to climate are expected, outflow is always present in—at least—one of the two corridors. This is consistent with faunal and isotope studies that report the existence of Mediterranean outflow in the Betic (e.g., Pérez-Asensio et al., 2012) and Rifian (e.g., Ivanovic et al., 2013) corridors prior to the Messinian Salinity Crisis. Regarding the exchange in the corridors, we find, again, that the shift from one- to two-way flow

occurs when the shallow corridor is deeper than about the mid-depth of the deeper corridor. This confirms that our results are robust and that the exchange pattern is not sensitive to the atmospheric conditions imposed.

3.4.3. Reassessment of the "siphon event"

Compositional changes in marine microfossil assemblages at the Tortonian-Messinian boundary led Benson et al. (1991) to propose the "siphon event". An influx of deep-water Atlantic ostracods to the western end of the Rifian corridor (Salé core in Bou Regreg valley; see Figure 3.1), coincident with a transition from tropical-epipelagic to temperate-mesopelagic planktic foraminifera, was interpreted as evidence for inflow of upwelled Atlantic waters. Benson et al. (1991) suggested that this inflow occupied the whole RiC while the BeC accommodated only outflow. The event is thought to have started about 7.2 Ma (Hodell et al., 1994) and may have ended 6.58 Ma on the basis of the presumed siphon expression in the Melilla basin (near the eastern end of the RiC) (van Assen et al., 2006).

None of our modelled exchange patterns matches the organisation of flows proposed for the siphon event. This suggests that the siphon hypothesis is incompatible with the physics of water exchange. However, combining model results with our knowledge of gateway evolution, it is possible to sketch an alternative scenario that is consistent with certain elements of the siphon scenario. In the gateways at 7.2 Ma, two important events occur: (1) rapid shoaling of Taza-Guercif basin in the central RiC from about 500 m to less than 100 m (Krijgsman et al., 1999b) and (2) opening of the Guadalhorce corridor of the BeC with a depth between 50 and 120 m (Martín et al., 2001; see locations in Figure 3.1). Although the existence of a second Betic connection prior to the crisis is still under debate (e.g., Soria et al., 1999; Hüsing et al., 2010), for simplicity we assume a single Betic corridor. In this context, immediately before 7.2 Ma, the RiC may have been the only Mediterranean-Atlantic connection, and therefore, two-way flow is expected. At 7.2 Ma, the shoaling of Taza-Guercif basin together with the opening of the Guadalhorce corridor may well have led to the northern corridor being deeper than the southern one. In this situation model calculations suggest that the BeC would have accommodated two-way flow while the RiC experienced only inflow (i.e., as in Figure 3.6i) or mostly inflow with minor outflow (see Figure 3.6g), depending on its exact depth compared to the BeC. Both

possibilities entail an increase in the relative importance of Atlantic-derived waters in the RiC at 7.2 Ma. In the first case (with RiC shallower than half the depth of BeC), the sole presence of Atlantic inflow would be consistent with the siphon hypothesis in the RiC. A possibility that cannot be ruled out based on the depth estimates is that the RiC was still the deeper corridor. In this case both corridors may have seen two-way flow. The possibility that the RiC was more than twice as deep as the BeC can be discarded because then, the BeC would be subject only to inflow and this is inconsistent with the presence of sedimentary structures in the Guadalhorce corridor indicating oceanward flow (Martín et al., 2001).

Does other observational evidence allow further constraint on the evolution of the Mediterranean-Atlantic exchange through the gateways? As yet, the available data are not conclusive. Ivanovic et al. (2013) present a first bottom-water record of the exchange through the RiC based on neodymium isotopes. Although the overall picture emerging is far from straightforward, the data do indicate that before the restriction of the RiC at 7.2 Ma, bottom waters in the Taza-Guercif basin are of Mediterranean origin. This is consistent with the presence of two-way flow in the RiC before the opening of the Guadalhorce corridor. It is important to note that for this same period, the Bou Regreg valley sections (situated somewhat south of the middle in the wide western end of the RiC, see Figure 3.1) only present Atlantic bottom waters (Ivanovic et al., 2013). Apparently, the Mediterranean outflow passing through the central RiC is not recorded at this location on the Atlantic side. In a wide section of a single gateway, the interface tilted southward by rotation may reach the bottom. Whereas within the central corridor (i.e., Taza-Guercif basin) only outflow would be recorded at the bottom, in the much wider Atlantic end of the RiC, inflow and outflow could be side by side on the gateway floor. Consequently, Mediterranean outflow may have passed to the north of the location of the Bou Regreg sections. The implication would be that we should not expect major changes at this site in response to variations in the depth of the RiC. The Bou Regreg neodymium signal is puzzling by all means; it indicates more Mediterranean-like water after 7.2 Ma and even after the RiC has closed, possibly due to reworking (Ivanovic et al., 2013). A new, detailed analysis of benthic foraminiferal assemblages from the Salé Briqueterie core in the Bou Regreg valley shows only minor compositional changes for the time interval proposed for the siphon and fails to show the "influx" of *Uvigerina peregrina* and *U. pygmaea* used as evidence for influx of deeper-water Atlantic taxa by Benson et al. (1991; A. Cutler, A

reexamination of the Miocene Morocco siphon event hypothesis using benthic foraminifera, unpublished MSc thesis, University of Birmingham, 2013). This casts doubt on the validity of the siphon hypothesis and thus supports the conclusions derived from our model results. The fact that faunal changes are only minor may again be an expression of the location of the section in the wide western portion of the gateway (see Figure 3.7). Seemingly in favour of the siphon hypothesis, several studies reported a cooling of waters of the RiC at the start of the siphon (e.g., Hodell et al., 1994; Cunningham and Collins, 2002). The flow configurations that we propose for the time interval corresponding to the siphon event actually entail a warming in the RiC, although our results prove to be not fully conclusive in this respect. The great shoaling of this corridor implies that the Atlantic inflow and the Mediterranean outflow (if present) come from shallower depths and carry higher temperature. If deep-water Atlantic organisms were able to reach the RiC at 7.2 Ma when this corridor was as shallow as 100 m, then this may have been due to upwelling in the Atlantic Ocean not captured by our model.

3.4.4. Further implications

The systematic behaviour of these gateways in terms of exchange patterns is useful to determine the depth of a corridor relative to the other. For instance, evidence for outflow in both gateways would not only automatically relate to two-way flow through both but also indicate that the shallow corridor was deeper than the mid-depth of the other gateway (Figures 3.4b and 3.4c). When evidence for inflow is found in a corridor, it is important to note that this could be an expression of rotational two-layer flow. In this case, as explained above, evidence from another location to the north of where evidence for inflow was found is required to determine if the corridor accommodated one- or two-layer flow. If one-layer flow occurred, this may be taken to indicate that the corridor was shallower than half the depth of the other one (Figures 3.4a and 3.4d). Our results also entail an important consequence regarding the reconstructions of the time of gateway closure. In a double-gateway configuration, the disappearance of evidence for outflow from the sedimentary record does not necessarily indicate that the gateway was closed. According to our results, estimates of the age of closure of the Guadalhorce corridor based on this criterion (Pérez-Asensio et al., 2012) are too old.

3.5. Conclusions

This model analysis offers, for the first time, physics-based insight into the functioning of the Late Miocene Betic and Rifian corridors that connected the Mediterranean and the Atlantic prior to the Messinian Salinity Crisis. Our results show that the water exchange through these two corridors depends predominantly on the depth of a corridor relative to the other. More specifically, both corridors present two-way flow (i.e., antiestuarine exchange) unless the shallow gateway is shallower than about the mid-depth of the deeper corridor. We show that the configuration of the flows postulated in the "siphon theory" by Benson et al. (1991) is unlikely from a physics perspective. Combining our model results with the information available regarding the evolution of the corridors, we propose new, model-based flow patterns for the time interval defined for the "siphon event". The finding that the exchange pattern varies systematically depending only on the depth ratio of the corridors allows us, even from limited geological evidence, to gain valuable insight regarding the double-gateway geometry: (i) outflow evidence in a corridor automatically relates to two-way flow; (ii) evidence for inflow could be the result of one-way flow or a rotational two-layer flow; in this case evidence from a location further north would clarify if this corresponded to one- or two-layer flow; (iii) one-way flow in a corridor indicates that this corridor was shallower than half the depth of the deeper gateway; (iv) outflow disappearance in a corridor does not necessarily indicate its closure; and (v) two-way flow in the two gateways indicates that the shallower corridor was deeper than the mid-depth of the other.

Acknowledgements

Chapter 4: Quantitative analysis of Paratethys sea level change during the Messinian Salinity Crisis

ABSTRACT

At the time of the Messinian Salinity Crisis in the Mediterranean Sea (i.e., the Pontian stage of the Paratethys), the Paratethys sea level dropped also. Evidence found in the sedimentary record of the Black Sea and the Caspian Sea has been interpreted to indicate that a sea level fall occurred between 5.6 and 5.5 Ma. Estimates for the magnitude of the fall range between tens of meters to more than 1500 m. The purpose of this study is to provide quantitative insight into the sensitivity of the water level of the Black Sea and the Caspian Sea to the hydrologic budget, for the case that the Paratethys is disconnected from the Mediterranean. Using a Late Miocene bathymetry based on a palaeographic map by Popov et al. (2004) we quantify the fall in sea level, the mean salinity, and the time to reach equilibrium for a wide range of negative hydrologic budgets. By combining our results with (i) estimates derived from a recent global Late Miocene climate simulation and (ii) reconstructed basin salinities, we are able to rule out a drop in sea level as large as 1000 m in the Caspian Sea during this time period. In the Black Sea, however, such a large sea level fall cannot be fully discarded.

4.1. Introduction

During the Eocene-Oligocene, as a consequence of the incipient formation of the Alpine chains, a new marine realm separated to the north of the Tethys Ocean: the Paratethys (Rögl, 1999). This large epicontinental sea extended over southern Europe and consisted of several sub-basins of which the Black, Caspian and Aral seas are the modern remnants. Later in time, during the Middle to Late Miocene, the progressive enclosure of the Paratethys gave rise to further differentiation between the Central Paratethys (Pannonian basin) and the Eastern Paratethys (Black Sea basin and Caspian basin; e.g., Rögl, 1996; see Figure 4.1a). The Paratethys sub-basins were episodically connected through shallow channels (e.g., Popov et al., 2006; Kroonenberg et al., 2005) and sporadic Mediterranean-Paratethys connections have been documented (e.g., Popov et al., 2006; Suc et al., 2011; Vasiliev et al., 2013).

In the Late Miocene, the Mediterranean Sea experienced the Messinian Salinity Crisis (5.97–5.33 Ma; Krijgsman et al., 1999a; Manzi et al., 2013). During this extreme geological event a thick sequence of evaporites was deposited in the basin in response to tectonic and glacio-eustatic restriction of the connection with the ocean (Roveri et al., 2014). The consensual view is that during the climax of the Messinian Salinity Crisis (from 5.61 to 5.55 Ma) the Mediterranean sea level dropped about 1500 m (e.g., Hsü et al., 1973; Clauzon et al., 1996). Such a fall would have terminated the inflow of Mediterranean waters into the Paratethys, but the Paratethyan water level would not simply mimic the Mediterranean drop due to the presence of sill(s). Instead, the water level of the Paratethys would be controlled locally by the interplay of tectonics (i.e., sill depth) and climate (i.e., hydrologic budget) after disconnection from the Mediterranean (e.g., Krijgsman et al., 2010). With a negative hydrologic budget (i.e., evaporation dominating over freshwater input by precipitation and runoff), the Paratethys sea level would have dropped. A sea level drop below the depth of the channels within the Paratethys would have potentially fragmented the sea into a series of individual sub-basins. From 5.6 to 5.5 Ma, roughly coincident with the climax of the Messinian Salinity Crisis, the Paratethys may indeed have experienced a drop in sea level (e.g., Hsü and Giovanoli, 1979; Popescu, 2006; Gillet et al., 2007; Krijgsman et al., 2010; Leever et al., 2010; Abdullayev et al., 2012; Munteanu et al., 2012). In Paratethys terminology, this occurred during the Pontian stage. The

amplitude of the fall in the Black Sea and the Caspian Sea during this stage is highly debated and estimates range from tens of meters to more than 1500 m.

In this paper, to provide a quantitative basis for the debate, we perform a model analysis of the sensitivity of the levels of the Late Miocene Black Sea and Caspian Sea to the hydrologic budget when the Paratethys is not connected to the Mediterranean Sea. Using a late Messinian bathymetry based on the palaeogeographic map of Popov et al. (2004) we quantify (i) the drop in sea level, (ii) the resulting average basin salinity, and (iii) the time needed for the sea level and salinity to reach equilibrium. This is done for a wide range of negative hydrologic budgets. In our calculations the drop in sea level is determined by the balance between evaporation minus precipitation (E─P) and river discharge (R). We first focus on the entire Paratethys and then study the Black Sea and the Caspian Sea separately. By using hydrologic budgets calculated for the Late Miocene Paratethys from the recent global climate model experiments of Marzocchi et al. (2015) and by comparing our results to salinity estimates inferred from geological data for this time interval, we aim to elucidate the magnitude of the sea level drop consistent with observations in the Black Sea and the Caspian Sea. In particular, we investigate whether a sea level drop of 1000 m or more is possible.

4.2. Model setup

4.2.1. Underlying equations

In this analysis the rate of sea level (SL) drop in the basin studied (i.e., entire Paratethys, Black Sea, or Caspian Sea) is controlled by the surface freshwater flux (i.e., E─P) and the river discharge R (Equation 4.1). With SL for sea level in m, E─P in m/yr, R in m^3/yr, sea level dependent surface area A in m^2, and time t in years, the governing equations reads,

$$\frac{d}{dt} SL = (E - P) - \frac{R}{A\,(SL)} \qquad (4.1)$$

Both E─P and R are assumed to be constant over time. The reduction of the surface area of the basin entailed by a drop in sea level increases the rate of the sea level rise due to river input. In all calculations E─P is greater than R/A at the outset.

Sea level drop and salinity are calculated for the steady state, which is reached when the two terms on the right-hand side become equal.

To calculate the salinity associated with a certain sea level drop, the initial salt content of the basin is divided by the remaining water volume. Over time the salinity of the Paratethys waters varied between marine and fresh (e.g., Schrader, 1978; Popov et al., 2006). To account for this, each calculation is initialised with a range of salinities: 10, 20, or 35 g/kg. Empirical and theoretical studies have shown that evaporation decreases when the salinity of the body of water increases (e.g., Salhotra et al., 1985). We will consider the effect of salinity on the evaporation using the expression proposed in Topper et al. (2013). This consists of a linear fit to observational data regarding the evaporation rate as a function of salinity reported in Warren (2006). In our model setup we do not distinguish between evaporation and precipitation and, consequently, this parameterisation also affects precipitation (i.e., E─P). Following Topper et al. (2013), we assume this to be a valid approach given that other parameterisations are more complex and entail more assumptions. The resulting expression reads,

$$E - P = (E - P)_o \cdot 1.0316 \cdot (1 - 8.75 \cdot 10^{-4} \cdot S) \qquad (4.2)$$

where S is salinity in g/kg and (E─P)$_o$ corresponds to the initial value of E─P before the sea level starts to drop. In each simulation E─P ranges from 0 to 3 m/yr. R is varied between the values that would contribute a sea level rise from 0 to 3 m/yr at the initial sea level, i.e. before any fall in sea level has occurred. In the Mediterranean Sea, the modern value of E─P is 0.6 m/yr (Mariotti et al., 2002) and model studies have yielded 1 m/yr for the Late Miocene (Gladstone et al., 2007). Estimates of present-day E─P are 0.1 m/yr in the Black Sea (Ünlüata et al., 1990) and 0.7 m/yr in the Caspian Sea (Ozyavas et al., 2010). At present the river runoff is 350 km^3/yr (0.8 m/yr) in the Black Sea (Ünlüata et al., 1990) and 301 km^3/yr (0.8 m/yr) in the Caspian Sea (Ozyavas et al., 2010). We therefore expect 0-3 m/yr to cover, by far, the range of E─P and R of the Late Miocene Paratethys.

4.2.2. Bathymetry and hypsometry

The bathymetry used for the calculations is built from the late Messinian palaeogeographic map of Popov et al. (2004), from which a gridded bathymetry with a uniform horizontal resolution of $1/20^o$ x $1/20^o$ is created. The deep and shallow domains distinguished on the palaeogeographic map are set to 2000 m and 100 m, respectively (Figure 4.1a). A smooth transition between these two domains is achieved by the implementation of a continental slope. This consists of a linear increase of the depth from the shelves to 2000 m. As in the present-day Black Sea and Caspian Sea, this slope is considered relatively steep and narrow (e.g., Staneva et al., 2001). Arguing that water depths greater than 1000 m only existed in the central depressions indicated on the map (Popov et al., 2006), the continental slope is inserted on the "deep side" of the outer edge of the shallow domains shown on the map (Figure 4.1a). Next, the horizontal area as a function of depth is computed from the surface until the seafloor at a vertical spacing of one meter (blue hypsometric curve in Figure 4.1b). Because in the bathymetry the shelf is considered 100 m deep starting right at the coastline, the hypsometry starts abruptly. This was found to create numerical instabilities and to correct for this we assume a linear transition between the surface area at 0 m and that at 100 m. To account for a more gradual decrease of the surface area from the continental slope to the deepest basin, we also adopt a linear transition from the surface area at 100 m and that at 2000 m (red curve in Figure 4.1b). Results presented in this paper are computed using the red hypsometric curve. We first focus on the entire Paratethys and, at a later stage, assuming that the gateways connecting the sub-basins were shallow (e.g., Popov et al., 2006), we study the Black Sea and the Caspian Sea separately. The hypsometric curves for the Black Sea and the Caspian Sea are calculated following the same procedure as for the Paratethys (Figure 4.1c and 4.1d). Volume as a function of depth (not shown) is calculated by integration of the red hypsometric curves.
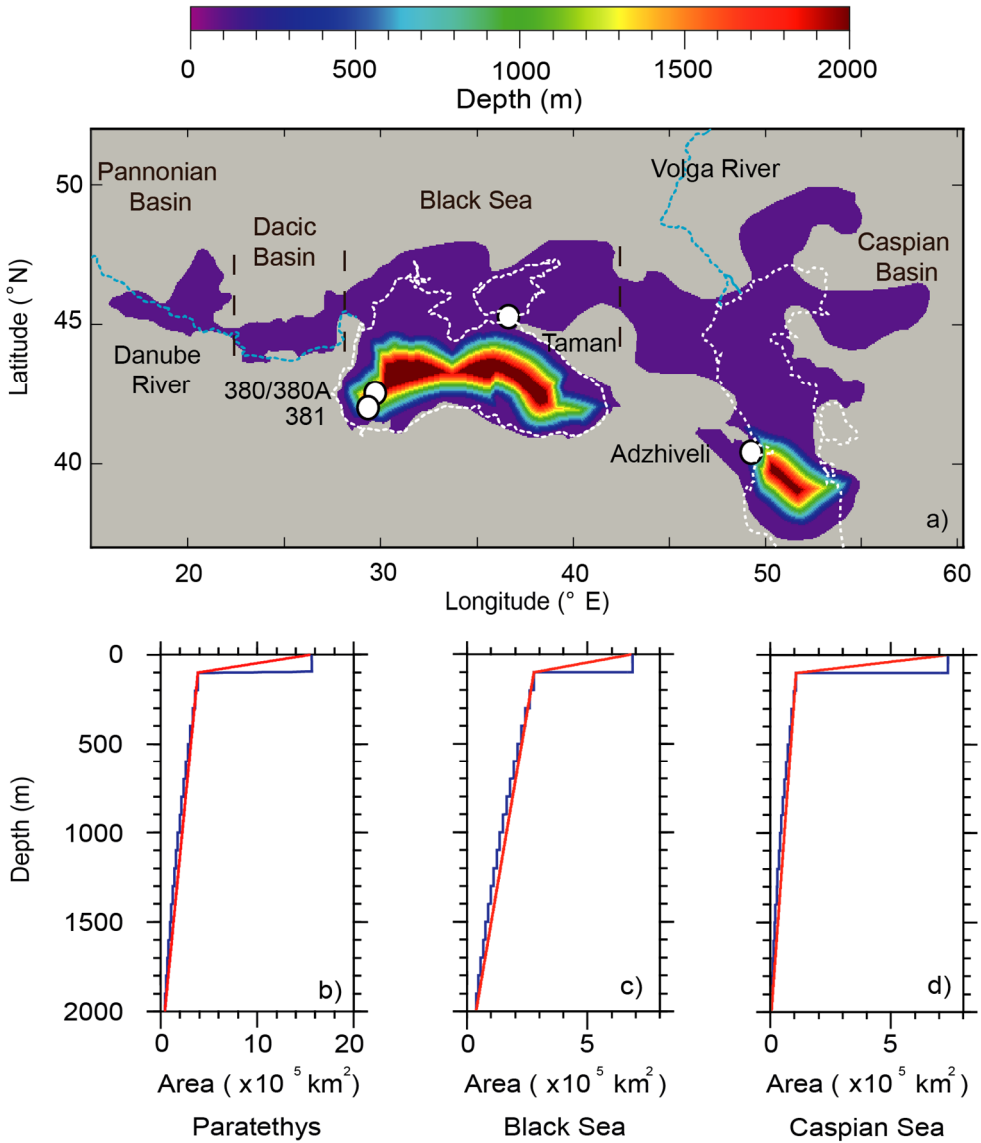
Figure 4.1. (Previous page). Panel (a) shows the late Messinian bathymetry constructed from the palaeogeographic map of Popov et al. (2004). The circles show the location of DSDP sites 380/380A and 381, Taman Peninsula (Russia), and Adzhiveli (Azerbaijan). White dashed lines indicate the present-day coastline of the Black Sea and the Caspian Sea and the blue dashed lines the modern Danube and Volga rivers. Panels (b) to (d) show the hypsometric curves for the Paratethys, the Black Sea and the Caspian Sea, respectively. The blue hypsometric curves are built from the palaeobathymetry of panel (a). In the red curves a linear decrease of the surface area from the surface until 100 m, as well as from 100 m until 2000 m is assumed. Results shown in this paper are calculated with the red curves.

4.2.3. Alternative parameterisations

To test the effect of other parameterisations we perform several additional experiments. We investigate the possibility that the river discharge increases progressively as the sea level drops due to the implied increase of the surface area of the drainage basins. In this case we assume that the river discharge is proportional to the surface area of the drainage basins, following Jauzein and Hubert (1984). When the sea level falls the newly desiccated area is added to the drainage basin. The surface area of the drainage basins at normal sea level is derived from the global Late Miocene climate simulations by Marzocchi et al. (2015).

Because the exact bathymetry of the Late Miocene Paratethys is uncertain, we also explore the sensitivity of results to bathymetric changes in the basins. To this end, we set the shelves to 250 m (instead of to 100 m). We also investigate the case where the continental slope is inserted on the shallow side of the shelf edge. Although this seems a less likely configuration, it does represent a useful alternative to test the robustness of our results. The corresponding hypsometries are presented in Figure 4.2. In this figure hypsometric curves of the modern Black Sea and Caspian Sea are also presented for comparison to the Miocene ones. An important feature is that in the present-day Black Sea and Caspian Sea hypsometric curves the deep domains of the basin occupy a surface area that takes intermediate values between the two Late Miocene curves. A summary of the surface areas and volumes calculated for the entire Paratethys, the Black Sea and the Caspian Sea is presented in Table 4.1.
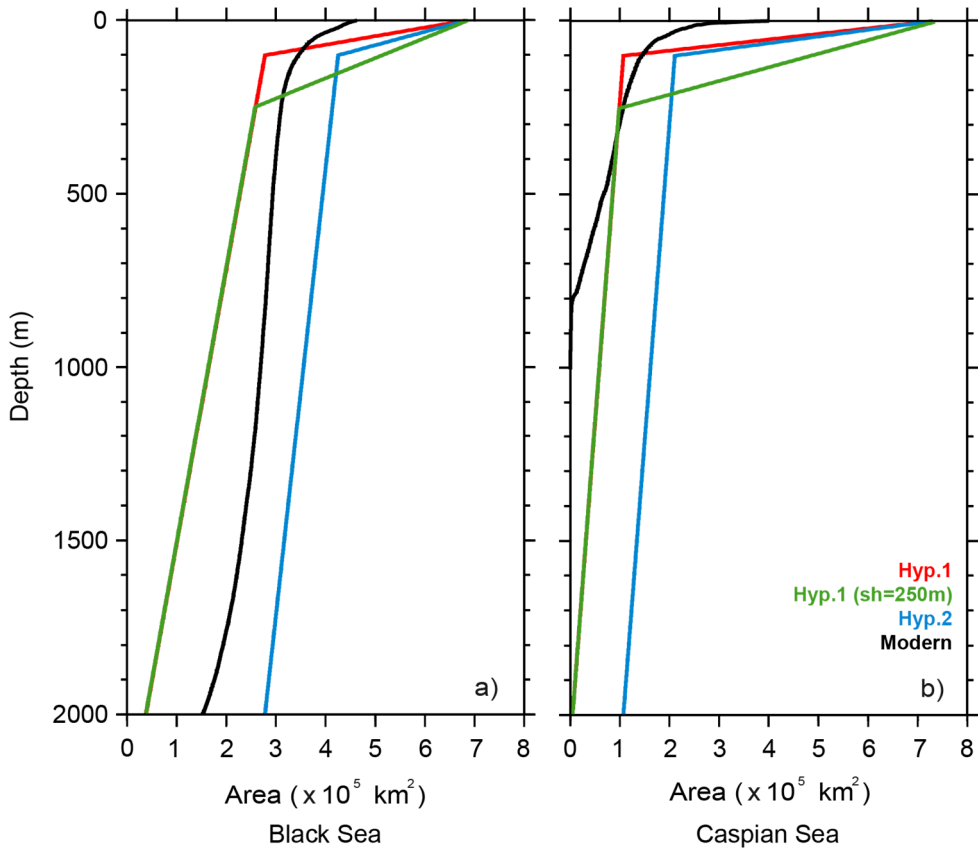
Figure 4.2. Present-day (black line) and Late Miocene (blue, red and green) hypsometries of the Black Sea (a) and the Caspian Sea (b). The red Late Miocene hypsometric curves are based on a bathymetry where the continental slope is introduced on the deep side of the shelf edge ("Hyp. 1"). The green curves differ from the red ones in that the shelves are set to 250 m (instead of 100 m; "Hyp. 1 (sh=250m.)"). The blue Late Miocene hypsometric curves are based on a bathymetry in which the continental slope is inserted on the shallow side of the shelf edge instead ("Hyp. 2"). Bathymetric data used to construct the present-day Black Sea and Caspian Sea hypsometries is extracted from the SRTM dataset (Farr and Kobrick, 2000) and the National Geographical Data Center of the NOAA, respectively.

		Total area (x10^5 km^2)	Area shallow domains (x10^5 km^2)	Area deep domains (x10^5 km^2)	Total volume (x10^5 km^3)	Volume shallow domains (x10^5 km^3)	Volume deep domains (x10^5 km^3)
Late Mioc. Parat.	Hyp. 1	15.6533	11.8057	3.8476	5.0485	0.9907	4.0578
	Hyp. 2	15.6533	9.2951	6.3582	10.8079	1.1162	9.6917
Late Mioc. Black Sea	Hyp. 1	6.8533	4.0751	2.7782	3.4872	0.4884	2.9988
	Hyp. 2	6.8533	2.6006	4.2527	7.2387	0.5621	6.6766
Late Mioc. Casp. Sea	Hyp. 1	7.3607	6.2913	1.0694	1.4878	0.4288	1.0590
	Hyp. 2	7.3607	5.2552	2.1055	3.4957	0.4807	3.0150

Table 4.1. Summary of the surface areas and volumes of the Late Miocene Paratethys, Black Sea and Caspian Sea. Shallow domains correspond to the shelves (i.e., depth smaller or equal 100 m) and deep domains include all depths greater than that. Hypsometry 1 (Hyp. 1) is built from a bathymetry in which the continental slope is introduced on the deep side of the shelf edge. In hypsometry 2 (Hyp. 2) this is done on the shallow side.

4.3. Analysis and results

4.3.1. Reference experiments

The amplitude of the sea level drop, the associated salinity, and the time required to reach equilibrium in the entire Paratethys, Black Sea and Caspian Sea are shown in Figures 4.3, 4.4, and 4.5. Since the river discharge corresponding to an equivalent rate of sea level rise which ranges from 0 to 3 m/yr, is greater when the basin occupies a larger surface area, the maximum R considered is greatest in the Paratethys, followed by the Caspian Sea and the Black Sea (Table 4.1). In these experiments the basins are initialised with a salinity of 10, 20, or 35 g/kg and E─P is considered to be either dependent or independent of salinity.

Nearly the entire range of E─P and R tested results in a sea level fall smaller than 100 m (in Figure 4.3 the purple colour dominates). For a specific basin, combinations of E─P and R with which the sea level drops below the shelves (i.e., below 100 m) are the same regardless of the initial salinity and E─P parameterisation. Comparing panels corresponding to the same basin, only subtle variations of the amplitude of the sea level drop appear when R is very small. When R is close to 0 m/yr the sea level drops between 1500 and 2000 m depending on the initial salinity of the basin and the way in which E─P is defined. For a given basin, the base level fall is greater when E─P is not a function of salinity (e.g., Figures 4.3a-4.3d). When E─P is parameterised as a function of salinity, E─P decreases linearly as salinity increases and this reduces the magnitude of the sea level drop compared to when E─P is constant. For this reason, in this case, in a certain basin, the sea level drops less when the basin is initialised with a higher salinity (e.g., panels 4.3b-4.3d). When E─P is independent of salinity the sea level drop remains the same regardless of the initial salinity prescribed. For this case we only consider an initial salinity of 20 g/kg.

For a given E─P, the absolute value of R required for a sea level drop below the shelves (i.e., larger than 100 m) is smaller in the Black Sea and the Caspian Sea individually than for the Paratethys as a whole (Figure 4.3). Once the sea level drops below the shelves the surface area of the basins becomes substantially smaller (see Figure 4.1 and Table 4.1). River discharge, which is assumed to be constant, is spread over a smaller area and contributes a greater sea level rise. When the horizontal surface area of the basin at levels deeper than the shelves is small, the balance between E─P and R will therefore be attained at higher positions of the sea level. When the Black Sea and the Caspian Sea are taken separately, the surface area below 100 m depth is smaller than when the entire Paratethys is considered. For this reason, the absolute value of R for which the sea level drops below the shelves is smaller for the Black Sea and the Caspian Sea individually. To achieve a sea level fall of 100 m or larger, a substantially smaller R is required for the Caspian Sea than for the Black Sea because in the Caspian Sea the deep domains of the basin occupy a considerably smaller area (Figure 4.1 and Table 4.1).
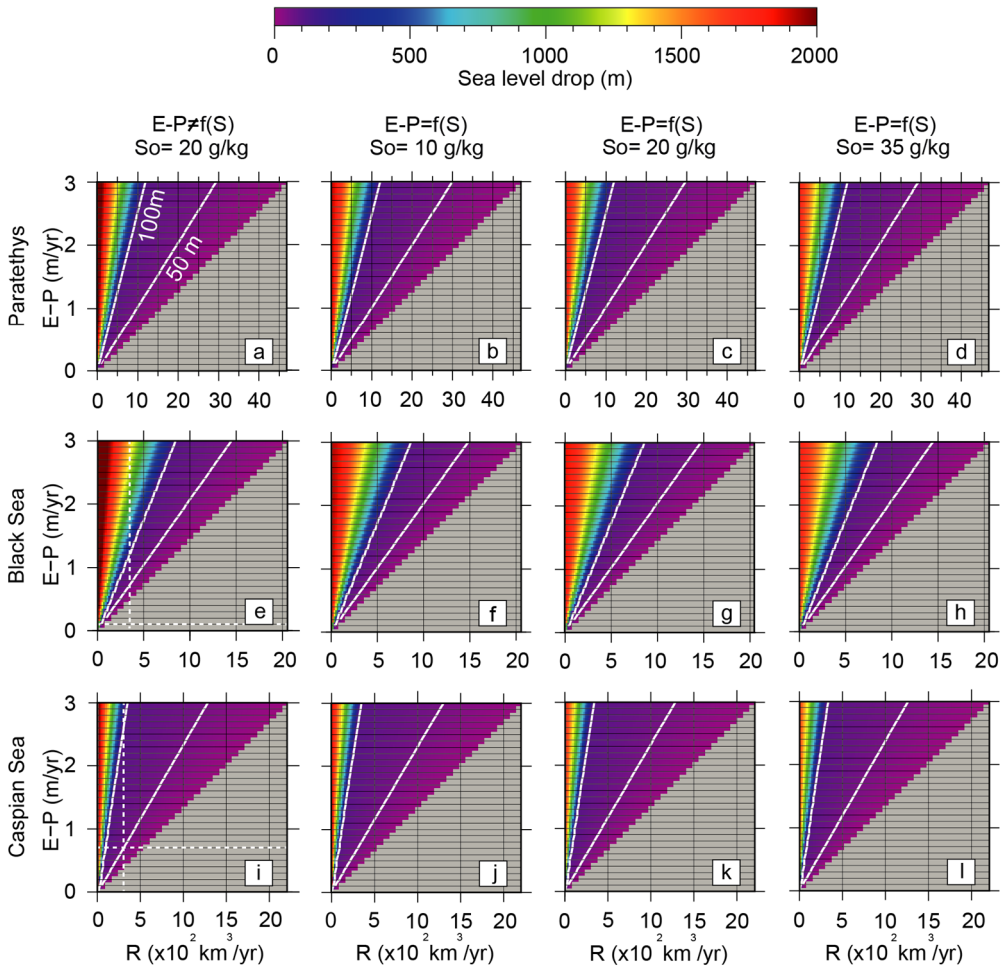
Figure 4.3. Drop in sea level for the entire Paratethys (a-d), the Black Sea (e-h), and the Caspian Sea (i- l) for a wide range of hydrologic budgets. As indicated in the figure, in the first panel of each row of four, E─P does not depend on salinity and the basins are initialised with a salinity of 20 g/kg. In the next three panels, E─P is a function of salinity and the initial salinity of the basins 10, 20, and 35 g/kg, respectively. White continuous lines indicate a sea level drop of 50 and 100 m. White dashed lines in panels (e) and (i) show the present-day hydrologic budgets of the Black Sea and the Caspian Sea, respectively. The Black Sea hydrologic budget derives from Ünlüata et al. (1990) and the Caspian Sea budget from Ozyavas et al. (2010). Grey areas denote regions where the hydrologic budget is positive.
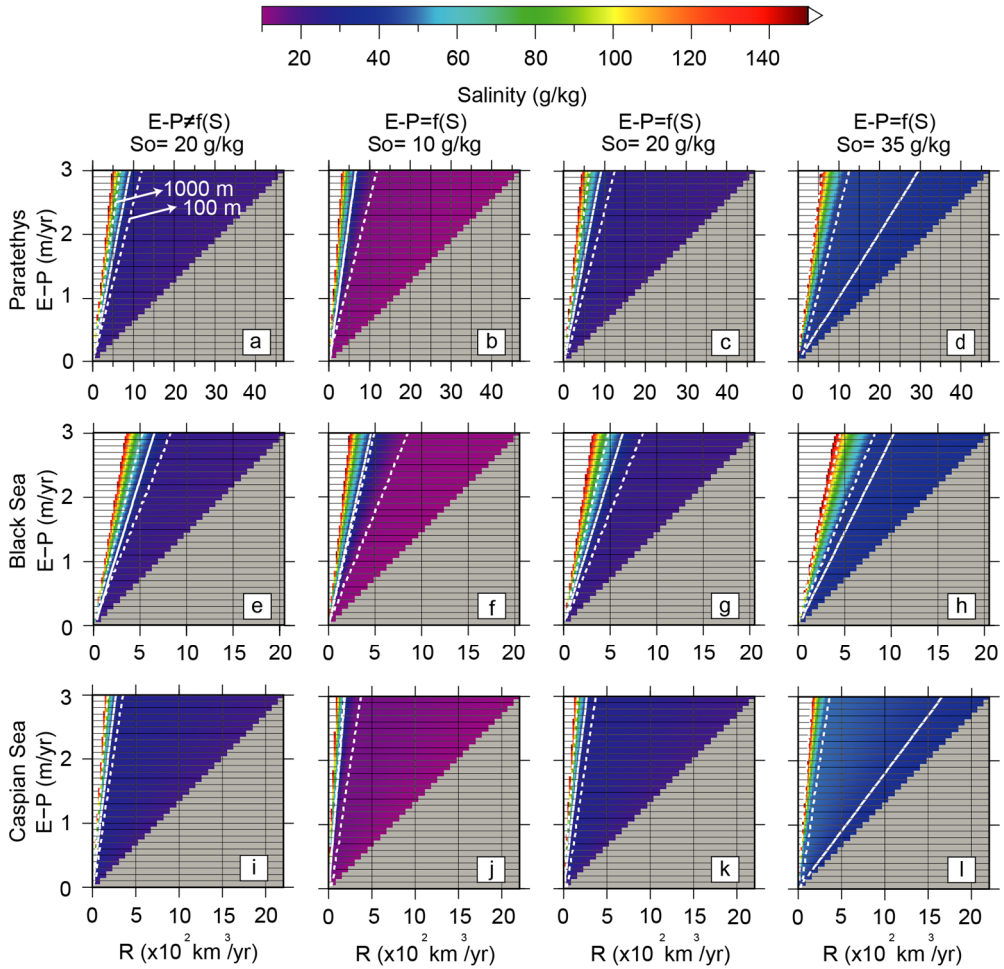
Figure 4.4. Salinity at equilibrium in the Paratethys (a-d), Black Sea (e-h) and Caspian Sea (i-l) for a wide range of hydrologic budgets. In the first panel of each row of four, E─P is not dependent on salinity and initial salinity is 20 g/kg. In the next three panels E─P is a function of salinity and the basins are initialised with 10, 20, or 35 g/kg, respectively. White continuous lines indicate a salinity of 40 g/kg and white dashed lines show the hydrologic budgets that correspond to a 100 and 1000 m sea level drop, as indicated in panel (a). The areas coloured in grey correspond to positive hydrologic budgets. Note that in panels (b), (f) and (j) the contours showing the 1000 m sea level drop and 40 g/kg closely overlap.

Salinity at equilibrium is shown in Figure 4.4. Given that no gypsum or halite was deposited in the Black Sea and in the Caspian Sea during the Late Miocene, we set the upper limit of the colour scale to 150 g/kg for a better visualisation of results (i.e., the value at gypsum saturation). Salinities greater than 150 g/kg are shown in white. Salinity only starts to rise substantially relative to the initial salinity of the basin when the sea level is below the shelves. Although the shelves occupy a large surface area, the volume from the surface to the shelf depth is only a small part of the total volume of the basin and the salt contained in the shelves is small. In the Black Sea the shelves occupy 59% of the total area but only contain about 14% of the total volume. This is even more pronounced in the Caspian Sea, where the numbers are 85% and 29%, respectively. Once the sea level drops below the shelves the surface area becomes substantially smaller in the Caspian Sea than in the Black Sea (Table 4.1). For a given sea level drop larger than the shelves, salinity would rise more in the Caspian Sea than in the Black Sea (e.g., see the 1000 m sea level drop contour of Figures 4.4e-4.4l).

Figure 4.5 shows the time to equilibrium for the entire Paratethys, the Black Sea and the Caspian Sea. For a given basin, essentially no deviations due to different E─P parameterisation and initial salinity occur. For brevity we here focus on the case where E─P is a function of salinity and the basins are initialised with a salinity of 10 g/kg. Time to equilibrium never exceeds 80-90 kyr. We observe that for most of the hydrologic budgets tested a steady state is reached within 10 kyr. Time to equilibrium is shortest for sea level drops over the shelves (i.e., smaller than 100 m). In the areas adjacent to the boundary between a positive and a negative hydrologic budget time to equilibrium is short, but slightly longer for small values of E─P and R. Time to equilibrium is longest when the sea level drops below the shelves because this entails the evaporation of a greater volume of water which takes longer, especially for small fluxes of R and E─P.
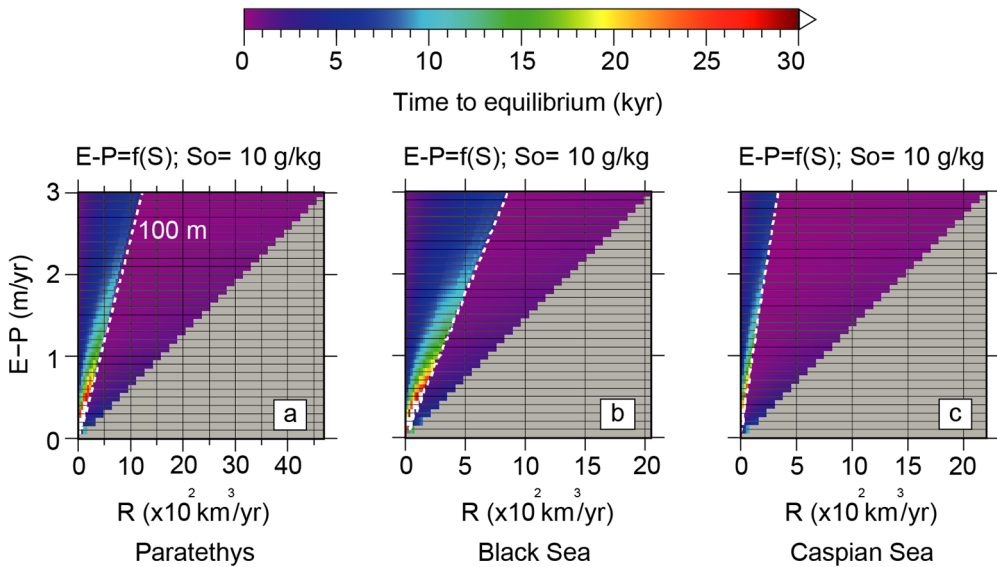
Figure 4.5. Time to reach equilibrium in the Paratethys (a), Black Sea (panel b), and Caspian Sea (c). E─P is parameterised as a function of salinity and the basins are set to an initial salinity of 10 g/kg. The discontinuous lines correspond with the hydrologic budgets for which the sea level drops 100 m. The grey regions of the plot indicate positive hydrologic budgets.

4.3.2. Additional experiments: Alternative parameterisations

For brevity, and because it proves representative, we will examine the role of the other parameterisations only for the case where E─P is a function of salinity and the basins have an initial salinity of 10 g/kg. Results obtained with river discharge depending on drainage area are depicted in panels (a) to (c) of Figure 4.6. Due to the increase in R, for a given E–P and starting value of R, the sea level falls less compared to the equivalent reference experiment (see Figures 4.3b, 4.3f, 4.3j). For this reason a specific hydrologic budget also entails a smaller salinity (not shown). Time to equilibrium proves not significantly different (not shown).

The sea level drop in the whole Paratethys, Black Sea and Caspian Sea when the shelves are set to a maximum depth of 250 m is shown in Figures 4.6d to 4.6f. Because we assume a linear decrease from the surface area at the surface to that at 250 m, shelves are deeper everywhere (see Figure 4.2). Notwithstanding the greater
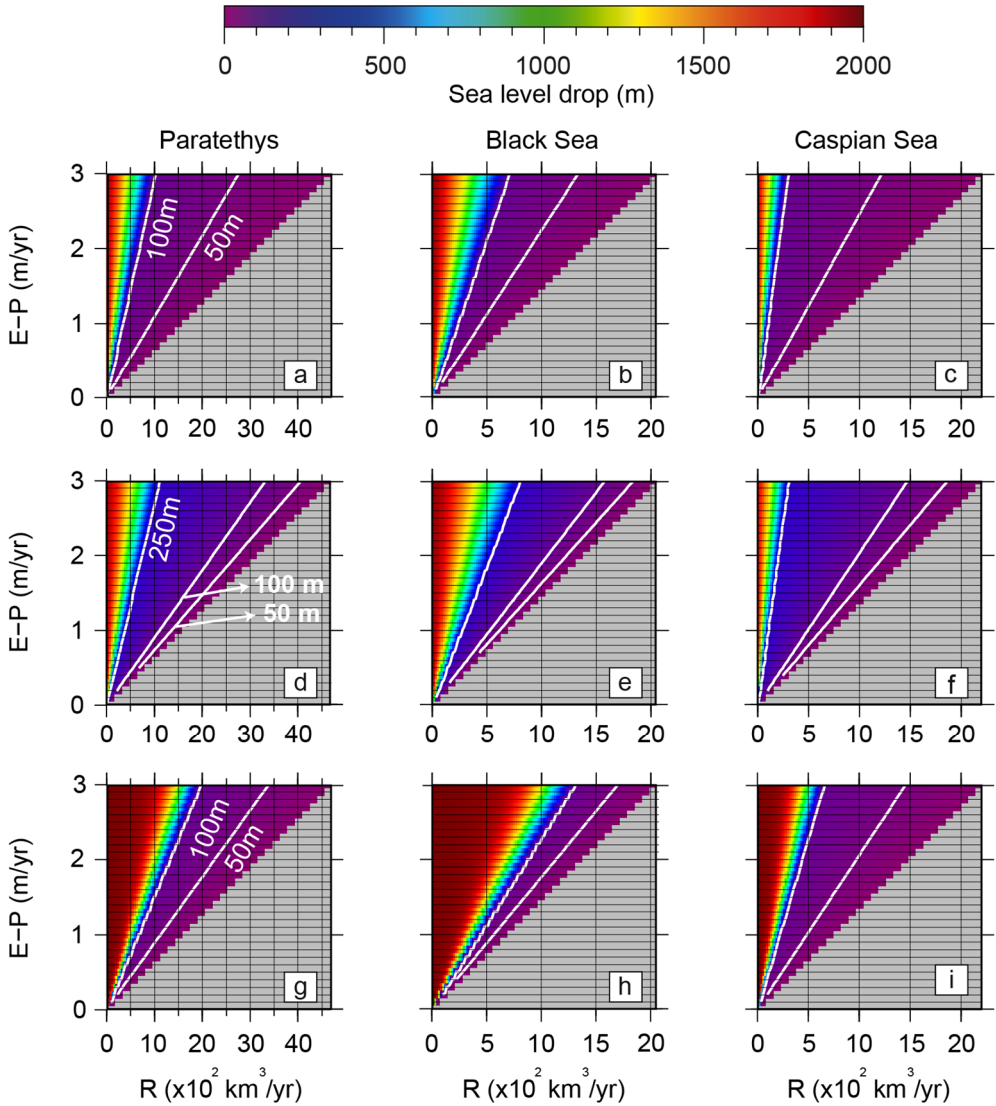
Figure 4.6. Sea level drop in the Paratethys as a whole (a, d, g), Black Sea (b, e, h) and Caspian Sea (c, f, i) as a function of the hydrologic budget and for several alternative parameterisations. E−P is a function of salinity and initial salinity of the basins is 10 g/kg. In panels (a) to (c) the river discharge is proportional to the surface area of the drainage basins as proposed by Jauzein and Hubert (1984). In panels (d) to (f) the shelves are set to 250 m. In panels (g) to (i) the continental slope is inserted on the shallow side of the shelf edge. White contours indicate a sea level drop of the amplitude specified in the figure. Grey areas correspond to positive hydrologic budgets.

depth of the shelves, the hydrologic budgets for which sea level drops below the shelves remain roughly unchanged compared to the equivalent reference experiment (cf. Figures 4.3b, 4.3f, 4.3j). Comparing these results to equivalent experiments with shallow shelves we find that a specific hydrologic budget now entails a slightly higher salinity (not shown). Because shelves are deeper, hydrologic budgets that drop the sea level over the shelves entail a greater fall in sea level and therefore higher salinity. For hydrologic budgets that correspond to sea level drops below the shelves salinity is slightly greater due to the deeper nature of the shelves, which increases the salt content of the basin. For each basin, time to equilibrium for sea level drops over the shelves is somewhat longer than that in the reference experiments, but it never exceeds 10 kyr (not shown). For larger falls in sea level time to equilibrium is very similar to that in the reference experiments (not shown).

Finally, we consider the case that the slope is introduced on the shallow side of the outer edge of the deep domains. The sea level drop for the entire Paratethys, the Black Sea and the Caspian Sea is shown in Figures 4.6g, 4.6h, and 4.6i, respectively. With this hypsometry, in a given basin and for a specific hydrologic budget, the sea level stabilises at greater depth than in the previous experiments (see Figure 4.3 and Figures 4.6a to 4.6f). This is a direct consequence of the fact that the deep domains of the basin are now more extensive and the area for which R/A balances E–P is only found at greater depth (Figure 4.6g-4.6i). Because of this, the associated salinity is also higher (not shown). It takes a longer time to reach equilibrium than in the equivalent reference experiment, especially when E─P and R are small (not shown). However, time to equilibrium never exceeds 10 kyr for sea level drops over the shelves and 100 kyr for sea level drops below them (not shown).

4.4. Discussion

4.4.1. A large intra-Pontian sea level drop in the Black Sea?

During Deep Sea Drilling Project Leg 42b a shallow-water stromatolitic dolomite unit, the so-called Pebbly Breccia, was recovered from the Black Sea at modern water depths deeper than 1700 m at sites 380A and 381 (see location in Figure 4.1; Ross et al., 1978). Based on biostratigraphic studies it was concluded that the Pebbly Breccia had a Late Miocene age (e.g., Gheorghian, 1978; Jousé and Mukhina, 1978). However, in the 1970s age control on the Paratethys record was poor and the age assigned to this unit was questioned (Kojumdgieva, 1979). This notwithstanding, Hsü and Giovanoli (1979) proposed that the unit formed in response to a 1600 m amplitude sea level fall coeval with the Messinian Salinity Crisis. Further studies correlated erosional surfaces observed in seismic profiles from the Black Sea to the Messinian Salinity Crisis, supporting the hypothesis that a sea level drop larger than 1500 m occurred during the Late Miocene (e.g., Gillet et al., 2003, 2007; Munteanu et al., 2012).

On the basis of new seismic surveys in the western Black Sea, Tari et al. (2015) conclude that that the Pebbly Breccia is allochthonous. Biostratigraphic and magnetostratigraphic studies have led to greatly improved age control on the Paratethyan successions (e.g., Vasiliev et al., 2005; Stoica et al., 2013) and new dating shows that the Pebbly Breccia is older than the Late Miocene (Grothe et al., 2014). Also, lithological and faunal evidence from Taman (Figure 4.1) has been interpreted to indicate a sea level drop of 50-100 m at 5.6 Ma (Krijgsman et al., 2010). However, the target section contains a hiatus at 5.6 Ma and the authors point out that their estimate must be considered a minimum. The seismic surveys of Tari et al. (2015) show that the Late Miocene incisions over the Black Sea palaeoslope have a subaqueous origin. This, they argue, excludes the possibility of a sea level drop as large as 1600 m.
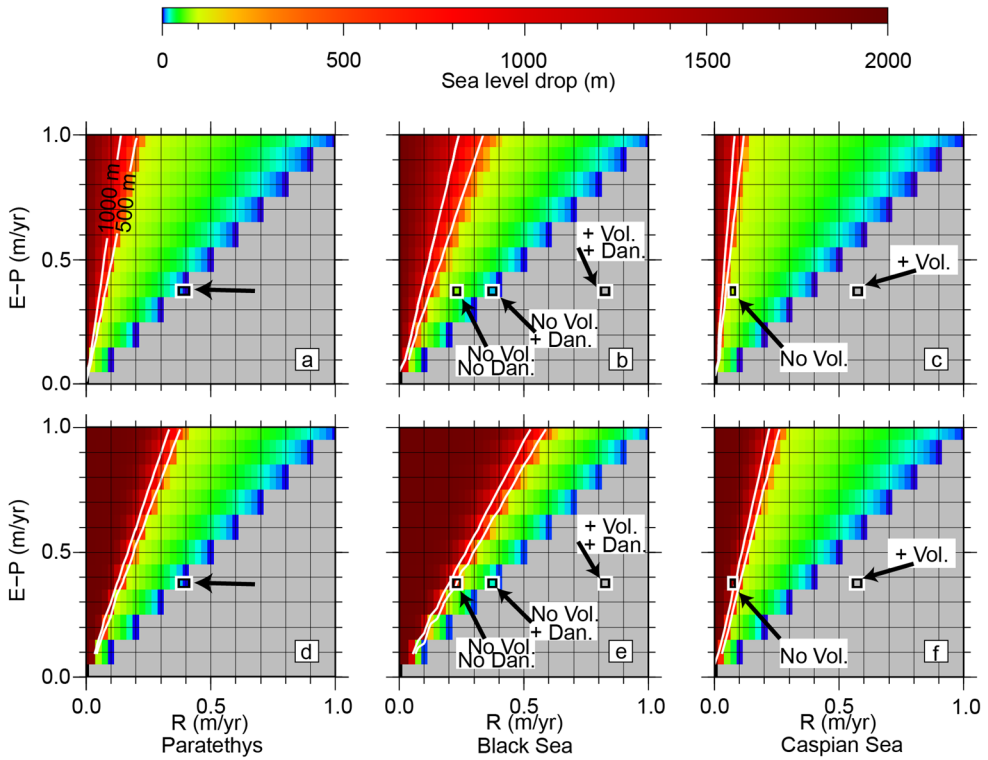
Figure 4.7. Estimated sea level drop for the entire Paratethys (a and d), Black Sea (b and e), and Caspian Sea (c and f). Note that the x-axis is now expressed in (m/yr). In all cases E—P is prescribed as a function of salinity and the basins are initialised with 10 g/kg. In (a) to (c), the hypsometry used for the calculations is built from a bathymetry where the continental slope is inserted on the deep side of the shelf edge. In panels (d) to (f), the hypsometry used for the calculations is constructed from a bathymetry where the continental slope is inserted on the shallow side of the shelf edge instead. The squares indicate the hydrologic budgets derived from the global climate simulations by Marzocchi et al. (2015). "Dan." and "Vol." refer to the Danube and Volga rivers, respectively. White lines indicate a sea level drop of 500 and 1000 m. Grey areas indicate positive hydrologic budgets.

Can we use our analysis to assess the likelihood of a large sea level drop in the Black Sea? We will assume that the level of the Paratethys does not simply follow the falling level of the Mediterranean, in other words, that the two are separated by a sill located higher than the lowered Mediterranean water surface. Arguing that the connection between the Black Sea and the Caspian Sea was shallow (e.g., Popov et al., 2006), we determine the hydrologic budgets that would cause a 1000 m sea level drop in the Black Sea basin in isolation. We take E─P to be no greater than 1 m/yr, the value proposed for the Mediterranean Sea during the Messinian Crisis (Gladstone et al., 2007). To achieve a 1000 m sea level drop in the Black Sea, R has to be close to 0.23 m/yr (i.e., 158 km^3/yr) or smaller if E─P is less than 1 m/yr (Figure 4.7b). This value of R is about two times smaller than the modern river discharge into the Black Sea (350 km^3/yr; Ünlüata et al., 1990) and is close to the present-day Danube River discharge (198.68 km^3/yr; Garnier et al., 2002).

While these numbers perhaps already speak against a large-magnitude drop, it would clearly help to have a constraint on the hydrologic budget at the time. For this we turn to Marzocchi et al. (2015) who performed experiments with a global ocean-atmosphere-vegetation coupled model for the Late Miocene. We calculated the annual mean hydrologic budget of the Paratethys averaged over the duration of the full Late Miocene precession cycle simulated by Marzocchi et al. (2015). The methodology, which is derived from Gladstone et al. (2007), and the hydrologic budgets calculated from the simulations of Marzocchi et al. (2015), are presented in the Supplementary material. In the hydrologic budget calculations the "en route" evaporation from the catchment area to the basin is not taken into account. This implies a slight overestimation of the runoff which may not have been larger than 5% (pers. comm., Rens van Beek; see also Torcellini et al., 2003). We account for this and also for the fact that, since the configuration of the Late Miocene drainage system is uncertain (e.g., Gillet et al., 2007; Munteanu et al., 2012), there are different possibilities as to the location of discharge of the Danube and the Volga (Figure 4.7 and see Figures 4.8a-4.8c also). It proves that only in the case that we assume that neither of these rivers enters the Black Sea, the hydrologic budget takes significantly negative values (i.e., E─P > R; Figure 4.7b). This would result in a sea level drop of about 75 m and corresponds to an equivalent freshwater flux (i.e., E─P─R) between 0.14 and 0.15 m/yr─which is substantially smaller than that of the present-day
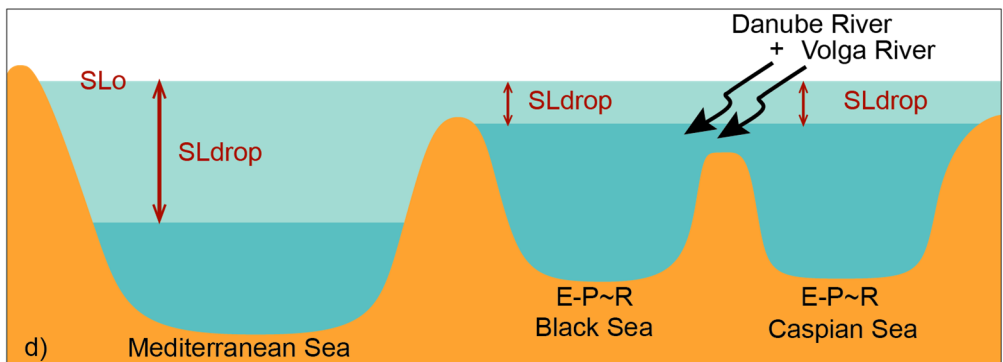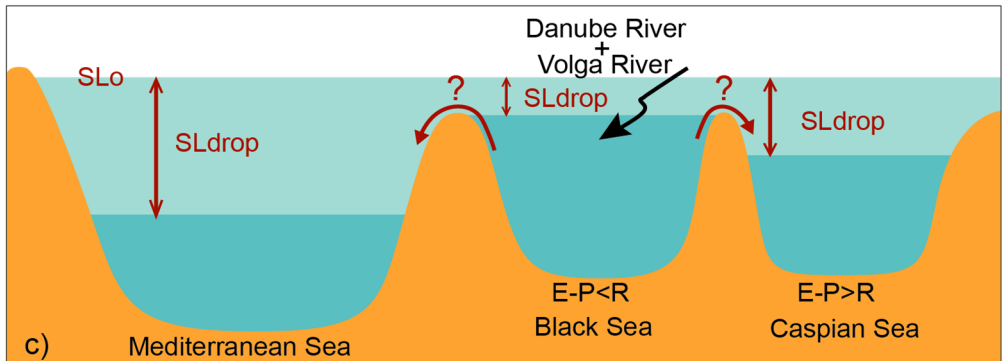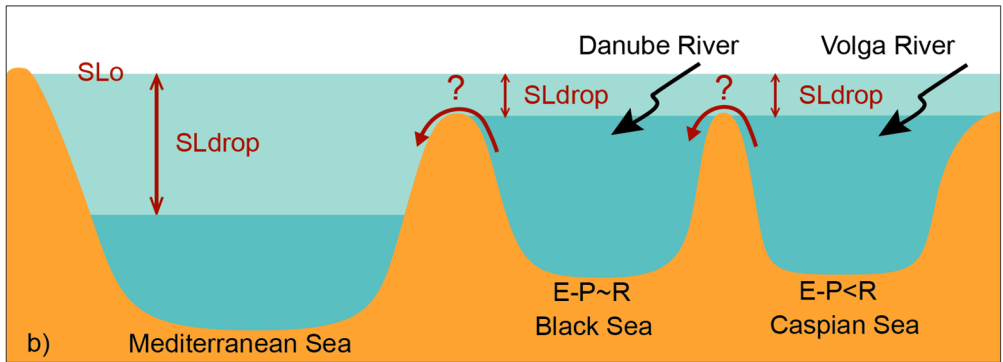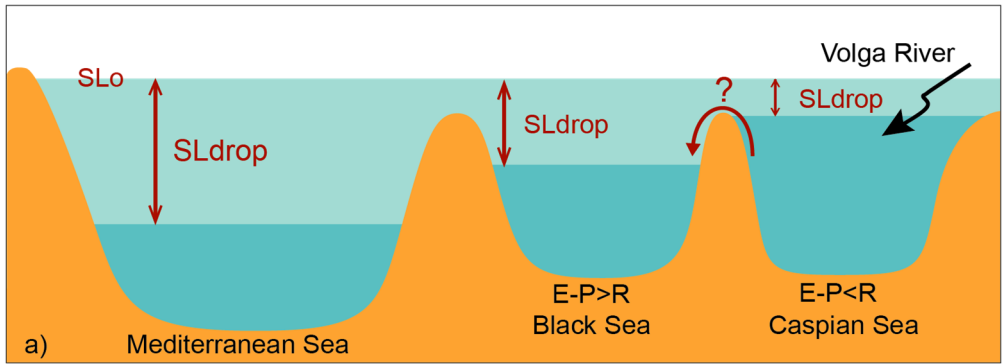
Figure 4.8. (Previous page). Schematic illustration of the sea level configuration in the Black Sea and the Caspian Sea for different configurations of the sills between the basins and using the hydrologic budgets from Marzocchi et al. (2015). In panels (a) to (c) the sill between the Mediterranean Sea and the Paratethys (most likely via the Aegean region; Popov et al., 2006) has a similar depth to that between Black Sea and the Caspian Sea. Once the Mediterranean sea level falls below the connecting sill, the Black Sea and the Caspian Sea become separated basins and develop their own hydrologic budgets. In panel (d) the sill between the Black Sea and the Caspian Sea is deeper than that to the Mediterranean. A lowering of the Mediterranean sea level below the sill does not separate the Black Sea and the Caspian Sea and both basins would have the same hydrologic budget. Initial sea level is indicated as SLo. Arrows between basins indicate possible overspilling from a basin into another.

Mediterranean Sea (0.5 m/yr). This indicates that even in the extreme case that none of the major rivers was flowing into the Black Sea the hydrologic budget calculated from the simulations by Marzocchi et al. (2015) does not correspond to a 1000 m sea level drop. In contradiction with the relatively small negative budgets inferred from Marzocchi et al. (2015), hydrogen isotopes measured on alkenones ($\delta D_{alkenone}$) from the Black Sea suggest prevailingly dry conditions and likely a strongly negative hydrologic budget for this time period (Vasiliev et al., 2013, 2015). As an alternative explanation, the heavy $\delta D_{alkenones}$ signal could represent a Mediterranean signal transferred into the Paratethys by evaporation.

Another way to constrain past sea level is via the salinity of the basin waters. Surface salinity observations reported by Schrader (1978) in sites 380/380A and 381 have recently been dated by van Baak et al. (in press) using a new high-resolution age model. In borehole 380/380A one of the diatom species used to reconstruct surface salinity (*Coscinodiscus stokesianus*) shows an abrupt increase in abundance during the time interval of the Messinian crisis. The salinity preference of this species is unknown and this causes salinity estimates to be subject to large uncertainty. Van Baak et al. (in press) considers both the possibility that this species represents fresh-to-brackish conditions (as done in Schrader, 1978) and the case that it indicates a marine environment. Comparing the estimated values just prior to 5.6 Ma with the maxima inferred for the interval from 5.6 to 5.5 Ma, the first possibility considered by van Baak et al. (in press) yields a change from a salinity of 3 to maximally 23 g/kg.

The second case gives a change from a salinity of 10 to, at the highest, 25 g/kg. Combined with our model calculations these changes would correspond to a sea level fall of 1400 m and 785 m, respectively (Figure 4.9). These values are clearly higher than those inferred from the climate model results. However, we must keep in mind that salinity reconstructions are uncertain to start with. Also, whereas the diatoms provide us with an estimate of sea-surface salinity, our model considers basin-averaged values. Salinity at shallow depths is more prone to change in response to surface processes and, for that reason, may show more extreme salinity variation.

To what extent are the insights reached so far robust in view of choices made in setting up our model? In Section 4.3.2 we find that in the case that the river discharge increases gradually as the sea level drops, for a given basin and a hydrologic budget, the sea level falls slightly less than in the equivalent reference experiment (Figure 4.3 and Figures 4.6a-4.6c). When the shelves are set to 250 m, a given combination of E─P and R results in a slightly larger sea level drop over the shelves relative to the equivalent reference experiment, but it does not affect the magnitude of sea level drops below the shelves (Figure 4.3 and Figures 4.6d-4.6f). These alternative parameterisations thus do not affect much the preceding discussion. In contrast, when the alternative hypsometric curve is considered (blue curve in Figure 4.2), a given hydrologic budget corresponds to a substantially greater sea level drop (Figure 4.3 and Figures 4.6g-4.6i). In Figure 7e we observe that when this hypsometry is used the Black Sea hydrologic budget derived from the simulations of Marzocchi et al. (2015) excluding the Danube and Volga rivers now results in a sea level drop of about 690 m. Surface salinity estimates from van Baak et al. (in press) correspond to a sea level drop of 1675 and 1080 m, respectively (see Figure 4.9b). Thus, as found with the reference hypsometry, a 1000 m sea level drop is possible on the basis of salinity reconstructions but it is not supported by the climate modelling of Marzocchi et al. (2015).
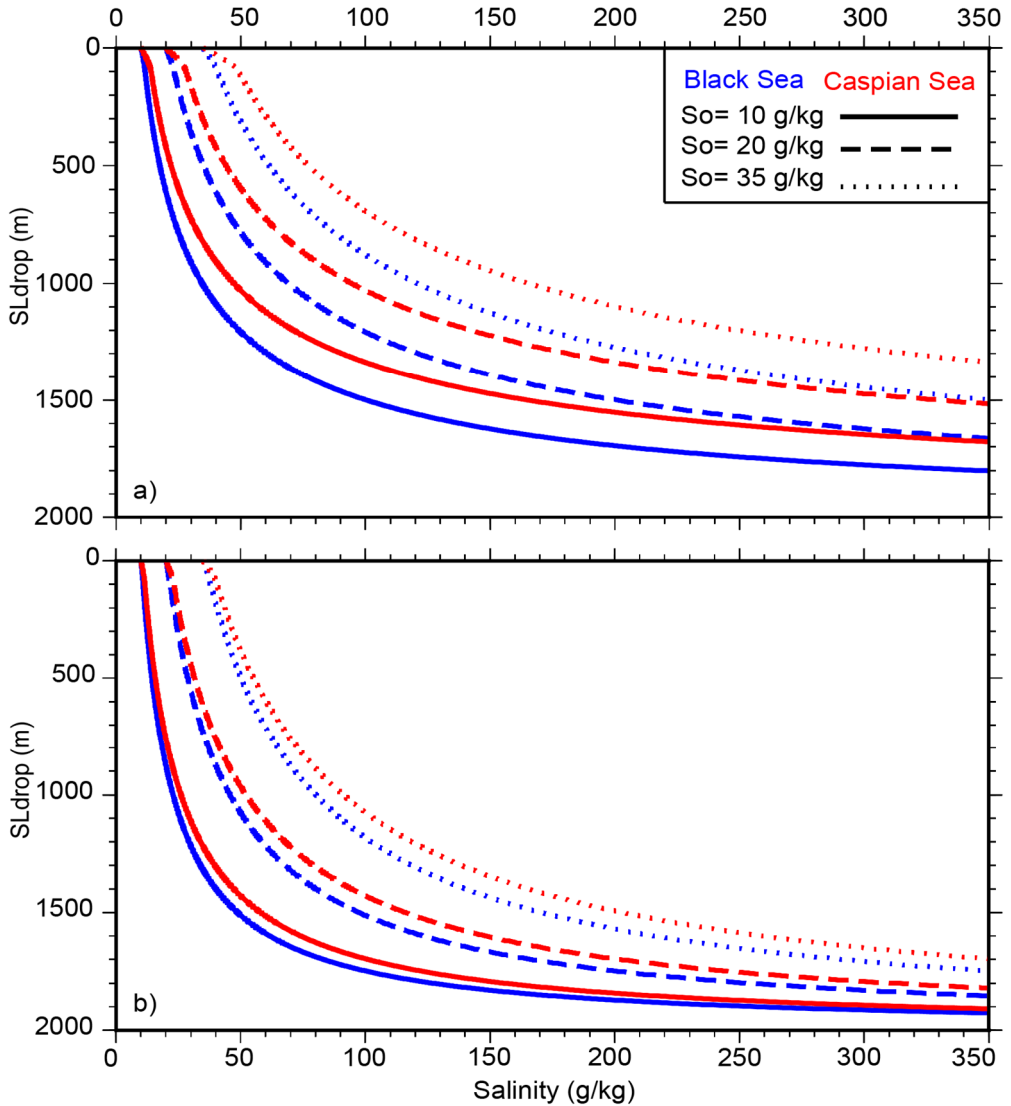
Figure 4.9. Salinity (g/kg) as a function of the sea level drop (m) in the Black Sea (blue lines) and Caspian Sea (red lines) when the basins are isolated. The basins are initialised with a salinity (So) of 10 g/kg (solid lines), 20 g/kg (dashed lines) and 35 g/kg (dotted lines). The hypsometries used are built from either a bathymetry in which the continental slope is introduced on the deep (a) or the shallow sides (b) of the shelf edge.

To summarise, the sea level drop calculated on the basis of model-derived hydrologic budgets differs from that based on geological salinity estimates. The budgets from the simulations of Marzocchi et al. (2015) never correspond to a sea level drop of 1000 m but salinity estimates would indicate sea level drops exceeding that value. However, salinity estimates for this time period are very uncertain and a 1000 m drop seems less likely to have occurred.

4.4.2. Did the Caspian sea level drop 1000 m during the Pontian?

One of the main arguments to postulate a large sea level fall in the Caspian Sea is the presence of a palaeo-Volga canyon through the Central Caspian Basin. This was interpreted to have formed in response to a base-level fall between 600 and 1500 m coeval with the Messinian Salinity Crisis (e.g., Jones and Simmons, 1996). However, the age of this canyon is poorly constrained. Another evidence in favour of a 1500 m sea level fall is the basinward shift of the depocenter observed in seismic profiles (Abdullayev et al., 2012). Similarly to the Black Sea, good age control has only been acquired lately. Using a high resolution age model, van Baak et al. (2015) argues for a sea level drop of 100-150 m in Adzhiveli section (southwestern Caspian Sea; see location in Figure 4.1a) between 5.6 and 5.5 Ma, in contrast with previous estimates.

We can apply our results by deriving the hydrologic budget that would cause the Caspian sea level to go down by 1000 m. As in the previous section, arguing that the connection between the Black Sea and the Caspian Sea was shallow, we study the Caspian Sea separately. Assuming again that E─P was equal or smaller than 1 m/yr we find that R has to be lower than about 0.1 m/yr (74 km^3/yr; Figure 4.7c). Based on the dimensions of the Volga canyon it has been proposed that at the time, the discharge of this river was at least as large as it is at present (e.g., Abdullayev et al., 2012). However, the required R for a sea level lowering is much smaller than the modern annual mean discharge of the Volga River (239.67 km^3/yr; Overeem et al., 2003). A 1000 m sea level drop and the simultaneous formation of a deeply incising palaeo-Volga canyon would thus seem incompatible.

Our calculations from the Late Miocene climate experiments of Marzocchi et al. (2015) indicate that the hydrologic budget of the Caspian Sea is positive if the Volga River flows there (Figure 4.7c and Figures 4.8a, 4.8b). In this situation overspilling from the Caspian Sea into the Black Sea would have occurred. If the Volga River is excluded from the river discharge into the Caspian Sea the equivalent surface freshwater flux (E─P─R) is close to 0.3 m/yr, which is smaller than that of the present-day Mediterranean Sea. This hydrologic budget corresponds to a sea level drop of about 100 m (Figure 4.7c), which is within the range proposed by van Baak et al. (2015). In this case, the Volga River would have drained into the Black Sea. Interestingly, the runoff of the Volga River calculated by Marzocchi et al. (2015) is so large that it causes the hydrologic budget of the basin in which it flows, in this case the Black Sea, to become positive. Thus, a simultaneous high-magnitude sea level drop in both the Black Sea and the Caspian Sea is not possible (Figures 4.7b and 4.7c). According to van Baak et al. (2015), salinity in the Caspian basin remained relatively stable at 10 g/kg from 5.6 to 5.5 Ma. We find that a sea level fall of 100-150 m would have increased salinity by 4-5 g/kg (from a salinity of 10 to 14-15 g/kg; Figure 4.9a), which is probably too small an increase to detect. The possibility of a 1000 m sea level drop at this time can be discarded because it would raise salinity to a value of 47 g/kg, which exceeds by far the brackish conditions inferred by van Baak et al. (2015; Figure 4.9a).

When the alternative hypsometric curve is considered, the hydrologic budget calculated from Marzocchi et al. (2015), for the case that the Volga and Danube rivers are not connected to this basin, corresponds to a sea level drop larger than 1000 m (Figure 4.7f). In the Caspian Sea, due to the small surface area occupied by the deep domains of the basin, R has to be very small to lower the sea level below the shelves. Once this value is reached, even small reductions of R, can have a large impact on the amplitude of the sea level drop. A sea level drop of 1000 m, according to our results, would cause a salinity increase from 10 to a value of 26 g/kg (Figure 4.9b). However, van Baak et al. (2015) reports no major environmental shifts during this period and estimates a constant salinity of 10 g/kg from 5.6 to 5.5 Ma, and a 1000 m sea level drop in the Caspian Sea can be ruled out. This result confirms that the alternative hypsometric curve represents a too extreme basin configuration and that the sea level drop in the Black Sea and the Caspian Sea may have been smaller than that inferred from this curve.

To summarise, by combining salinity estimates derived from field observations and Late Miocene hydrologic budgets we are able to discard a 1000 m sea level drop in the Caspian Sea from 5.6 to 5.5 Ma. For an isolated Caspian Sea, a drop in sea level below the shelves would only happen if the Volga does not flow there.

4.4.3. Further implications

So far in this discussion, we have studied each of the basins in isolation arguing that the connection between the Black Sea and the Caspian Sea was shallow (Popov et al., 2006). We now use our analysis to look into the possibility that the Black Sea and the Caspian Sea remained united during this time interval. This scenario necessarily requires the connection between the Mediterranean Sea and the Paratethys to be shallower than the channel between the Black Sea and the Caspian Sea (Figure 4.8d). For the Paratethys as a whole the model results derived from the simulations of Marzocchi et al. (2015) predict a hydrologic budget close to neutral (Figures 4.7a and 4.7d). Any drop in excess of the level of the sill between the Paratethys and the Mediterranean Sea would thus seem unlikely and the Black Sea and the Caspian Sea would remain connected (Figures 4.7a, 4.7d and 4.8d). In other words, if the Paratethys sea level drop induced by the Mediterranean level lowering is not enough to isolate the basins, further sea level drop would not occur.

In this case, the connectivity between the Black Sea and the Caspian Sea may have been relatively poor due to the presence of a shallow gateway between them. Whereas, for this reason, the same salinity values are not expected in both basins, one would expect a similar evolution of salinity over time in the Black Sea and the Caspian Sea. In contrast with this, van Baak et al. (in press, 2015) report important salinity fluctuations in the Black Sea but a relatively stable environment in the Caspian Sea during this time interval. Overall, based on salinity estimates, it would appear unlikely that the basins remained together from 5.6 to 5.5 Ma. This implies that the connection between the Mediterranean Sea and the Paratethys was most likely not shallower than the channel between the Black Sea and the Caspian Sea.

4.5. Conclusions

We have shown that a relatively simple analysis provides valuable quantitative constraints on the sensitivity of sea level of the Paratethys basins to the hydrologic budget. The model approach allows us to study sea level fall and salinity change in a consistent way and provides a framework to interpret the spatially limited observations on the scale of entire (sub-)basins. The following conclusions have been reached independent of data:

- In the Caspian Sea, a smaller river discharge is required for a sea level drop below the shelves than in the Black Sea.

- Basin salinity only rises significantly for sea level drops below the shelves.

- For a given basin, time to equilibrium is typically not longer than 10 kyr. When E─P and R are small time to equilibrium is longer, but it never reaches 100 kyr.

- Climate-model derived hydrologic budgets indicate that the Volga River renders the hydrologic budget of the basin in which it terminates positive. A sea level drop below the shelves at the same time in the Black Sea and the Caspian Sea thus seems unlikely.

Combining our model analysis with the available data, two further conclusions could be drawn regarding the possibility of a large sea level fall from 5.6 to 5.5 Ma:

- A 1000 m sea level drop in the Black Sea can be ruled out based on the Late Miocene hydrologic budgets from Marzocchi et al. (2015). Salinity reconstructions, although very uncertain, would leave open this possibility. Even excluding the Volga and the Danube rivers from the discharge into the Black Sea proves not to be enough to lower the Black sea level by 1000 m.

- A sea level drop in the Caspian Sea of 1000 m or more, is unlikely. The Caspian sea level only drops below the shelves if the Volga River is much smaller than at present or absent. A large sea level drop coeval with the formation of a deep Volga canyon is unlikely.

Acknowledgements

Supplementary material

The climate model simulations by Marzocchi et al. (2015) were performed with the UK Hadley Centre Coupled Model (HadCM3L, version 4.5). This is a fully coupled ocean-atmosphere global circulation model, coupled also to a dynamic vegetation model (TRIFFID). The ocean and atmosphere components have a horizontal resolution of 3.75° longitude by 2.5° latitude. The model has 19 vertical levels for the atmosphere and 20 levels for the ocean. The Late Miocene palaeogeography used in these simulations derives from Markwick (2007; Figure S4.1). See Marzocchi et al. (2015) and references therein, for the details of the model setup.

In order to calculate the hydrologic budget for the Paratethys, seven drainage basins were defined as proposed by Gladstone et al. (2007) but with the addition of the Amu Darya catchment (Figure S4.1). The hydrologic budget is calculated in the same way as in Gladstone et al. (2007), by considering precipitation and evaporation separately over each catchment and over the Paratethys itself. Here, "en-route" evaporation from the catchments to the Paratethys is not taken into account, but this is unlikely to be an important source of error. Exchange with the Mediterranean Sea is not included because there is no Mediterranean-Paratethys connection in the palaeogeography used. Precipitation and evaporation values are obtained from an ensemble of 22 climate simulations through a Late Miocene precession cycle. We computed the annual mean hydrologic budget, averaged over the full precession cycle, for the Paratethys as a whole, the Black Sea and the Caspian Sea.

In the palaeogeography adopted in our sea level calculations, the Paratethys is slightly smaller than in the palaeogeography used by Marzocchi et al. (2015; Figure S4.1). In order to obtain a correct representation of the sea level dynamics implied by the climate model runs, we convert the river discharge derived from the climate model in litre/year, to the equivalent rate of sea level rise in metre/year by dividing it through the basin area of the climate model palaeogeography. The value thus obtained is then used in our calculations. Note that directly using the hydrologic budget predicted by the climate models (i.e., in litre/year) would render the budget used in our calculations only wetter and any inferred sea level drop less. To calculate E─P the total evaporative loss over the entire Paratethys is considered to be uniformly distributed over the surface area of the Paratethys.
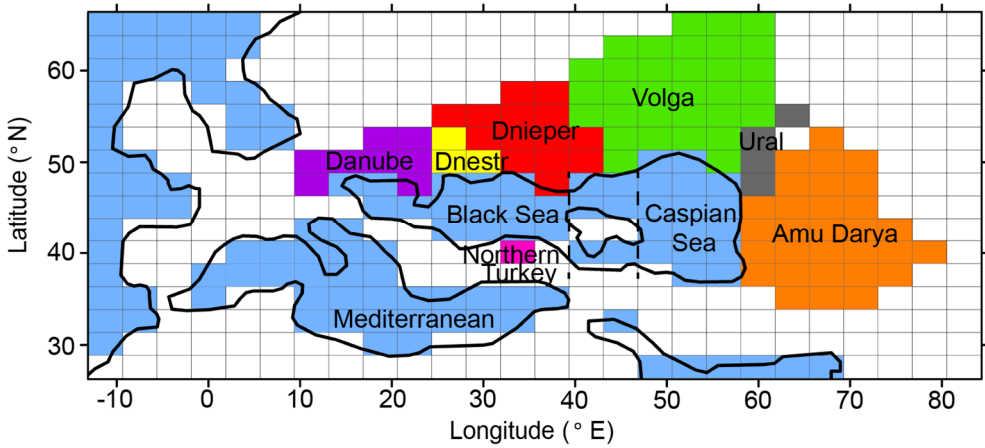
Figure S4.1. Late Miocene drainage basins (modified from Gladstone et al., 2007) used for the hydrologic budget calculations from the climate simulations of Marzocchi et al. (2015). The basins are represented at the model's resolution and the Late Miocene coastline used in the climate simulations is also outlined. The dashed lines indicate the eastern limit of the Black Sea and the western limit of the Caspian Sea, as adopted in Marzocchi et al. (2015). Which drainage basin is connected to each of the two sub-basins is specified in Table S4.1.

Runoff into the Black Sea	Volume flux (l/yr)	Equivalent rate of sea level rise over the Paratethys (m/yr)	Equivalent rate of sea level rise over the Black Sea (m/yr)
Danube	$1.8383 \cdot 10^{14}$	0.0601	0.1380
Dnestr	$8.7565 \cdot 10^{13}$	0.0286	0.0655
Dnepr	$2.3398 \cdot 10^{14}$	0.0765	0.1750
Northern Turkey	$6.0471 \cdot 10^{12}$	0.0020	0.0045
Runoff into the Caspian Sea	**Volume flux (l/yr)**	**Equivalent rate of sea level rise over the Paratethys (m/yr)**	**Equivalent rate of sea level rise over the Caspian Sea (m/yr)**
Volga	$6.3140 \cdot 10^{14}$	0.2064	0.5154
Ural	$3.8597 \cdot 10^{13}$	0.0126	0.0315
Amu Darya	$5.0416 \cdot 10^{13}$	0.0165	0.0412
E−P (m/yr)	**Over the Paratethys**	**Over the Black Sea**	**Over the Caspian Sea**
	0.3830	0.3830	0.3830

Table S4.1. Mean annual Paratethys hydrologic budget averaged over the duration of one full Late Miocene precession cycle derived from the climate simulations by Marzocchi et al. (2015).

Bibliography

Abdullayev, N. R., G. W. Riley, and A. P. Bowman (2012), Regional controls on lacustrine sandstone reservoirs: The Pliocene of the South Caspian basin, in: *Lacustrine sandstone reservoirs and hydrocarbon systems,* ed. by: Baganz, O. W., Y. Bartov, K. Bohacs, and D. Nummedal, pp. 71─98.

Alhammoud, B., P. Th. Meijer, and H. A. Dijkstra (2010), Sensitivity of the Mediterranean thermohaline circulation to gateway depth: A model investigation, *Palaeoceanography* **25**(2), PA2220, doi: 10.1029/2009PA001823.

Allen, M. B., and H. A. Armstrong (2008), Arabia–Eurasia collision and the forcing of mid Cenozoic global cooling, *Palaeogeography, Palaeoclimatology, Palaeoecology* **265**(1), pp. 52─58, doi: 10.1016/j.palaeo.2008.04.021.

Báldi, T. (1980), The early history of the Paratethys, *Bulletin of the Hungarian Geological Society* **110**(3─4), pp. 468─471.

Barker, P. F. (2001), Scotia Sea regional tectonic evolution: implications for mantle flow and palaeocirculation, *Earth-Science Reviews* **55**(1), pp. 1─39, doi: 10.1016/S0012-8252(01)00055-1.

Bartoli, G., M. Sarnthein, M. Weinelt, H. Erlenkeuser, C. D. Garbe-Schönberg, and D. W. Lea (2005), Final closure of Panama and the onset of northern hemisphere glaciation, *Earth and Planetary Science Letters* **237**(1), pp. 33–44, doi: 10.1016/j.epsl.2005.06.020.

Bellahsen, N., F. Mouthereau, A. Boutoux, M. Bellanger, O. Lacombe, L. Jolivet, and Y. Rolland (2014), Collision kinematics in the western external Alps, *Tectonics* **33**(6), pp. 1055–1088, doi: 10.1002/2013TC003453.

Benson, R. H. (1978), The palaeoecology of the Ostracodes of DSDP Leg 42-A, *Initial Report Deep Sea Drilling Project* **42**(1), pp. 777–787.

Benson, R. H., K. Rakic-El Bied, and G. Bonaduce (1991), An important current reversal (influx) in the Rifian Corridor (Morocco) at the Tortonian-Messinian boundary: the end of the Tethys ocean, *Palaeoceanography* **6**(1), pp. 165─192, doi: 10.1029/90PA00756.

Berggren, W. A., and C. D. Hollister (1977), Plate tectonics and palaeocirculation—commotion in the ocean, *Tectonophysics* **38**(1), pp. 11─48, doi: 10.1016/0040-1951(77)90199-8.

Bicchi, E., E. Ferrero, and M. Gonera (2003), Palaeoclimatic interpretation based on Middle Miocene planktonic foraminifera: the Silesia Basin (Paratethys) and Monferrato (Tethys)

records, *Palaeogeography, Palaeoclimatology, Palaeoecology* **196**(3), pp. 265─303, doi: 10.1016/S0031-0182(03)00368-7.

Blumberg, A. F., and G. L. Mellor (1987), A description of a three-dimensional coastal ocean circulation model, *Coastal and Estuarine Sciences* **4**, pp. 1─16, doi: 10.1029/CO004p0001.

Böhme, M., M. Winklhofer, and A. Ilg (2011), Miocene precipitation in Europe: Temporal trends and spatial gradients, *Palaeogeography, Palaeoclimatology, Palaeoecology* **304**(3), pp. 212─218, doi: 10.1016/j.palaeo.2010.09.028.

Bosellini, F. R., and C. Perrin (2008), Estimating Mediterranean Oligocene-Miocene sea-surface temperatures: An approach based on coral taxonomic richness, *Palaeogeography, Palaeoclimatology, Palaeoecology* **258**(1), pp. 71─88, doi: 10.1016/j.palaeo.2007.10.028.

Bryden, H. L., and H. M. Stommel (1984), Limiting processes that determine basic features of the circulation in the Mediterranean Sea, *Oceanologica Acta* **7**(3), pp. 289─296.

Bryden, H. L., and T. H. Kinder (1991), Steady two-layer exchange through the Strait of Gibraltar, *Deep Sea Research Part A, Oceanographic Research Papers* **38**(1), S445─S463, doi:10.1016/S0198-0149(12)80020-3.

Burton, K. W., H. F. Ling, and R. K. O'Nions (1997), Closure of the Central American Isthmus and its effect on deep-water formation in the North Atlantic, *Nature* **386**, pp. 382─385, doi: 10.1038/386382a0.

Bush, A. B. (1997), Numerical simulation of the Cretaceous Tethys circumglobal current, *Science* **275**(5301), pp. 807─810, doi: 10.1126/science.275.5301.807.

Butzin, M., G. Lohmann, and T. Bickert (2011), Miocene ocean circulation inferred from marine carbon cycle modeling combined with benthic isotope records, *Palaeoceanography* **26**(1), PA1203, doi: 10.1029/2009PA001901.

Cane, M. A., and P. Molnar (2001), Closing of the Indonesian seaway as a precursor to east African aridification around 3-4 million years ago, *Nature* **411**(6834), pp. 157─162, doi: 10.1038/35075500.

Cita, M. B., and S. Gartner (1973), The stratotype Zanclean foraminiferal and nannofossil biostratigraphy, *Rivista Italiana di Palaeontologia* **79**(4), pp. 503─588.

Clauzon, G., J. P. Suc, F. Gautier, A. Berger, and M. F. Loutre (1996), Alternate interpretation of the Messinian salinity crisis: Controversy resolved?, *Geology* **24**(4), pp. 363─366, doi: 10.1130/0091-7613(1996)024<0363:AIOTMS>2.3.CO;2.

Clauzon, G., J. P. Suc, S. -M. Popescu, M. Marunteanu, J. L. Rubino, F. Marinescu, and M. C. Melinte (2005), Influence of Mediterranean sea-level changes on the Dacic Basin (Eastern Paratethys) during the late Neogene: the Mediterranean Lago Mare facies

deciphered, *Basin Research* **17**(3), pp. 437─462, doi: 10.1111/j.1365-2117.2005.00269.x.

Coates, A. G., L. S. Collins, M. P. Aubry, and W. A. Berggren (2004), The geology of the Darien, Panama, and the late Miocene-Pliocene collision of the Panama arc with northwestern South America, *Geological Society of America Bulletin* **116**(11─12), pp. 1327─1344, doi: 10.1130/B25275.1.

Cohen, K. M., S. C. Finney, P. L. Gibbard, and J. -X. Fan (2013; updated), *The ICS International Chronostratigraphic Chart*, Episodes 36, pp.199─204.

Coleman, R. G. (1974), Geologic Background of the Red Sea, in: *The Geology of Continental Margins*, ed. by: Burk, C. A., and C. L. Drake, Springer Berlin Heidelberg, pp. 743─751, doi: 10.1007/978-3-662-01141-6_55.

Cunningham, K. J., and L. S. Collins (2002), Controls on facies and sequence stratigraphy of an upper Miocene carbonate ramp and platform, Melilla basin, NE Morocco, *Sedimentary Geology* **146**(3), pp. 285─304, doi: 10.1016/S0037-0738(01)00131-2.

Dall´Antonia, B. (2003), Deep-sea ostracods as indicators of palaeoceanographic changes: a case from the middle-late Miocene of southern Italy (Central Mediterranean), *Terra Nova* **15**(1), pp. 52–60, doi: 10.1046/j.1365-3121.2003.00464.x.

Dall´Antonia, B., A. Di Stefano, and L. M. Foresi (2001), Integrated micropalaeontological study (ostracods and calcareous plankton) of the Langhian western Hyblean successions (Sicily, Italy), *Palaeogeography, Palaeoclimatology, Palaeoecology* **176**(1), pp. 59─80, doi: 10.1016/S0031-0182(01)00326-1.

deConto, R. M. (2009), Plate tectonics and climate changes, in: *Encyclopedia of paleoclimatology and ancient environments*, ed. by: Gornitz, V., Springer, Dordrecht, The Netherlands, p. 789.

Dercourt, J., M. Gaetani, B. Vrielynck, E. Barrier, B. Biju-Duval, M. F. Brunet, J. P. Cadet, S. Crasquin, and M. Sandulescu, eds. (2000), *Atlas Peri-Tethys: Palaeogeographical Maps*, CCGM/CGMW, Paris.

Drakopoulos, P. G., and A. Lascaratos (1999), Modelling the Mediterranean Sea climatological forcing, *Journal of Marine Systems* **20**(1), pp. 157─173, doi: 10.1016/S0924-7963(98)00080-3.

Farr, T. G., and M. Kobrick (2000), Shuttle Radar Topography Mission produces a wealth of data, *Eos, Transactions, American Geophysical Union* **81**, pp. 583─585.

Flower, B. P., and J. P. Kennett (1994), The middle Miocene climatic transition: East Antarctic ice sheet development, deep ocean circulation and global carbon cycling, *Palaeogeography, Palaeoclimatology, Palaeoecology* **108**(3), pp. 537─555, doi: 10.1016/0031-0182(94)90251-8.

REFERENCES

Garnier, J., G. Billen, E. Hannon, S. Fonbonne, Y. Videnina, and M. Soulie (2002), Modelling the transfer and retention of nutrients in the drainage network of the Danube River, *Estuarine, Coastal and Shelf Science* **54**(3), pp. 285−308, doi:10.1006/ecss.2000.0648.

Gebhardt, H. (1999), Middle to Upper Miocene benthonic foraminiferal palaeoecology of the Tap Marls (Alicante Province, SE Spain) and its palaeoceanographic implications, *Palaeogeography, Palaeoclimatology, Palaeoecology* **145**(1), pp. 141−156, doi: 10.1016/S0031-0182(98)00110-2.

Gheorghian, M. (1978), Micropaleontological investigations of the sediments from sites 379, 380, and 381 of leg 42B, in: *Initial Reports of the Deep Sea Drilling* Project, volume 42, part 2*, ed. by: Ross, D. A., and Y. P. Neprochnov, U. S. Government Printing Office, Washington, D. C., pp. 783−787.

Gillet, H., G. Lericolais, J. P. Rehault, and C. Dinu (2003), La stratigraphie oligo-miocène et la surface d'érosion messinienne en mer Noire, stratigraphie sismique haute resolution, *Comptes Rendus Geoscience* **335**(12), pp. 907−916, doi:10.1016/j.crte.2003.08.008.

Gillet, H., G. Lericolais, and J. P. Réhault (2007), Messinian event in the Black Sea: evidence of a Messinian erosional surface, *Marine Geology* **244**(1), pp. 142−165, doi:10.1016/j.margeo.2007.06.004.

Gladstone, R., R. Flecker, P. Valdes, D. Lunt, and P. Markwick (2007), The Mediterranean hydrologic budget from a Late Miocene global climate simulation, *Palaeogeography, Palaeoclimatology, Palaeoecology* **251**(2), pp. 254−267, doi: 10.1016/j.palaeo.2007.03.050.

Grothe, A., F. Sangiorgi, Y. R. Mulders, I. Vasiliev, G-. J. Reichart, H. Brinkhuis, M. Stoica, and W. Krijgsman (2014), Black Sea desiccation during the Messinian Salinity Crisis: Fact or fiction?, *Geology* **42**(7), pp. 563−566, doi: 10.1130/G35503.1.

Hallam, A. (1969), Faunal realms and facies in the Jurassic, *Palaeontology* **12**(1), pp. 1−18.

Hamon, N., P. Sepulchre, V. Lefebvre, and G. Ramstein (2013), The role of the eastern Tethys seaway closure in the middle Miocene Climatic Transition (ca. 14 Ma), *Climate of the Past* **9**, pp. 2687−2702, doi: 10.5194/cp-9-2687-2013.

Harzhauser, M., and W. E. Piller (2007), Benchmark data of a changing sea— palaeogeography, palaeobiogeography and events in the Central Paratethys during the Miocene, *Palaeogeography, Palaeoclimatology, Palaeoecology* **253**(1), pp. 8−31, doi:10.1016/j.palaeo.2007.03.031.

Harzhauser, M., A. Kroh, O. Mandic, W. E. Piller, U. Göhlich, M. Reuter, and B. Berning (2007), Biogeographic responses to geodynamics: A key study all around the Oligo–

Miocene Tethyan Seaway, *Zoologischer Anzeiger-A Journal of Comparative Zoology* **246**(4), pp. 241–256, doi: 10.1016/j.jcz.2007.05.001.

Harzhauser, M., M. Reuter, W. E. Piller, B. Berning, A. Kroh, and O. Mandic (2009), Oligocene and Early Miocene gastropods from Kutch (NW India) document an early biogeographic switch from Western Tethys to Indo-Pacific, *Paläontologische Zeitschrift* **83**(3), pp. 333–372, doi: 10.1007/s12542-009-0025-5.

Haug, G. H., and R. Tiedemann (1998), Effect of the formation of the Isthmus of Panama on Atlantic Ocean thermohaline circulation, *Nature* **393**(6686), pp. 673–676, doi: 10.1038/31447.

Heinze, C., and T. J. Crowley (1997), Sedimentary response to ocean gateway circulation changes, *Paleoceanography* **12**(6), pp. 742–754, doi: 10.1029/97PA02050.

Hernández-Molina, F. J., D. A. V. Stow, C. A. Alvarez-Zarikian, G. Acton, A. Bahr, B. Balestra, E. Ducassou, R. Flood, J. A. Flores, S. Furota, P. Grunert, D. Hodell, F. Jimenez-Espejo, J. K. Kim, L. Krissek, J. Kuroda, B. Li, E. Llave, J. Lofi, L. Lourens, M. Miller, F. Nanayama, N. Nishida, C. Richter, C. Roque, H. Pereira, M. F. Sanchez Goñi, F. J. Sierro, A. D. Singh, C. Sloss, Y. Takashimizu, A. Tzanova, A. Voelker, T. Williams, and C. Xuan (2014), Onset of Mediterranean outflow into the North Atlantic, *Science* **344**(6189), pp. 1244–1250, doi: 418 10.1126/science.1251306.

Herold, N., M. Huber, R. D. Müller, and M. Seton (2012), Modeling the Miocene climatic optimum: Ocean circulation, *Palaeoceanography* **27**(1), PA1209, doi: 10.1029/2010PA002041.

Hodell, D. A., R. H. Benson, D. V. Kent, A. Boersma, and K. Rakic-El Bied (1994), Magnetostratigraphic, biostratigraphic, and stable isotope stratigraphy of an Upper Miocene drill core from the Salé Briqueterie (northwestern Morocco): A high-resolution chronology for the Messinian stage, *Palaeoceanography* **9**(6), pp. 835–855, doi: 10.1029/94PA01838.

Hsü, K. J., W. B. F. Ryan, and M. B. Cita (1973), Late Miocene desiccation of the Mediterranean, *Nature* **242**(5395), pp. 240–244.

Hsü, K. J., and F. Giovanoli (1979), Messinian event in the Black Sea, *Palaeogeography, Palaeoclimatology, Palaeoecology* **29**, pp. 75–93, doi: 10.1016/0031-0182(79)90075-0.

Hüsing, S. K., W. J. Zachariasse, D. J. J. van Hinsbergen, W. Krijgsman, W. Inceöz, M. Harzhauser, O. Mandic, and A. Kroh (2009), Oligocene-Miocene basin evolution in SE Anatolia, Turkey: constraints on the closure of the eastern Tethys gateway, *Geological Society, London, Special Publications* **311**(1), pp. 107–132, doi: 10.1144/SP311.4.

Hüsing, S. K., O. Oms, J. Agustí, M. Garcés, T. J. Kouwenhoven, W. Krijgsman, and W. -J. Zachariasse (2010), On the late Miocene closure of the Mediterranean-Atlantic gateway

through the Guadix basin (southern Spain), *Palaeogeography, Palaeoclimatology, Palaeoecology* **291**(3), pp. 167─179, doi: 10.1016/j.palaeo.2010.02.005.

Ivanovic, R. F., R. Flecker, M. Gutjahr, and P. J. Valdes (2013), First Nd isotope record of Mediterranean-Atlantic water exchange through the Moroccan Rifian Corridor during the Messinian Salinity Crisis, *Earth and Planetary Science Letters* **368**, pp. 163─174, doi:10.1016/j.epsl.2013.03.010.

Ivanovic, R. F., P. J. Valdes, L. Gregoire, R. Flecker, and M. Gutjahr (2014), Sensitivity of modern climate to the presence, strength and salinity of Mediterranean-Atlantic exchange in a global general circulation model, *Climate Dynamics* **42**(3─4), pp. 859─877, doi: 10.1007/s00382-013-1680-5.

Jauzein, A., and P. Hubert (1984), Les bassins oscillants: Un modèle de genèse des séries salines, *Bulletin des Sciences géologiques* **37**(3), pp. 267─282.

Jolivet, L., and C. Faccenna (2000), Mediterranean extension and the Africa-Eurasia collision, *Tectonics* **19**(6), pp. 1095─1106, doi: 10.1029/2000TC900018.

Jolivet, L., R. Augier, C. Robin, J. P. Suc, and J. M. Rouchy (2006), Lithospheric-scale geodynamic context of the Messinian salinity crisis, *Sedimentary Geology* **188**, pp. 9─33, doi: 10.1016/j.sedgeo.2006.02.004.

Jones, R. W., and M. D. Simmons (1996), A review of the stratigraphy of Eastern Paratethys (Oligocene-Holocene), *Bulletin Natural History Museum Geology Series* **52**, pp. 25─50.

Jordi, A., and D. -P. Wang (2012), sbPOM: A parallel implementation of Princeton Ocean Model, *Environmental Modelling & Software* **38**, pp. 59─61, doi: 10.1016/j.envsoft.2012.05.013.

Jousé, A. P., and V. V. Mukhina (1978), Diatom units and the paleogeography of the Black Sea in the late Cenozoic (DSDP, Leg 42B), in: *Intial Reports of the Deep Sea Drilling Project,* volume 42, part 2, ed. by: Ross, D. A., and Y. P. Neprochnov, U. S. Government Printing Office, Washington, D. C., pp. 903─950.

Karami, M. P. (2011), *Palaeoceanography of the Miocene Mediterranean Sea and Paratethys: Regional ocean modelling of the response to closure of the Tethys Seaway*, Ph.D. thesis, Utrecht University, The Netherlands, pp. 67─108.

Karami, M. P., P. Th. Meijer, H. A. Dijkstra, and M. J. R. Wortel (2009), An oceanic box model of the Miocene Mediterranean Sea with emphasis on the effects of closure of the eastern gateway, *Palaeoceanography* **24**(4), PA4023, doi: 10.1029/2008PA001679.

Karami, M. P, A. De Leeuw, W. Krijgsman, P. Th. Meijer, and M. J. R. Wortel (2011), The role of gateways in the evolution of temperature and salinity of semi-enclosed basins: An oceanic box model for the Miocene Mediterranean Sea and Paratethys, *Global and Planetary Change* **79**(1), pp. 73─88, doi: 10.1016/j.gloplacha.2011.07.011.

Kennett, J. P. (1977), Cenozoic evolution of Antarctic glaciation, the circum-Antarctic Ocean, and their impact on global palaeoceanography, *Journal of Geophysical Research* **82**, pp. 3843─3860, doi: 10.1029/JC082i027p03843.

Kocsis, L., T. W. Vennemann, D. Fontignie, C. Baumgartner, A. Montanari, and B. Jelen (2008), Oceanographic and climatic evolution of the Miocene Mediterranean deduced from Nd, Sr, C, and O isotope compositions of marine fossils and sediments, *Palaeoceanography* **23**(4), PA4211, doi: 10.1029/2007PA001540.

Kocsis, L., A. Dulai, M. A. Bitner, T. Vennemann, and M. Cooper (2012), Geochemical compositions of Neogene phosphatic brachiopods: Implications for ancient environmental and marine conditions, *Palaeogeography, Palaeoclimatology, Palaeoecology* **326**, pp. 66─67, doi: 10.1016/j.palaeo.2012.02.004.

Kojumdgieva, E. (1979), Critical notes on the stratigraphy of Black Sea boreholes (Deep Sea Drilling Project, Leg 42B), *Geologica Balcanica* **9**, pp.107–110.

Krapp, M., and J. H. Jungclaus (2011), The Middle Miocene climate as modelled in an atmosphere-ocean biosphere model, *Climate of the Past* **7**(4), pp. 1169─1188, doi: 10.5194/cp-7-1169-2011.

Krijgsman, W., F. J. Hilgen, I. Raffi, F. J. Sierro, and D. S. Wilson (1999a), Chronology, causes and progression of the Messinian salinity crisis, *Nature* **400**(6745), pp. 652─655, doi: 10.1038/23231.

Krijgsman, W., C. G. Langereis, W. -J. Zachariasse, M. Boccaletti, G. Moratti, R. Gelati, S. Iaccarino, G. Papani, and G. Villa (1999b), Late Neogene evolution of the Taza-Guercif Basin (Rifian Corridor, Morocco) and implications for the Messinian salinity crisis, *Marine Geology* **153**(1), pp. 147─160, doi: 10.1111/j.1365-3121.2004.00564.x.

Krijgsman, W., M. Stoica, I. Vasiliev, and V. V. Popov (2010), Rise and fall of the Paratethys Sea during the Messinian Salinity Crisis, *Earth and Planetary Science Letters* **290**(1), pp. 183─191, doi:10.1016/j.epsl.2009.12.020.

Kroonenberg, S. B., M. D. Simmons, N. I. Alekseevski, E. Aliyeva, M. B. Allen, D. N. Aybulatov, A. Baba-Zadeh, E. N. Babyukova, C. E. Davies, D. J. Hinds, R. M. Hoogendoorn, D. Huseynov, B. Ibrahimov, P. Mamedov, I. Overeem, G. V. Rusakov, S. F. Suleymanova, A. A. Svitoch, and S. J. Vincent (2005), Two deltas, two basins, one river, one sea: The modern Volga delta as an analogue of the Neogene Productive Series, South Caspian Basin, in: *SEPM Special Publication: River Deltas - Concepts, Models and Examples*, SEPM, Tulsa, Oklahoma, U.S.A., pp. 231–256.

Latimer, J. C., and G. M. Filippelli (2002), Eocene to Miocene terrigenous inputs and export production: Geochemical evidence from ODP Leg 177, Site 1090, *Palaeogeography, Palaeoclimatology, Palaeoecology* **182**(3), pp. 151–164, doi: 10.1016/S0031-0182(01)00493-X.

REFERENCES

Leever, K. A., L. Matenco, T. Rabagia, S. Cloetingh, W. Krijgsman, and M. Stoica (2010), Messinian sea level fall in the Dacic Basin (Eastern Paratethys): palaeogeographical implications from seismic sequence stratigraphy, *Terra Nova* **22**(1), pp. 12─17, doi: 10.1111/j.1365-3121.2009.00910.x.

Leigh, E. G., A. O'Dea, and G. J. Vermeij (2014), Historical biogeography of the Isthmus of Panama, *Biological Reviews* **89**(1), pp. 148─172, doi: 10.1111/brv.12048.

Livermore, R., C. D. Hillenbrand, M. Meredith, and G. Eagles (2007), Drake Passage and Cenozoic climate: an open and shut case?, *Geochemistry, Geophysics, Geosystems* **8**(1), Q01005, doi: 10.1029/2005GC001224.

Locarnini, R. A., A. V. Mishonov, J. I. Antonov, J. P. Boyer, H. E. Garcia, O. K. Baranova, M. Zweng, C. R. Paver, J. R. Reagan, D. R. Johnson, M. Hamilton, and D. Seidov (2013), Temperature NOAA Atlas NESDIS 73, in: *World Ocean Atlas,* volume 1, ed. by: Levitus, S., and A. Mishonov, p.40.

Lunt, D. J., P. J. Valdes, A. Haywood, and I. C. Rutt (2008), Closure of the Panama Seaway during the Pliocene: implications for climate and Northern Hemisphere glaciation, *Climate Dynamics* **30**(1), pp. 1─18, doi: 10.1007/s00382-007-0265-6.

Maier-Reimer, E., U. Mikolajewicz, and T. Crowley (1990), Ocean general circulation model sensitivity experiment with an open Central American Isthmus, *Paleoceanography* **5**(3), pp. 349─366, doi: 10.1029/PA005i003p00349.

Manzi, V., R. Gennari, F. Hilgen, W. Krijgsman, S. Lugli, M. Roveri, and F. J. Sierro (2013), Age refinement of the Messinian salinity crisis onset in the Mediterranean, *Terra Nova* **25**(4), pp. 315─322, doi: 10.1111/ter.12038.

Mariotti, A., M. V. Struglia, N. Zeng, and K.-M. Lau (2002), The hydrological cycle in the Mediterranean region and implications for the water budget of the Mediterranean Sea, *Journal of Climate* **15**(13), pp. 1674─1690, doi: 10.1175/1520-0442(2002)015<1674:THCITM>2.0.CO;2.

Markwick, P. (2007), The palaeogeographic and palaeoclimatic significance of climate proxies for data-model comparisons, in: *Deep-time perspectives on climate change: Marrying the signal from computer models and biological proxies*, ed. by: Williams, M., A. M. Haywood, F. J. Gregory, and D. N. Schmidt, The Micropalaeontology Society, Special Publication, The Geological Society, London, pp. 251–312.

Martín, J. M., J. C. Braga, and C. Betzler (2001), The Messinian Guadalhorce corridor: the last northern, Atlantic-Mediterranean gateway, *Terra Nova* **13**(6), pp. 418─424, doi: 10.1046/j.1365-3121.2001.00376.x.

Martín, J. M., J. C. Braga, J. Aguirre, and A. Puga-Bernabéu (2009), History and evolution of the North-Betic Strait (Prebetic Zone, Betic Cordillera): a narrow, early Tortonian, tidal-

dominated, Atlantic-Mediterranean marine passage, *Sedimentary Geology* **216**(3), pp. 80─90, doi: 10.1016/j.sedgeo.2009.01.005.

Marzocchi, A., D. J. Lunt, R. Flecker, C. D. Bradshaw, A. Farnsworth, and F. J. Hilgen (2015), Orbital control on late Miocene climate and the North African monsoon: insight from an ensemble of sub-precessional simulations, *Climate of the Past* **11**, pp. 1271─1295, doi: 10.5194/cp-11-1271-2015.

McKenzie, D. P., D. Davies, and P. Molnar (1970), Plate tectonics of the Red Sea and East Africa, *Nature* **226**(5242), pp. 243─248, doi: 10.1038/226243a0.

Meijer, P. Th. (2012), Hydraulic theory of sea straits applied to the onset of the Messinian Salinity Crisis, *Marine Geology* **326**, pp. 131–139, doi: 10.1016/j.margeo.2012.09.001.

Meijer, P. Th., and H. A. Dijkstra (2009), The response of Mediterranean thermohaline circulation to climate change: a minimal model, *Climate of the Past* **5**(4), pp. 713─720, doi: 10.1029/97JC02720.

Meulenkamp, J. E., and W. Sissingh (2003), Tertiary palaeogeography and tectonostratigraphic evolution of the Northern and Southern Peri-Tethys platforms and the intermediate domains of the African–Eurasian convergent plate boundary zone, *Palaeogeography, Palaeoclimatology, Palaeoecology* **196**(1), pp. 209–228, doi: 10.1016/S0031-0182(03)00319-5.

Mikolajewicz, U., E. Maier-Reimer, T. J. Crowley, and K. Y. Kim (1993), Effect of Drake and Panamanian Gateways on the circulation of an ocean model, *Paleoceanography* **8**(4), pp. 409–426, doi: 10.1029/93PA00893.

Montes, C., A. Cardona, C. Jaramillo, A. Pardo, J. C. Silva, V. Valencia, C. Ayala, L. C. Pérez-Angel, L. A. Rodríguez-Parra, V. Ramírez, and H. Niño (2015), Middle Miocene closure of the Central American Seaway, *Science* **348**(6231), pp. 226–229, doi: 10.1126/science.aaa2815.

Müller, R. D., M. Sdrolias, C. Gaina, and W. R. Roest (2008), Age, spreading rates, and spreading asymmetry of the world's ocean crust, *Geochemistry, Geophysics, Geosystems* **9**(4), pp. 1525–2027, doi: 10.1029/2007GC001743.

Munteanu, I., L. Matenco, C. Dinu, and S. Cloetingh (2012), Effects of large sea-level variations in connected basins: the Dacian–Black Sea system of the Eastern Paratethys, *Basin Research* **24**(5), pp. 583─597, doi: 10.1111/j.1365-2117.2012.00541.x.

Nong, G. T., R. G. Najjar, D. Seidov, and W. H. Peterson (2000), Simulation of ocean temperature change due to the opening of Drake Passage, *Geophysical Research Letters* **27**(17), pp. 2689─2692, doi: 10.1029/1999GL011072.

REFERENCES

Omta, A. W., and H. A. Dijkstra (2003), A physical mechanism for the Atlantic-Pacific flow reversal in the early Miocene, *Global and Planetary Change* **36**(4), pp. 265−276, doi: 10.1016/S0921-8181(02)00221-7.

Overeem, I., A. Veldkamp, L. Tebbens, and S. B. Kroonenberg (2003), Modelling Holocene stratigraphy and depocentre migration of the Volga delta due to Caspian Sea-level change, *Sedimentary Geology* **159**(3), pp. 159−175, doi:10.1016/S0037-0738(02)00256-7.

Ozyavas, A., S. D. Khan, and J. F. Casey (2010), A possible connection of Caspian Sea level fluctuations with meteorological factors and seismicity, *Earth and Planetary Science Letters* **299**(1), pp. 150−158, doi: 10.1016/j.epsl.2010.08.030.

Pérez-Asensio, J. N., J. Aguirre, G. Schmiedl, and J. Civis (2012), Impact of the restriction of the Atlantic-Mediterranean gateway on the Mediterranean Outflow Water and eastern Atlantic circulation during the Messinian, *Palaeoceanography* **27**(3), PA3222, doi: 10.1029/2012PA002309.

Pfister, P. L., T. F. Stocker, J. Rempfer, and S. P. Ritz (2014), Influence of the Central American Seaway and Drake Passage on ocean circulation and neodymium isotopes: A model study, *Paleoceanography* **29**(12), pp. 1214–1237, doi: 10.1002/2014PA002666.

Pippèrr, M., and B. Reichenbacher (2010), Foraminifera from the borehole Altdorf (SE Germany): Proxies for Ottnangian (early Miocene) palaeoenvironments of the Central Paratethys, *Palaeogeography, Palaeoclimatology, Palaeoecology* **289**(1), pp. 62−80, doi: 10.1016/j.palaeo.2010.02.009.

Popescu, S. -M. (2006), Late Miocene and early Pliocene environments in the southwestern Black Sea region from high-resolution palynology of DSDP Site 380A (Leg 42B), *Palaeogeography, Palaeoclimatology, Palaeoecology* **238**(1), pp. 64−77, doi: 10.1016/j.palaeo.2006.03.018.

Popov, S. V, F. Rögl, A. Y. Rozanov, F. F. Steiniger, I. G. Shcherba, and M. Kovac (2004), *Lithological-Paleogeographic maps of Paratethys: 10 Maps Late Eocene to Pliocene*, Courier Forschungsinstitut Senckenberg, Frankfurt/Main.

Popov, S. V., I. G. Shcherba, L. B. Ilyina, L. A. Nevesskaya, N. P. Paramonova, S. O. Khondkarian, and I. Magyar (2006), Late Miocene to Pliocene palaeogeography of the Paratethys and its relation to the Mediterranean, *Palaeogeography, Palaeoclimatology, Palaeoecology* **238**(1), pp. 91−106, doi: 10.1016/j.palaeo.2006.03.020.

Prange, M., and M. Schulz (2004), A coastal upwelling seesaw in the Atlantic Ocean as a result of the closure of the Central American Seaway, *Geophysical Research Letters* **31**(17), L17207, doi: 10.1029/2004GL020073.

Ramsay, A. T., C. W. Smart, and J. C. Zachos (1998), A model of early to middle Miocene deep ocean circulation for the Atlantic and Indian Oceans, *Geological Society, London, Special Publications* **131**(1), pp. 55─70, doi: 10.1144/GSL.SP.1998.131.01.04.

Rögl, F. (1996), Stratigraphic correlation of the Paratethys Oligocene and Miocene, *Journal of Alpine Geology* **41**, pp. 65─73.

Rögl, F. (1999), Mediterranean and Paratethys. Facts and hypotheses of an Oligocene to Miocene paleogeography (short overview), *Geologica Carpathica* **50**(4), pp. 339─349.

Ross, D. A., Y. P. Neprochnov, K. J. Hsü, P. Stoffers, P. Supko, E. S. Trimonis, S. F. Percival, A. J. Erickson, E. T. Degens, J. M. Hunt, F. T. Manheim, M. Senalp, and A. Traverse (1978), *Initial reports of the Deep Sea Drilling Project*, volume 42, part 2, U. S. Government Printing Office, Washington, D. C., doi:10.2973/dsdp.proc.42-2.1978.

Roveri, M., R. Flecker, W. Krijgsman, J. Lofi, S. Lugli, V. Manzi, J. F. Sierro, A. Bertini, A. Camerlenghi, G. de Lange, R. Govers, F. G. Hilgen, C. Hübscher, P. Th. Meijer, and M. Stoica (2014), The Messinian Salinity Crisis: Past and future of a great challenge for marine sciences, *Marine Geology* **352**, pp. 25─58, doi: 10.1016/j.margeo.2014.02.002.

Ryan, W. B. F. (1978), Messinian badlands on the southeastern margin of the Mediterranean Sea, *Marine Geology* **27**(3), pp. 349─363, doi: 10.1016/0025-3227(78)90039-7.

Ryan, W. B. F., and M. B. Cita (1978), The nature and distribution of Messinian erosional surfaces—Indicators of a several-kilometer-deep Mediterranean in the Miocene, *Marine Geology* **27**(3), pp. 193─230, doi: 10.1016/0025-3227(78)90032-4.

Salhotra, A. M., E. E. Adams, and D. R. F. Harleman (1985), Effect of salinity and ionic composition on evaporation: Analysis of Dead Sea evaporation pans, *Water Resources Research* **21**(9), pp. 1336─1344, doi: 10.1029/WR021i009p01336.

Sannino, G., A. Bargagli, and V. Artale (2002), Numerical modeling of the mean exchange through the Strait of Gibraltar, *Journal of Geophysical Research* **107**(C8), 3094, doi: 10.1029/2001JC000929.

Santisteban, C., and C. Taberner (1983), Shallow marine and continental conglomerates derived from coral reef complexes after desiccation of a deep marine basin: the Tortonian-Messinian deposits of the Fortuna Basin, SE Spain, *Journal of the Geological Society* **140**(3), pp. 401─411, doi: 10.1144/gsjgs.140.3.0401.

Schmid, S. M., O. A. Pfiffner, N. Froitzheim, G. Schönborn, and E. Kissling (1996), Geophysical-geological transect and tectonic evolution of the Swiss-Italian Alps, *Tectonics* **15**(5), pp. 1036─1064, doi: 10.1029/96TC00433.

Schneider, B., and A. Schmittner (2006), Simulating the impact of the Panamanian seaway closure on ocean circulation, marine productivity and nutrient cycling, *Earth and Planetary Science Letters* **246**(3), pp. 367─380, doi:10.1016/j.epsl.2006.04.028.

REFERENCES

Schrader, H. -J. (1978), Quaternary through Neogene history of the Black Sea, deduced from the paleoecology of diatoms, silicoflagellates, ebridians, and chrysomonads, in: *Intial Reports of the Deep Sea Drilling Project,* volume 42, part 2, ed. by: Ross, D. A., and Y. P. Neprochnov, U. S. Government Printing Office, Washington, D. C., pp. 789—901.

Seneš, J. (1973), Correlation hypotheses of the Neogene Tethys and Paratethys, *Giornale di Geologia* **39**(2), pp. 271—286.

Sepulchre, P., T. Arsouze, Y. Donnadieu, J.-C. Dutay, C. Jaramillo, J. Le Bras, E. Martin, C. Montes, and A. J. Waite (2014), Consequences of shoaling of the Central American Seaway determined from modeling Nd isotopes, *Palaeoceanography* **29**(3), pp. 176—189, doi: 10.1002/2013PA002501.

Sijp, W. P., and M. H. England (2004), Effect of the Drake Passage throughflow on global climate, *Journal of Physical Oceanography* **34**(5) pp. 1254—1266, doi: 10.1175/1520-0485(2004)034<1254:EOTDPT>2.0.CO;2.

Sijp, W. P., M. H. England, and M. Huber (2011), Effect of the deepening of the Tasman Gateway on the global ocean, *Palaeoceanography* **26**(4), PA4207, doi: 10.1029/2011PA002143.

Smeed, D. A. (2000), Hydraulic control of three-layer exchange flows: application to the Bab al Mandab, *Journal of Physical Oceanography* **30**(10), pp. 2574—2588, doi: 10.1175/1520-0485(2000)030<2574:HCOTLE>2.0.CO;2.

Soria, J. M., J. Fernández, and C. Viseras (1999), Late Miocene stratigraphy and palaeogeographic evolution of the intramontane Guadix Basin (Central Betic Cordillera, Spain): implications for an Atlantic-Mediterranean connection, *Palaeogeography, Palaeoclimatology, Palaeoecology* **151**(4), pp. 255—266, doi:10.1016/S0031-0182(99)00019-X.

Soto-Navarro, J., F. Criado-Aldeanueva, J. García-Lafuente, and A. Sánchez-Román (2010), Estimation of the Atlantic inflow through the Strait of Gibraltar from climatological and in situ data, *Journal of Geophysical Research: Oceans* **115**, C10023, doi: 10.1029/2010JC006302.

Staneva, J. V., D. E. Dietrich, E. V. Stanev, and M. J. Bowman (2001), Rim current and coastal eddy mechanisms in an eddy-resolving Black Sea general circulation model, *Journal of Marine Systems* **31**(1), pp. 137—157, doi: 10.1016/S0924-7963(01)00050-1.

Stanley, S. M. (1995), New horizons for palaeontology, with two examples: the rise and fall of the cretaceous supertethys and the cause of the modern ice age, *Journal of Paleontology* **69**(6), pp. 999—1007.

Steininger, F. F., C. Müller, and F. Rögl (1988), Correlation of central Paratethys, eastern Paratethys, and Mediterranean Neogene stages, *American Association of Petroleum Geologists* **45**, pp. 79─88.

Steppuhn, A., A. Micheels, G. Geiger, and V. Mosbrugger (2006), Reconstructing the Late Miocene climate and oceanic flux using the AGCM ECHAM4 coupled to a mixed-layer ocean model with adjusted heat flux correction, *Palaeogeography, Palaeoclimatology, Palaeoecology* **238**(1), pp. 399─423, doi: 10.1016/j.palaeo.2006.03.037.

Stoica, M., I. Lazăr, W. Krijgsman, I. Vasiliev, D. Jipa, and A. Floroiu (2013), Paleoenvironmental evolution of the East Carpathian foredeep during the late Miocene–early Pliocene (Dacian Basin; Romania), *Global and Planetary Change* **103**, pp. 135─148, doi: 10.1016/j.gloplacha.2012.04.004.

Suc, J. P., D. Do Couto, M. C. Melinte-Dobrinescu, R. Macalet, F. Quillévéré, G. Clauzon, I. Csato, J. -L. Rubino, and S. -M. Popescu (2011), The Messinian Salinity Crisis in the Dacic Basin (SW Romania) and early Zanclean Mediterranean–Eastern Paratethys high sea-level connection, *Palaeogeography, Palaeoclimatology, Palaeoecology* **310**(3), pp. 256─272, doi:10.1016/j.palaeo.2011.07.018.

Tari, G., M. Fallah, W. Kosi, J. Floodpage, J. Baur, Z. Bati, and N. O. Sipahioğlu (2015), Is the impact of the Messinian Salinity Crisis in the Black Sea comparable to that of the Mediterranean?, *Marine and Petroleum Geology* **66**(1), pp. 135─148 doi: 10.1016/j.marpetgeo.2015.03.021.

Timmermans, M. -L. E., and L. J. Pratt (2005), Two-layer rotating exchange flow between two deep basins: Theory and application to the Strait of Gibraltar, *Journal of Physical Oceanography* **35**(9), pp. 1568─1592, doi: 10.1175/JPO2775.1.

Toggweiler, J. R., and H. Bjornsson (2000), Drake Passage and palaeoclimate, *Journal of Quaternary Science* **15**(4), pp. 319─328.

Topper, R. P. M, R. Flecker, P. Th. Meijer, and M. J. R. Wortel (2011), A box model of the Late Miocene Mediterranean Sea: Implications for combined [87]Sr/[86]Sr and salinity data, *Palaeoceanography* **26**(3), PA3223, doi: 10.1029/2010PA002063.

Topper, R. P. M., and P. Th. Meijer (2013), A modeling perspective on spatial and temporal variations in Messinian evaporite deposits, *Marine Geology* **336**, pp. 44─60, doi:10.1016/j.margeo.2012.11.009.

Topper, R. P. M., and P. Th. Meijer (2015), Changes in Mediterranean circulation and water characteristics due to restriction of the Atlantic connection: a high-resolution ocean model, *Climate of the Past* **11**, pp. 233─251, doi: 10.5194/cp-11-233-2015.

Torcellini, P. A., N. Long, and R. Judkoff (2003), Consumptive water use for US power production, ASHRAE Winter Meeting, Anaheim, California.

REFERENCES

Ünlülata, Ü., T. Oğuz, M. A. Latif, and E. Özsoy (1990), On the physical oceanography of the Turkish Straits, in: *The physical oceanography of sea straits*, ed. by: Pratt, L. J., Springer Netherlands, pp. 25−60, doi: 10.1007/978-94-009-0677-8_2.

van Assen, E., K. F. Kuiper, N. Barhoun, W. Krijgsman, and F. J. Sierro (2006), Messinian astrochronology of the Melilla Basin: Stepwise restriction of the Mediterranean-Atlantic connection through Morocco, *Palaeogeography, Palaeoclimatology, Palaeoecology* **238**(1), pp. 15−31, doi: 10.1016/j.palaeo.2006.03.014.

van Baak, C. G. C., E. P. Radionova, L. A. Golovina, I. Raffi, K. F. Kuiper, I. Vasiliev, and W. Krijgsman (in press), Messinian events in the Black Sea, doi: 10.1111/ter.12177.

van Baak, C. G. C., M. Stoica, A. Grothe, E. Aliyeva, and W. Krijgsman (2015), Mediterranean-Parathethys connectivity during the Messinian salinity crisis, in: *Mediterranean-Parathethys connectivity during the late Miocene to Recent: Unravelling geodynamic and paleoclimatic causes of sea-level change in semi-isolated basins*, PhD thesis, Chapter 7, Utrecht University, The Netherlands, pp. 177–205.

Vasiliev, I., W. Krijgsman, M. Stoica, and C. G. Langereis (2005), Mio-Pliocene magnetostratigraphy in the southern Carpathian foredeep and Mediterranean–Parathethys correlations, *Terra Nova* **17**(4), pp. 376−384, doi: 10.1111/j.1365-3121.2005.00624.x.

Vasiliev, I., A. G. Iosifidi, A. N. Khramov, W. Krijgsman, K. Kuiper, C. G. Langereis, V. V. Popov, M. Stoica, V. A. Tomsha, and S. V. Yudin (2011), Magnetostratigraphy and radio-isotope dating of upper Miocene–lower Pliocene sedimentary successions of the Black Sea Basin (Taman Peninsula, Russia), *Palaeogeography, Palaeoclimatology, Palaeoecology* **310**(3), pp. 163−175, doi:10.1016/j.palaeo.2011.06.022.

Vasiliev, I., G-. J. Reichart, and W. Krijgsman (2013), Impact of the Messinian Salinity Crisis on Black Sea hydrology—Insights from hydrogen isotopes analysis on biomarkers, *Earth and Planetary Science Letters* **362**, pp. 272−282, doi:10.1016/j.epsl.2012.11.038.nzi.

Vasiliev, I., G-. J. Reichart, A. Grothe, J. S. Sinninghe Damsté, W. Krijgsman, F. Sangiorgi, J. W. H. Weijers, and L. van Roij (2015), Recurrent phases of drought in the upper Miocene of the Black Sea region, *Palaeogeography, Palaeoclimatology, Palaeoecology* **423**, pp. 18−31, doi: 10.1016/j.palaeo.2015.01.020.

Vergnaud-Grazzini, C. (1983), Reconstruction of Mediterranean Late Cenozoic hydrography by means of carbon isotope analyses, *Utrecht Micropaleontological Bulletins* **30**, pp. 25−47.

von der Heydt, A., and H. A. Dijkstra (2005), Flow reorganizations in the Panama Seaway: A cause for demise of Miocene corals?, *Geophysical Research Letters* **32**(2), L02609, doi: 10.1029/2004GL020990.

von der Heydt, A., and H. A. Dijkstra (2006), Effect of ocean gateways on the global ocean circulation in the late Oligocene and early Miocene, *Palaeoceanography* **21**(1), PA1011, doi: 10.1029/2005PA001149.

Wang, C., X. Li, X. Hu, and L. F. Jansa (2002), Latest marine horizon north of Qomolangma (Mt Everest): implications for closure of Tethys Seaway and collision tectonics, *Terra Nova* **14**(2), pp. 114─120, doi: 10.1046/j.1365-3121.2002.00399.x.

Warren, J. K. (2006), Depositional chemistry and hydrology, in: *Evaporites: Sediments, resources, and hydrocarbons*, ed. by: Warren, J. K., Springer-Verlag, New York.

Woodruff, F., and S. M. Savin (1989), Miocene deepwater oceanography, *Palaeoceanography* **4**(1), pp. 87─140, doi: 10.1029/PA004i001p00087.

Wortel, M. J. R., and W. Spakman (2000), Subduction and slab detachment in the Mediterranean-Carpathian region, *Science* **290**(5498), pp. 1910─1917, doi: 10.1126/science.290.5498.1910.

Wright, J. D., K. G. Miller, and R. G. Fairbanks (1992), Early and middle Miocene stable isotopes: Implications for deep water circulation and climate, *Palaeoceanography* **7**(3), pp. 357─389, doi: 10.1029/92PA00760.

You, Y., M. Huber, R. D. Müller, C. J. Poulsen, and J. Ribbe (2009), Simulation of the Middle Miocene Climate Optimum, *Geophysical Research Letters* **36**(4), L04702, doi: 10.1029/2008GL036571.

Zachos, J. C., M. Pagani, L. Sloan, E. Thomas, and K. Billups (2001), Trends, rhythms, and aberrations in global climate 65 Ma to present, *Science* **292**(5517), pp. 686─693, doi*:* 10.1126/science.1059412.

Zavatarelli, M., and G. L. Mellor (1995), A numerical study of the Mediterranean Sea circulation, *Journal of Physical Oceanography* **25**(6), pp. 1384─1414, doi: 10.1175/1520-0485(1995)025<1384:ANSOTM>2.0.CO;2.

Zhang, Z., G. Ramstein, M. Schuster, C. Li, C. Contoux, and Q. Yan (2014), Aridification of the Sahara desert caused by Tethys Sea shrinkage during the Late Miocene, *Nature* **513**(7518), pp. 401─404, doi: 10.1038/nature13705.

Summary

During the Early Miocene (23-16 Ma; Ma = million years in the past) several marine gateways existed in the broader Mediterranean region. These seaways connected the Mediterranean Sea to the Indo-Pacific Ocean to the east, to the Atlantic Ocean to the west, and to the Paratethys—the predecessor of the Black Sea, Caspian Sea and Aral Sea—to the north. Tectonically-driven palaeogeographic changes resulted in the modern land-locked configuration of the Mediterranean Sea and its satellite basins. As part of this, the opening and closure of marine gateways, together with climate, triggered changes in the palaeoceanography of both the Mediterranean Sea and the Paratethys. These changes are preserved in the sedimentary record but, because our techniques for reconstruction of the past conditions are limited and the record itself is incomplete, interpretation of the geological evidence in terms of the underlying causes is subject to uncertainty and discussion. In this thesis I explore the alternative (and complementary) approach of applying regional-scale numerical models to gain physics-based understanding into the role of marine gateways in the palaeoceanography of the Miocene (23-5 Ma) Mediterranean Sea and Paratethys. The comparison of model results to geological data allows me to determine which scenarios are consistent with data, as well as to specify the conditions under which these arise.

I first focus on the closure of the marine gateway that connected the Mediterranean to the Indo-Pacific until the Early to Middle Miocene: the Indian Gateway. In particular, I examine the effect of the shoaling and closure of this gateway on Mediterranean circulation, the exchange with the adjacent oceans and, to a lesser extent, Mediterranean and Paratethys water properties. Results obtained with a regional-scale ocean circulation model show that when the Indian Gateway is deep (1000 m), the patterns of exchange are not dependent on factors such as climate, Atlantic Gateway depth and presence or absence of net westward flow in the ocean gateways. When the Indian Gateway is shallow (200 m) the exchange with the adjacent oceans is very sensitive to the previously mentioned factors. After closure more than a single Mediterranean-Atlantic exchange pattern is possible depending

on the Atlantic Gateway depth and climate. By combining model results with the available geological data, flow configurations consistent with observations for different stages of the process of closure are proposed. Specific attention is given to the exchange pattern with the Atlantic Ocean after closure, for which I compare model results to observations of Langhian age (16-14 Ma) from the western and central Mediterranean Sea.

In the Late Miocene, before the Messinian Salinity Crisis, the Mediterranean and the Atlantic were connected by two marine gateways: the Betic and Rifian corridors. Using a regional-scale ocean circulation model I investigate the patterns of exchange through this double gateway. Results show that two exchange patterns are possible depending on the relative depths of the gateways. More specifically, the deep corridor always presents two-layer flow (i.e., oceanic inflow at the surface and outflow at depth); the shallow corridor accommodates two-layer flow if it is deeper than the mid-depth of the deeper corridor and one-layer flow (i.e., Atlantic inflow) if this is shallower than half the depth of the deeper one. Model results allow the discard of the "siphon theory", according to which the Rifian corridor accommodated only Atlantic inflow and the Betic corridor Mediterranean outflow. With the model results as a basis, the geological data from the gateways are interpreted in terms of new scenarios, consistent with physics, for the time interval proposed for the "siphon event". Knowledge of the systematic behaviour of the double gateway in terms of exchange patterns is useful to reconstruct gateway geometries from the incomplete geological data.

In the Late Miocene, during the Messinian Salinity Crisis in the Mediterranean, the Paratethys sea level dropped. Estimates for the amplitude of the sea level drop in the main Paratethys sub-basins (Black Sea and Caspian Sea) range from a few meters to more than 1600 m. In this thesis I examine the sensitivity of the Black and Caspian sea levels to hydrologic budgets, assuming disconnection of these basins from the Mediterranean Sea. For that I quantify, for a wide range of negative hydrologic budgets (evaporative loss exceeds freshwater input), the sea level drop, the resulting salinity, and the time required to reach such a fall in sea level. Comparing the model results to (i) a set of Late Miocene hydrologic budgets calculated from a global climate simulation and (ii) to salinity estimates inferred from geological evidence, a 1000 m sea level drop in the Caspian Sea can be

discarded. In the Black Sea, whereas such a dramatic fall appears unlikely, it cannot be fully ruled out.

Samenvatting

Gedurende het Vroeg Miocene tijdvak (23-16 Ma; Ma = miljoen jaar geleden) bestonden er meerdere zeestraten in het toenmalige Middellandse Zeegebied. Deze zeestraten verbonden de proto-Middellandse Zee met de Indo-Pacifische Oceaan in het oosten, met de Atlantische Oceaan in het westen, en met de Paratethys - de voorloper van de Zwarte Zee, de Kaspische Zee en het Aralmeer - in het noorden. Door tektoniek gedreven paleogeografische veranderingen resulteerden in het hedendaagse door land ingesloten karakter van de Middellandse Zee en de aangrenzende bekkens. Als onderdeel hiervan veroorzaakten de opening en de sluiting van de zeestraten, samen met het klimaat, veranderingen in de paleoceanografie van zowel de Middellandse Zee als de Paratethys. Deze veranderingen zijn bewaard gebleven in de sedimenten die zich afzetten op de zeebodem. Omdat onze technieken voor de reconstructie van de omstandigheden in het verleden beperkt zijn en de stratigrafie zelf incompleet is, is de interpretatie van het geologische archief in termen van de onderliggende oorzaken onzeker en onderwerp van discussie. In dit proefschrift onderzoek ik de alternatieve (en aanvullende) benadering van de toepassing van numerieke modellen op regionale schaal om fysisch onderbouwd inzicht te krijgen in de rol van zeestraten in de palaeoceanografie en de zeespiegel van de Middellandse Zee en Paratethys tijdens het Mioceen (23-5 Ma). De vergelijking van de modelresultaten met geologische gegevens stelt mij in staat te bepalen welke scenario's consistent zijn met de data, alsmede te specficeren wat de omstandigheden waren waaronder deze zich hebben voltrokken.

Ik richt me eerst op de sluiting van de zeestraat die tot het Vroeg- tot Midden-Mioceen de Middellandse Zee met de Indo-Pacifische Oceaan verbond: de Indische zeestraat. In het bijzonder onderzoek ik het effect van het ondieper worden en de sluiting van deze zeestraat op de circulatie in de Middellandse zee, de wateruitwisseling met de aangrenzende oceanen en, in mindere mate, de eigenschappen van het water van de Middellandse Zee en de Paratethys. De resultaten verkregen met een oceaancirculatiemodel op regionale schaal tonen aan dat wanneer de Indische zeestraat diep is (1000 m), de patronen van uitwisseling niet afhankelijk

zijn van factoren zoals klimaat, diepte van de Atlantische zeestraat of de aan- of afwezigheid van een netto westwaartse stroom in de zeestraten. Wanneer de Indische zeestraat ondiep (200 m) is, is de uitwisseling met de aangrenzende oceanen zeer gevoelig voor de genoemde factoren. Na sluiting is meer dan één uitwisselingspatroon tussen de Middellandse Zee en de Atlantische oceaan mogelijk, afhankelijk van de diepte van de Atlantische zeestraat en het klimaat. Door de modelresultaten te combineren met de beschikbare geologische gegevens ben ik in staat de configuratie van stroming voor te stellen die consistent is met waarnemingen voor de verschillende fasen van het sluitingsproces. Specifieke aandacht wordt gegeven aan het uitwisselingspatroon met de Atlantische Oceaan na de sluiting, waarvoor ik mijn resultaten vergelijk met waarnemingen aan sedimenten van Langhien ouderdom (16-14 Ma) uit de centrale en westelijke Middellandse Zee.

In het Laat-Mioceen, en wel vóór de saliniteitscrisis van het Messinien, waren de Middellandse Zee en de Atlantische Oceaan verbonden door twee dicht bij elkaar gelegen zeestraten: de Betische en Rif-zeestraat. Met behulp van een algemeen oceaancirculatiemodel op regionale schaal en een Laat-Miocene paleogeografie onderzoek ik de uitwisselingspatronen door deze dubbele zeestraat. De resultaten laten zien dat er twee patronen mogelijk zijn, afhankelijk van de relatieve diepte van de zeestraten. Meer specifiek vertoont de diepe zeestraat altijd een tweelagen-stroming (dat wil zeggen, instroom aan het oppervlak en uitstroom op diepte); de ondiepe zeestraat biedt een tweelagen-stroming als deze dieper is dan de helft van de diepte van de diepere zeestraat en een éénlaagse stroming indien deze ondieper is dan de helft van de diepte van de diepere zeestraat. De modelresultaten stellen mij in staat om de zogenaamde "sifon theorie" te weerleggen. Volgens deze theorie zou door de Rif-zeestraat alleen instroom van Atlantisch water zijn opgetreden, terwijl door de Betische straat alleen uitstroom vanuit de Middellandse Zee plaatsvond. Met de uitkomsten van het model als basis worden geologische observaties gedaan in de zeestraten, voor het tijdsinterval voorgesteld voor de "sifon", geïnterpreteerd in termen van nieuwe scenario's, nu wel consistent met de achterliggende natuurkunde. Kennis van de systematiek van het uitwisselingspatroon in de zeestraten is nuttig om de geometrie van de zeestraten te reconstrueren uit de incomplete geologische data.

In het Laat-Mioceen, gedurende de saliniteitscrisis van het Messinien, daalde de zeespiegel van de Paratethys. Schattingen voor de grootte van de zeespiegeldaling in de belangrijkste sub-bekkens van de Paratethys (de Zwarte Zee en de Kaspische

Zee) variëren van enkele meters tot meer dan 1600 m. In dit proefschrift onderzoek ik de gevoeligheid van de zeespiegel van de Zwarte Zee en de Kaspische Zee voor hydrologische budgetten, aannemend dat deze bekkens van de Middelandse Zee zijn afgesloten. Hiervoor kwantificeer ik voor een breed scala van negatieve hydrologische budgetten (d.w.z. verlies door verdamping overschrijdt de aanvoer van zoetwater), de daling van de zeespiegel, het resulterende zoutgehalte, en de tijd die nodig is om de desbetreffende daling van de zeespiegel te bereiken. Vergelijking van de modelresultaten met een set van Laat-Mioceen hydrologische budgetten afgeleid van een recente globale klimaatsimulatie en met schattingen van het zoutgehalte afgeleid uit geologisch observaties, maakt het mogelijk een zeespiegeldaling van 1000 m in de Kaspische Zee te verwerpen. In de Zwarte Zee kan een dergelijke daling niet volledig worden uitgesloten, hoewel zo een dramatische daling onwaarschijnlijk lijkt.

Resumen

Durante el Mioceno Inferior (23-16 Ma; Ma = millones de años en el pasado) existieron varios corredores marinos en la región Mediterránea. Éstos conectaban el Mar Mediterráneo con el Indo-Pacífico al este, el Atlántico al oeste, y el Paratetis—predecesor de los mares Negro, Caspio y de Aral—al norte. Cambios paleogeográficos, que incluyen la apertura y el cierre de estos estrechos marinos, dieron lugar a la configuración actual del Mar Mediterráneo y sus cuencas satélite. La cambiante geometría de los estrechos marinos (impulsada por la tectónica de placas), en combinación con el clima, modificó sustancialmente la paleoceanografía del Mar Mediterráneo y del Paratetis. Estos cambios quedaron preservados en el registro sedimentario, que constituye una herramienta fundamental para la realización de reconstrucciones paleoambientales. El estudio de los sedimentos, sin embargo, no permite determinar los procesos causantes de las condiciones ambientales observadas, ni tampoco conocer si dichas condiciones son aplicables al resto de la cuenca o representan un fenómeno local. En esta tesis aplico modelos numéricos de escala regional para comprender, mediante las leyes de la física, la influencia de los estrechos marinos en la paleoceanografía del Mar Mediterráneo y el Paratetis durante el Mioceno (23-5 Ma). La comparación de los resultados de los modelos con información procedente del registro sedimentario permite determinar los escenarios modelados consistentes con los datos de campo, así como las condiciones necesarias para la generación de los mismos.

En primer lugar estudio el cierre del estrecho marino que conectó el Mar Mediterráneo con el Indo-Pacífico hasta el Mioceno Inferior-Mioceno Medio: el Estrecho del Índico. En particular, examino la influencia de la somerización y el cierre de este estrecho en (i) la circulación termohalina del Mar Mediterráneo, (ii) el intercambio de aguas entre el Mediterráneo y los océanos adyacentes y (iii) las propiedades de las aguas del Mediterráneo y el Paratetis. Los resultados, obtenidos con un modelo de circulación oceánica de escala regional, muestran que cuando el Estrecho del Índico es profundo (1000 m) los patrones de intercambio de aguas con el Atlántico y el Pacífico no dependen de factores tales como el clima, la

profundidad del Estrecho del Atlántico y la presencia (o ausencia) de transporte neto de agua hacia el oeste en los estrechos oceánicos. Cuando el Estrecho del Índico es somero (200 m), el intercambio de aguas con los océanos adyacentes es muy sensible a los factores mencionados anteriormente. Tras el cierre del Estrecho del Índico existen múltiples patrones posibles en cuanto al intercambio de aguas con el Atlántico en función de la profundidad del Estrecho del Atlántico y el clima. La comparación de los resultados obtenidos con datos geológicos permite establecer los posibles patrones de intercambio de aguas en los estrechos durante las diferentes etapas del proceso de cierre. Presto especial atención al intercambio de aguas entre el Mediterráneo y el Atlántico tras el cierre del Estrecho del Índico, para lo cual utilizo datos de campo procedentes del Mediterráneo central y occidental de edad Langhiense (16-14 Ma).

En el Mioceno Superior, con anterioridad a la Crisis de Salinidad del Messiniense, el Mediterráneo y el Atlántico estuvieron conectados por los corredores Bético y Rifeño. Utilizando un modelo de circulación oceánica de escala regional investigo el intercambio de aguas a través de estos corredores. Los resultados indican que hay dos patrones posibles en cuanto al intercambio de aguas en función de la profundidad relativa de un corredor con respecto al otro. Concretamente, el corredor más profundo siempre presenta flujo bicapa. Éste consiste en entrada de aguas Atlánticas hacia el Mediterráneo en superficie y salida de aguas Mediterráneas en profundidad. El corredor más somero presenta (i) flujo bicapa, si la profundidad de éste es superior a la mitad de la profundidad máxima del otro corredor y (ii) únicamente entrada de aguas Atlánticas, si éste es menos profundo que la mitad de la profundidad del corredor más profundo. Los resultados obtenidos permiten descartar la "teoría del sifón", que propone que el corredor Rifeño presentaba exclusivamente influjo de aguas Atlánticas y el Bético salida de aguas Mediterráneas hacia el Atlántico. Utilizando los resultados del modelo y datos de campo procedentes de los corredores propongo posibles patrones de intercambio de aguas durante el intervalo temporal del "sifón". El sistemático intercambio de aguas encontrado en los corredores en función de sus profundidades relativas resulta de gran utilidad para reconstruir las geometrías de los corredores a partir del limitado registro sedimentario y, por tanto, recrear la sucesión de acontecimientos que culminó en la crisis de salinidad.

En el Mioceno Superior, durante la Crisis de Salinidad del Messiniense en el Mediterráneo, el nivel del mar Paratetis cayó. Estimaciones de la amplitud del descenso del nivel del mar en las principales cuencas del Paratetis (Mar Negro y Mar Caspio) varían desde unos pocos metros hasta más de 1600 m. En esta tesis analizo la sensibilidad de los niveles del Mar Negro y del Mar Caspio a múltiples balances hidrológicos cuando el Paratetis está desconectado del Mar Mediterráneo. Cuantifico la caída del nivel del mar, la salinidad resultante y el tiempo necesario para alcanzar dicho nivel del mar, asumiendo múltiples balances hidrológicos negativos (pérdida evaporativa excede a la entrada de agua dulce). La comparación de los resultados modelados con (i) una colección de balances hidrológicos calculados para el Paratetis durante el Mioceno Superior y (ii) estimaciones de salinidad obtenidas a partir del registro sedimentario, permite descartar un descenso del nivel del mar de 1000 m en el Mar Caspio. En el Mar Negro, aunque una caída del nivel del mar tan acusada parece poco probable, ésta no se puede descartar completamente.

Acknowledgements

"I don't want to believe. I want to know"
Carl Sagan

As someone who is passionate about the ocean, I consider myself lucky to have had the opportunity to investigate the palaeoceanography of the of the ancient Mediterranean and Paratethys seas during my PhD. This project has been as exciting as challenging, and the completion of this thesis would not have been possible without those people that, in one way or another, helped me over the last years. First and foremost, I would like to thank my (co-)supervisor, **Paul Meijer**. Paul was always very enthusiastic about my research and we had many interesting and inspiring discussions. He was always willing to help and he squeezed his agenda many times to find time for me, especially in the last stages of the thesis. He not only reinforced my achievements, but also supported me when I had difficulties. Thanks, Paul!

I would also like to express my gratitude to my supervisor, **Rinus Wortel**. His support and great interest in my research are highly appreciated. He gave me advice on how to improve the structure and style of my manuscripts. He also helped me with the paperwork for the PhD application and carefully revised the Dutch summary of the thesis.

A big thanks to **Theo van Zessen**, who efficiently solved all my computer-related problems. I would also like to acknowledge **Ton Markus** for helping me to create and improve some of the illustrations of this thesis. I thank **Ildikó Csikós**, **Margreet Evertman** and **Jan-Willem de Blok** for their help with multiple administrative tasks.

I am very grateful to the members of the **reading committee**—Henk Dijkstra, Rachel Flecker, Jesús García Lafuente, Gert de Lange and Wout Krijgsman. Their comments were very valuable and helped me to polish the last version of the thesis manuscript.

During my PhD I worked with colleagues from other groups and institutions. I acknowledge **Anna von der Heydt** for her interest in the Indian Gateway work. I

thanks for being the way you are. For their unconditional love and support, I thank my grandmothers **Lola** and **Antonia**. I am very grateful to my aunt **Laura**, who gave me valuable advice on how to improve the layout of this thesis. Thanks also to my boyfriend **Sergio**, who has been by my side during the Dutch adventure.

To those of you that I may have forgotten to mention, also thanks! In my favour I would say that it is not easy to summarise the experiences of four years in a couple of pages.

Last, but not least, I would like to dedicate again this thesis to my grandfather and friend, **Pepe**. He was, is, and will always be one the most important persons to me. *Porque desde el día en que te fuiste, solo sueño con volver a verte.*

Curriculum Vitae

28 Nov. 1985   Born in Valencia, Spain

2003   High school graduation with
                                   honours
                                   Valencia, Spain

2004-2009   BSc in Marine Sciences with
                                   honours
                                   University of Alicante, Spain

2009-2010   MSc in Analysis and Management
                                   of Mediterranean Ecosystems
                                   University of Alicante / University
                                   of Elche, Spain

2011-2015   PhD candidate
                                   Tectonophysics group
                                   Utrecht University,
                                   The Netherlands